H-INFINITY MIXED SENSITIVITY OPTIMIZATION FOR A FOUR AXIS GIMBAL PLATFORM

EZEL YALÇINKAYA

SEPTEMBER 2022

ÇANKAYA UNIVERSITY

GRADUATE SCHOOL OF NATURAL AND APPLIED SCIENCES

DEPARTMENT OF ELECTRICAL AND ELECTRONICS ENGINEERING

MASTER'S THESIS IN
ELECTRICAL AND ELECTRONICS ENGINEERING

H-INFINITY MIXED SENSITIVITY OPTIMIZATION FOR A FOUR AXIS GIMBAL PLATFORM

EZEL YALÇINKAYA

SEPTEMBER 2022

ABSTRACT

H-INFINITY MIXED SENSITIVITY OPTIMIZATION FOR A FOUR AXIS GIMBAL PLATFORM

YALÇINKAYA, Ezel
Master of Science in Electrical and Electronics Engineering

Supervisor: Assist. Prof. Dr. Oğuzhan ÇİFDALÖZ
September 2022, 155 pages

Recently; gimbal systems are employed in a wide range of engineering applications, including military and commercial systems such as missiles, drones, attack helicopters etc. These systems are commonly used for target tracking, surveillance, mapping, image processing, and providing high resolution images with electro-optical or infrared cameras. The main purpose of using these systems is to point the optical system to the desired point regardless of the platform's movement and to compensate the disturbance effects in order to ensure that system is stabilized during the motion. It is important to design multi axis gimbal systems for tracking the desired target and point when it comes to precise targeting and observation.

This study addresses the detailed mathematical modelling and H_∞ mixed sensitivity control design of a four axis gimbal system. Firstly, the four-axis gimbal system is modeled separately for each axis, and the system's kinematic and dynamic models are thoroughly analyzed. After determining the system dynamics, controllers are designed with the H_∞ mixed sensitivity method, which is one of the robust control design methods for system control.

Finally, proposed system modelling and control design are simulated in MATLAB and Simulink environments. Results are presented with figures and tables in the thesis.

Keywords: Four-Axis Gimbal System, Mathematical Modeling, Controller Design, H_∞ Mixed Sensitivity, Stabilization.

ÖZ

DÖRT EKSENLİ GİMBAL PLATFORMU İÇİN H-SONSUZ KARMA HASSASİYET OPTİMİZASYONU

YALÇINKAYA, Ezel

Elektrik-Elektronik Mühendisliği Yüksek Lisans

Danışman: Dr. Öğr. Üyesi Oğuzhan ÇİFDALÖZ

Eylül 2022, 155 sayfa

Günümüzde gimbal sistemleri füzeler, insansız hava araçları, keşif gözlem helikopterleri gibi askeri ve bazı ticari amaçlı olmak üzere birçok mühendislik uygulamalarında kullanılmaktadır. Genellikle bu sistemler üzerinde taşıdıkları faydalı yük olan elektro-optik veya kızılötesi kameralarla hedef takibi, gözetleme, haritalama, görüntü işleme, yüksek çözünürlüğe sahip görüntü elde etmek amacıyla kullanılırlar. Bu sistemlerin kullanılmasındaki temel amaç, faydalı yükün; üzerinde bulunduğu platformun hareketinden bağımsız olarak istenilen konumlara yönlenmesi ve bu yönlenme sırasında sistemin kararlı olmasıdır. Hassas hedefleme ve gözlemleme söz konusu olduğunda gimbal sistemlerinin çok eksenli olarak tasarlanması istenilen hedef ve noktayı takip etme konusunda önemlidir.

Bu çalışma, dört eksenli bir gimbal sisteminin detaylı olarak matematiksel modellenmesi ve kontrolü üzerine odaklanmıştır. İlk olarak, dört eksenli gimbal sistemi her eksen ayrı ayrı olacak şekilde incelenmiş, kinematik ve dinamik denklemleri detaylı olarak analiz edilmiştir. Sistem dinamiklerinin belirlenmesinden sonra sistem kontrolü için gürbüz kontrol tasarım metotlarından biri olan H_∞ karma hassasiyet yöntemi ile kontrolcüler tasarlanmıştır.

Son olarak, önerilen sistem modellemesi ve kontrol tasarımı MATLAB/Simulink ortamları kullanılarak simule edilmiş olup sonuçlar tezde grafik ve tablolarla sunulmuştur.

Anahtar Kelimeler: Dört Eksenli Gimbal Sistemi, Matematiksel Modelleme, Kontrolcü Tasarımı, H_∞ Karma Hassasiyet, Stabilizasyon.

To my beloved family...

ACKNOWLEDGMENTS

I would like to express my deepest gratitude to my supervisor Assist. Prof. Dr. Oğuzhan Çifdalöz for his helpful criticism, guidance, motivation, profound knowledge and patience in the progress and preparation of this thesis. I have learnt a great deal from him, and it would not have been possible without his help. I would also like to thank my thesis committee members, Assoc. Prof. Dr. Erdem Akagündüz and Assist. Prof. Dr. Halit Ergezer for their valuable contributions.

I would also like to deeply thank my dear group-mate partner Sanem Meral, who has always been with me throughout my undergraduate and graduate life for all the support she has given me. I would like to thank my dear friends Baran Ayana, Almıla İkizoğlu, and Onur Öztürk, for being with me, for always giving me motivation and believing that I will succeed. Without them, my academic life would not have been enjoyable in any aspects.

Furthermore I would like to thank my friends and colleagues, Ömer Yaman, Dr. Nurgül Gökgöz Küçüksakallı, Melis Çıkış, Doruk Eren, İrem Gökdağ and Aydan Demirbüken for their support and friendship throughout my thesis studies. I would also like to thank İsmail Çırak for his encouragement and support throughout the thesis preparation process.

The support and understanding of my family was very important for me to complete this thesis. I would like to thank my dear brother Demiralp Yalçınkaya, his beloved wife Gözde Yalçınkaya and my dear niece Beren Yalçınkaya for always standing by me and supporting me in every decision I made. Also I would like to express my sincere gratitude to Sevgi Koşan, Erhan Koşan, Dr. Sevhan Turan, Dr. Bilal Turan and my lovely cousin Bartu Turan for always being there for me whenever I needed them.

Last but not least, I especially would like to greatly thank my mother, Nazlı Yalçınkaya and my father, Metin Yalçınkaya for their endless love, inspiration, support and guidance all through out my life. I would like to express my gratitude to them for always believing in and encouraging me. Without them, none of these achievements could have been possible. I will forever be in their debt for everything they did to this day and will do from now on. Hence, I dedicate this work to them.

TABLE OF CONTENTS

LIST OF TABLES

LIST OF FIGURES

LIST OF SYMBOLS AND ABBREVIATIONS

ISP	Inertially Stabilized Platform
DOF	Degree of Freedom
LTI	Linear Time Invariant
LQG	Linear Quadratic Gaussian
LQR	Linear Quadratic Regulator
MIMO	Multiple Input Multiple Output
SISO	Single Input Single Output
n	Navigation Frame
b	Body Frame
A	Outer Azimuth Frame
E	Outer Elevation Frame
e	Inner Elevation Frame
a	Inner Azimuth Frame
p, q, r	Roll, Pitch, Yaw Rates
ϕ, θ, ψ	Euler Angles

CHAPTER 1

INTRODUCTION

1.1 Background

ISPs (inertial stabilization platforms) are used in a wide range of engineering applications, including weapon systems, telescopes, cameras, military and commercial systems such as missiles, drones, attack helicopters etc. Gimbal systems, which are mechanical structures used to provide inertial stabilization; they can be considered as a combination of motor, bearings and mounted gyroscopes. In general, at least two orthogonal gimbals are preferred in most applications [11].

When the gimbal systems are mounted on moving platforms, such as an aircraft, ground vehicles, ships or a spacecraft, because of the base movements, inertial dynamics and sometimes environmental disturbances the system becomes a complex system [13, 15].

Despite, the specifications and configurations differing greatly, the main purpose of using these systems is to point the optical system to the desired point regardless of the platform's motions, vibrations and to compensate the disturbance effects in order to ensure that system is stabilized during motion [7, 11, 21]. All of these disturbances can result in decreased pointing accuracy of the ISPs [16].

This thesis consists of two main parts: modeling of a four-axis gimbal platform and the controller design of a four axis gimbal system. In the model analysis part, a detailed mathematical modeling of the system was made. In the control design section, a controller design was made with H_∞ mixed sensitivity, which is one of the robust control methods.

Also this thesis is organized as follows:

In this first chapter, background information, motivation for carrying out this thesis work and literature survey is given together with the objectives and contributions. In Chapter 2, firstly the gimbal mechanism is explained in detail. Secondly, notation, preliminaries, reference coordinate frames and transformation matrices have been determined. Thirdly, the kinematic equations are formulated in detail for each axis. In order to better understand the system, dynamic analysis are made and kinematic equations and dynamic equations were combined. Then, the four-axis gimbal model was represented in a state space, and their LTI models are obtained by the Jacobian linearization technique. In Chapter 3, firstly, the H_∞ mixed sensitivity optimization problem is explained in general terms. Afterwards, controllers are designed with the H_∞ mixed sensitivity method in different configurations as SISO and MIMO structures for the four-axis gimbal platform. In chapter 3 includes the simulation results of the proposed method. In chapter 4 summarizes the thesis. Then the important results derived throughout the thesis are explained. Chapter 4 is concluded by discussing some future applications.

1.2 Literature Survey

Since gimbal systems are basically guidance systems, they are frequently used in civil and military applications for pointing systems as well as imaging systems. In this part of the thesis, the gimbal mechanism and some studies on the control of the gimbal mechanism are discussed. This section provides an overview of gimbal systems, mathematical modeling of these systems, and controller design methods for them. When gimbal systems are examined, it is seen that two axis, three axis and four axis system structures are based [1, 9, 12, 14, 22, 25].

When the gimbal structures are examined, it is seen that they are handled in different rotation configurations. A gimbal design with a yaw-pitch structure is examined in the [27]. The designed gimbal is used as a laser and radar pointing system. Gimbal mechanism is used with direct-drive brushless direct current motor. In this study, the encoder is preferred as the angular position sensor. Also, PID (Proportional-Integral Differential) and PIV (Proportional-Integral-Velocity) control methods are developed as control methods. PIV type controller have been applied to achieve better results.

A two-axis gimbal system design and real-time control of the system are done in [4]. For the control of the gimbal system, LQG/LTR (Linear Quadratic Gaussian/Loop Transfer Recovery), H_∞ and μ controller structures were used and compared. In this study, it is seen that the H_∞ controller has the best performance in low frequency regions due to its high gain. While the LQG/LTR controller performs best in the mid-frequency region, the μ controller performs better near the cut-off frequencies. The H_∞ controller shows the worst performance in the mid-frequency region. Again, H_∞ controller performans better in high frequency regions. Because of its high gain, the LQG/LTR controller is expressed as the controller with the worst performance in this frequency range. In [4], it is suggested to use the H_∞ controller in cases where the working region represents low frequencies, and the μ controller in cases where the working region represents the entire frequency region.

Within the scope of the literature research, it has been seen that two axis structure are frequently used in gimbal mechanisms. The reason for this is that images are two-dimensional in imaging or pointig systems, and two-dimensional position information is sufficient for target pointing or tracking operations. Gimbal mechanisms with three or more axes are preferred to meet various requirements such as higher payload, increased field of view, and improved operational performance. It has been understood that it is important to design these systems as multi-axis when it comes to target tracking [18, 19]. The gimbal frame transformations, kinematics and dynamics equations of the considered systems have been investigated in different studies [9, 24, 26].

In [9], the equations of motion are derived using the moment equation and Lagrange equations, and it is shown that the equations can be formulated in such a way that natural interpretations can be given. Also that gimbals are rigid bodies, that have inertia cross couplings and have no mass unbalance. Static and dynamic mass unbalance dynamics of 2-DOF gimbal system in detail. The torque relationships have been derived considering the angular motion of the base body and the dynamic unbalance. According to the dynamic mass unbalance, the equations for the gimbals' motion were derived and introduced in two formulations. [23]

In [20], the impact of dynamical mass unbalance is included, but the center of gravity offsets, rotation axes misalignments and disturbance forces/moments are not explicitly modeled. Besides, in [3, 24, 28] researchers have simplified their gimbal models by neglecting static and dynamic mass unbalance effects and all gimbals have been designed as decoupled.

After the detailed mathematical model examinations in the literature, studies for general control systems are included. Many control design methods have been investigated on gimbal systems and successful results have been achieved in robust control-based linear quadratic methods [5, 6, 29], H_∞ method [2, 17, 30] and μ-synthesis [32] controller studies as well as classical control methods.

CHAPTER 2

MODEL ANALYSIS

In this chapter, the four axis gimbal system is modeled in detail to create a realistic simulation environment and describe the big picture before diving into controller design and simulation results.

In the modeling of the four axis gimbal systems, firstly the gimbal mechanism is explained in detail. Secondly, the notation, reference coordinate frames and transformation matrices used in four-axis gimbal modeling are described. Then, the kinematic equations are formulated in detail for each axis. After that, physical dynamic analysis is performed in order to better understand the friction and force effects that the gimbal system model is exposed to, and the system motions are examined under two titles as decoupled and coupled. As a result of these motion analysis, the effect of the friction force in the coupled system has been correctly integrated into the dynamic models and the full dynamic model of the four axis gimbal system has been schematized.

In the full dynamic model in which kinematic equations and dynamic block diagrams are integrated, it is seen that the four-axis gimbal system structure is non-linear with multiple inputs and multiple outputs (MIMO). Therefore, all the system's nonlinear state space equations are obtained, and the system is linearized at some equilibrium point. Finally, the linearized system's transfer functions are created and shown in detail.

2.1 Four-Axis Gimbal Model

The mechanism of the four-axis gimbal model shown in Fig 2.1 consists of four interconnected revolute joints which has one degree of freedom (one axis) of rotation. The primary mission of these systems is to rotate the payload, which could be a camera, a gun, a telescope, or any other device on the inner frame, with respect to the base platform. For that purpose, the mechanical design is conducted in such a way that the outer azimuth frame (A), outer elevation frame (E), inner elevation frame (e) and inner azimuth frame (a), respectively.

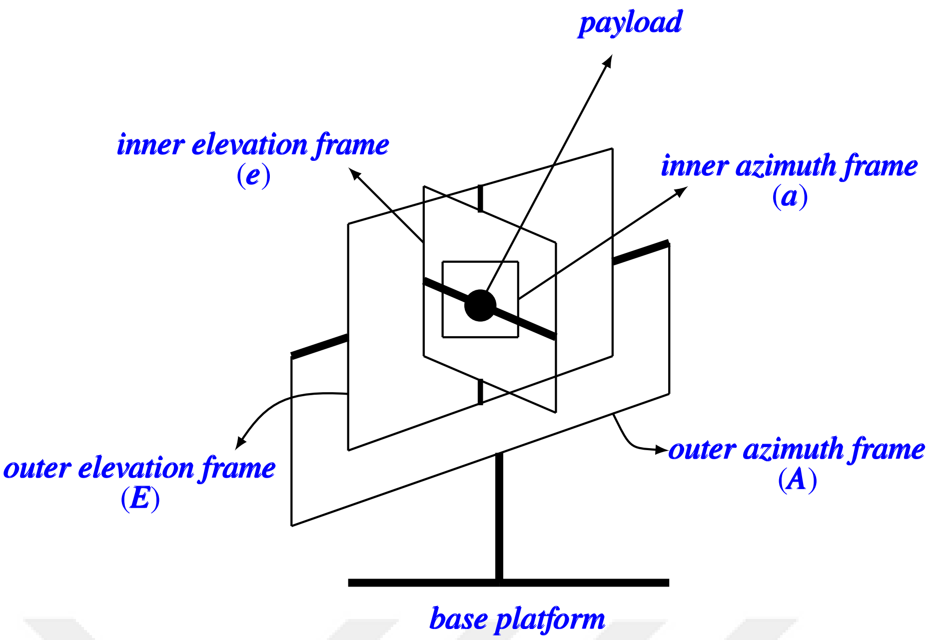

Figure 2.1: Four axis gimbal mechanism.

The four-axis gimbal system is thought to be mounted on any moving vehicle that rotates and translates according to a chosen inertial reference frame, and it is known that the vehicle's angular velocity and the translational acceleration will have a direct effect on the gimbal system.

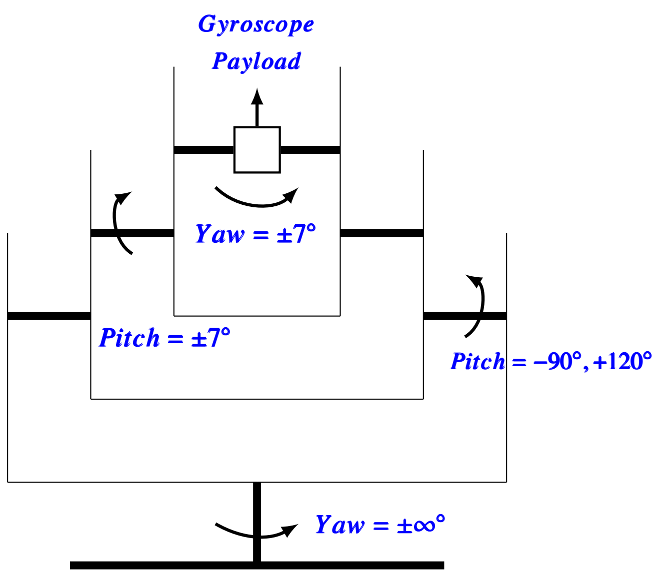

Figure 2.2: Top view of four axis gimbal model mechanism.

When the gimbal mechanism is examined in more detail; it is seen that the angular motion of the outer azimuth frame effects the outer elevation frame, inner elevation frame and inner azimuth frames. Likewise, the outer elevation frame affects inner elevation frame and inner azimuth frames. Fig 2.2 shows the top view of the four axis gimbal model mechanism given in Fig 2.1. In addition, the mechanical limits of rotation of each axis are given here.

In contrast to outer axes; which have a large rotational capacity but a low controller bandwidth, inner axes have few degrees of freedom but a large controller bandwidth. Inner frames; which are effective for angular stabilization in the inertial coordinate system, are used for fine tuning.

Four brushless direct current (DC) motors operate the full frame of the four-axis gimbal system seperately. Angular position sensors are performed by four absolute encoders mounted within the revolute joints, which are joining the outer azimuth frame, outer elevation frame, inner elevation frame and inner azimuth frame respectively. In this way; these sensors are measured angular position of the each frames with respect to base platform. No relative angular rate sensor is assumed.

Moreover, the gyroscope is located on the inner azimuth frame of the four axis gimbal to measure the angular rates of the inner azimuth frame with respect to the inertial reference frame.

2.2 Notation and Preliminaries

The notation used in this study is based on [8, 31]. Rotational transformation of a vector, x^b, in frame F_b into a vector, x^a in frame F_a is described as

$$x^a = C_b^a x^b$$

where F_a and F_b are orthogonal and right handed, subscript b in C_b^a denotes the *reference frame*, superscript a in C_b^a denotes the *target frame*, and x^a is the representation of the vector x^b in frame F_a. Since C_b^a is orthonormal, and $(C_b^a)^{-1} = (C_b^a)^T = C_a^b$ from which it follows $x^b = C_a^b x^a$.

The angular velocity of the *k-frame* relative to the *m-frame*, as resolved in the *p-frame*, is represented by ω_{mk}^p.

Roll, *pitch*, and *yaw* rotations are expressed mathematically as direction cosine matrices as:

$$R_1(\phi) \triangleq \begin{bmatrix} 1 & 0 & 0 \\ 0 & \cos\phi & \sin\phi \\ 0 & -\sin\phi & \cos\phi \end{bmatrix} \tag{2.1}$$

$$R_2(\theta) \triangleq \begin{bmatrix} \cos\theta & 0 & -\sin\theta \\ 0 & 1 & 0 \\ \sin\theta & 0 & \cos\theta \end{bmatrix} \tag{2.2}$$

$$R_3(\psi) \triangleq \begin{bmatrix} \cos\psi & \sin\psi & 0 \\ -\sin\psi & \cos\psi & 0 \\ 0 & 0 & 1 \end{bmatrix} \tag{2.3}$$

2.3 Reference Coordinate Frames and Transformations

To describe the method presented in this thesis, the *inertial frame (i-frame)*, the *earth frame (e-frame)*, the *navigation frame (n-frame)*, and the *body frame (b-frame)* need to be known. These are defined as presented in [31].

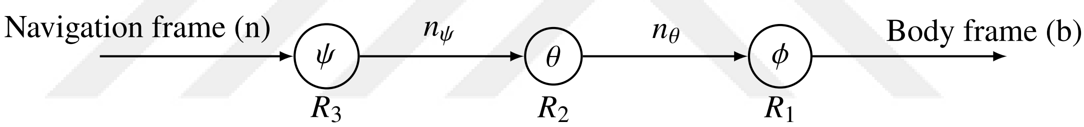

Figure 2.3: Sequence of Rotations.

The following is the transformation matrices from navigation to body frame:

$$C_n^b = R_1(\phi)R_2(\theta)R_3(\psi) \tag{2.4}$$

The transformation matrix from the body frame to the navigation frame is constructed by transposing C_n^b [31].

$$C_b^n = (C_n^b)^T = \begin{bmatrix} \cos\psi\cos\theta & \cos\psi\sin\phi\sin\theta - \sin\psi\cos\phi & \cos\psi\sin\theta\cos\phi + \sin\psi\sin\phi \\ \cos\theta\sin\psi & \sin\psi\sin\theta\sin\phi + \cos\psi\cos\phi & \sin\psi\sin\theta\cos\phi - \sin\phi\cos\psi \\ -\sin\theta & \sin\phi\cos\theta & \cos\phi\cos\theta \end{bmatrix} \tag{2.5}$$

ϕ, θ, and ψ are known as the *Euler Angles* and have the following connections to the body angular rates:

$$\begin{bmatrix} \dot{\phi} \\ \dot{\theta} \\ \dot{\psi} \end{bmatrix} = \begin{bmatrix} 1 & \sin\phi\tan\theta & \cos\phi\tan\theta \\ 0 & \cos\phi & -sin\phi \\ 0 & \sin\phi/cos\theta & \cos\phi/cos\theta \end{bmatrix} \begin{bmatrix} p \\ q \\ r \end{bmatrix} \tag{2.6}$$

where p, q, r are the body *roll*, *pitch*, *yaw* rates of the platform, respectively [31].

2.4 Kinematic Equations of Four-Axis Gimbal Platform

This section describes the kinematics of the four axis gimbal system which mechanizations are azimuth, elevation, elevation, and azimuth frames respectively from the outside to the inside. All frames of the four-axis gimbal platform, which are divided into inner and outer axes, have been investigated separately.

Table 2.1: Symbol Descriptions.

Symbol	Description
A	Outer Azimuth Frame
E	Outer Elevation Frame
e	Inner Elevation Frame
a	Inner Azimuth Frame (gyroscope)
$\psi_o, \theta_o, \theta_i, \psi_i$	Gimbal Angular Positions (encoders)

In the analysis that follows, A and E stand for the outer azimuth and outer elevation frames, respectively, e denotes the inner elevation frame, and a denotes the inner azimuth frame of the four axis gimbal. ψ_o, θ_o, θ_i, and ψ_i denote the outer azimuth angle, outer elevation angle, inner elevation angle, and the inner azimuth angle, respectively. These gimbal angular positions are measured by encoders. Thereafter, the kinematic equations of the four axis gimbal will be derived and combined with the dynamical model.

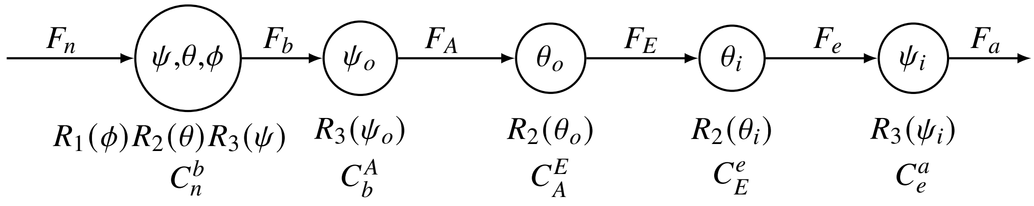

Figure 2.4: Reference frames and their rotational relations for a four axis gimbal.

The four axis gimbal model's reference frames and rotation relations are shown in Fig 2.4 above. The rotational relationship shown here is important as it provides the basis for kinematic equations. Furthermore, F_n denotes the navigation reference frame, F_b the body reference frame, F_A the outer azimuth reference frame, F_E the outer elevation reference frame, F_e the inner elevation reference frame, and F_a the inner azimuth reference frame.

2.4.1 Outer Azimuth Frame Kinematics

The angular rates of the outer azimuth frame with respect to the inertial frame as resolved in the outer azimuth frame is given by

$$d_A \triangleq \omega_{iA}^{A} = \omega_{ib}^{A} + \omega_{bA}^{A} = C_b^A \omega_{ib}^{b} + \omega_{bA}^{A} = R_3(\psi_o)\omega_{ib}^{b} + \omega_{bA}^{A} = R_3(\psi_o)\begin{bmatrix} p \\ q \\ r \end{bmatrix} + \begin{bmatrix} 0 \\ 0 \\ \dot{\psi}_o \end{bmatrix}. \tag{2.7}$$

Components of d_A are given by

$$d_A = \begin{bmatrix} p_A \\ q_A \\ r_A \end{bmatrix} = \begin{bmatrix} p\cos\psi_o + q\sin\psi_o \\ q\cos\psi_o - p\sin\psi_o \\ \dot{\psi}_o + r \end{bmatrix}. \tag{2.8}$$

If a *virtual* 3-axis rate gyro was mounted on the axis of rotation of the outer azimuth frame, it would measure d_A.

2.4.2 Outer Elevation Frame Kinematics

The angular rates of the outer elevation frame with respect to the inertial frame as resolved in the outer elevation frame is given by

$$d_E \triangleq \omega_{iE}^{E} = \omega_{iA}^{E} + \omega_{AE}^{E} = C_A^E \omega_{iA}^{A} + \omega_{AE}^{E} = R_2(\theta_o) d_A + \begin{bmatrix} 0 \\ \dot{\theta}_o \\ 0 \end{bmatrix}. \tag{2.9}$$

Components of d_E are given by

$$d_E = \begin{bmatrix} p_E \\ q_E \\ r_E \end{bmatrix} = \begin{bmatrix} p_A \cos\theta_o - r_A \sin\theta_o \\ q_A + \dot{\theta}_o \\ p_A \sin\theta_o + r_A \cos\theta_o \end{bmatrix} = \begin{bmatrix} (p\cos\psi_o + q\sin\psi_o)\cos\theta_o - (\dot{\psi}_o + r)\sin\theta_o \\ q\cos\psi_o - p\sin\psi_o + \dot{\theta}_o \\ (p\cos\psi_o + q\sin\psi_o)\sin\theta_o + (\dot{\psi}_o + r)\cos\theta_o \end{bmatrix}. \tag{2.10}$$

If a *virtual* 3-axis rate gyro was mounted on the axis of rotation of the outer elevation axis, it would measure d_E.

2.4.3 Inner Elevation Frame Kinematics

The angular rates of the inner elevation frame with respect to the inertial frame as resolved in the inner elevation frame is given by

$$d_e \triangleq \omega_{ie}^e = \omega_{iE}^e + \omega_{Ee}^e = C_E^e \omega_{iE}^E + \omega_{Ee}^e = R_2(\theta_i) d_E + \begin{bmatrix} 0 \\ \dot{\theta}_i \\ 0 \end{bmatrix}. \tag{2.11}$$

Components of d_e are given by

$$d_e = \begin{bmatrix} p_e \\ q_e \\ r_e \end{bmatrix} = \begin{bmatrix} p_E \cos\theta_i - r_E \sin\theta_i \\ q_E + \dot{\theta}_i \\ p_E \sin\theta_i + r_E \cos\theta_i \end{bmatrix} = \begin{bmatrix} (p\cos\psi_o + q\sin\psi_o)\cos(\theta_o + \theta_i) - (\dot{\psi}_o + r)\sin(\theta_o + \theta_i) \\ q\cos\psi_o - p\sin\psi_o + \dot{\theta}_o + \dot{\theta}_i \\ (p\cos\psi_o + q\sin\psi_o)\sin(\theta_o + \theta_i) + (\dot{\psi}_o + r)\cos(\theta_o + \theta_i) \end{bmatrix}. \tag{2.12}$$

If a *virtual* 3-axis rate gyro was mounted on the axis of rotation of the inner elevation frame, it would measure d_e.

2.4.4 Inner Azimuth Frame Kinematics

The angular rates of the inner azimuth frame with respect to the inertial frame as resolved in the inner azimuth frame is given by

$$\omega_{ia}^a = \omega_{ie}^a + \omega_{ea}^a = C_e^a \omega_{ie}^e + \omega_{ea}^a = R_3(\psi_i) d_e + \begin{bmatrix} 0 \\ 0 \\ \dot{\psi}_i \end{bmatrix}. \tag{2.13}$$

Components of ω_{ia}^{a} are given by

$$\omega_{ia}^{a} = \begin{bmatrix} w_x \\ w_y \\ w_z \end{bmatrix} = \begin{bmatrix} p_e \cos\psi_i + q_e \sin\psi_i \\ q_e \cos\psi_i - p_e \sin\psi_i \\ r_e + \dot{\psi}_i \end{bmatrix} \tag{2.14}$$

$$= \begin{bmatrix} (p\cos\psi_o + q\sin\psi_o)\cos(\theta_o+\theta_i)\cos\psi_i - (\dot{\psi}_o + r)\sin(\theta_o+\theta_i)\cos\psi_i + (q\cos\psi_o - p\sin\psi_o + \dot{\theta}_o + \dot{\theta}_i)\sin\psi_i \\ (q\cos\psi_o - p\sin\psi_o + \dot{\theta}_o + \dot{\theta}_i)\cos\psi_i - (p\cos\psi_o + q\sin\psi_o)\cos(\theta_o+\theta_i)\sin\psi_i + (\dot{\psi}_o + r)\sin(\theta_o+\theta_i)\sin\psi_i \\ (p\cos\psi_o + q\sin\psi_o)\sin(\theta_o+\theta_i) + (\dot{\psi}_o + r)\cos(\theta_o+\theta_i) + \dot{\psi}_i \end{bmatrix}. \tag{2.15}$$

and are measured by an *actual 3-axis rate gyro* that is mounted on the axis of rotation of the inner azimuth frame.

2.5 Dynamic Analysis of Four-Axis Gimbal Platform

Before dealing with creating the detailed kinematic and dynamic equations of the four axis gimbal platform, the system was first thought to be making linear motion in order to better understand the system. In this direction, analysis is made, and the obtained linear motion equations are converted into rotational motion equations and integrated into the four axis gimbal platform dynamical model.

2.5.1 Analysis of a Two Block System

Two blocks with masses m_1 and m_2 are placed on a surface, as shown in Fig 2.5. The friction coefficient between the ground and the block with mass m_1 of these two blocks is b_1; the friction coefficient between the block with mass m_1 and block with mass m_2 is b_2. The forces applied to blocks with masses m_1 and m_2 are F_1 and F_2, respectively. The reaction of the block with mass m_1 against the F_1 force applied to the block with mass m_1 will be in the opposite direction $b_1\dot{x}_1$. Similarly, in response to the F_2 force applied to the block with mass m_2, the response of the block with mass m_2 is in the opposite direction $b_2(\dot{x}_2 - \dot{x}_1)$, and its reaction is observed from over the *relative velocity*. Furthermore, the applied force F_2 will have a reaction on the block with mass m_1 as shown in Fig 2.5. All force responses are shown in accordance with Newton's laws. [10]

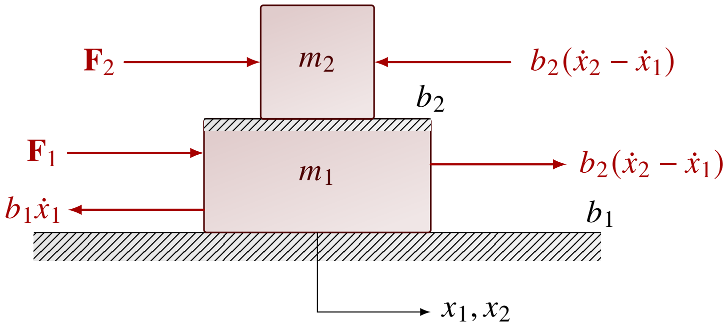

Figure 2.5: Dynamical analysis of a two block system.

The force equations of the system given in Fig 2.5 are expressed in Equation 2.16 below.

$$\begin{aligned} m_1\ddot{x}_1 &= F_1 - b_1\dot{x}_1 + b_2(\dot{x}_2 - \dot{x}_1) \\ m_2\ddot{x}_2 &= F_2 - b_2(\dot{x}_2 - \dot{x}_1) \end{aligned} \tag{2.16}$$

Decoupled System: If there is no friction between the two blocks. In other words, if $b_2 = 0$, these two equations become independent of each other as shown in Equation 2.17. Hence, they become decoupled.

$$\begin{aligned} m_1\ddot{x}_1 &= F_1 - b_1\dot{x}_1 \\ m_2\ddot{x}_2 &= F_2 \end{aligned} \tag{2.17}$$

Coupled System: If the friction between the two blocks is not zero, it is easier to explain the dynamics in terms of the relative positions. These equations become dependent of each other as shown in Equation 2.18. Hence, they become coupled.

$$\begin{aligned} m_1\ddot{x}_1 &= F_1 - b_1\dot{x}_1 + b_2(\dot{x}_2 - \dot{x}_1) \\ m_2(\ddot{x}_2 - \ddot{x}_1) &= F_2 - b_2(\dot{x}_2 - \dot{x}_1) - m_2\ddot{x}_1 \end{aligned} \tag{2.18}$$

So by setting,

$$
\begin{aligned}
q_1 &= x_1 \\
\dot{q}_1 &= \dot{x}_1 \\
\ddot{q}_1 &= \ddot{x}_1 \\
q_2 &= x_2 - x_1 \\
\dot{q}_2 &= \dot{x}_2 - \dot{x}_1 \\
\ddot{q}_2 &= \ddot{x}_2 - \ddot{x}_1
\end{aligned}
$$

The parameters are set as described above, and Equation 2.19 expresses the final form of linear force equations.

$$
\begin{aligned}
m_1\ddot{q}_1 &= F_1 - b_1\dot{q}_1 + b_2\dot{q}_2 \\
m_2\ddot{q}_2 &= F_2 - b_2\dot{q}_2 - m_2\ddot{q}_1
\end{aligned}
\tag{2.19}
$$

Furthermore, the linear force equations derived in Equation 2.19 have been verified under various conditions and are shown below.

- $b_1 = 0$, $b_2 = 0$ and $F_1 = 0$

$$
\left.
\begin{aligned}
m_1\ddot{q}_1 &= 0 \\
m_2\ddot{q}_2 &= F_2 - m_2\ddot{q}_1
\end{aligned}
\right\}
\begin{aligned}
\ddot{q}_1 = 0 \Rightarrow \dot{q}_1 = 0 \Rightarrow \dot{x}_1 = 0 \Rightarrow \dot{q}_2 = \dot{x}_2 \\
\ddot{x}_1 = 0 \Rightarrow \ddot{q}_2 = \ddot{x}_2 \\
\ddot{q}_2 = \frac{1}{m_2}F_2 \Rightarrow \ddot{x}_2 = \frac{1}{m_2}F_2
\end{aligned}
\tag{2.20}
$$

- $b_1 = 0$, $b_2 = 0$ and $F_2 = 0$

$$
\left.
\begin{aligned}
m_1\ddot{q}_1 &= F_1 \\
m_2\ddot{q}_2 &= -m_2\ddot{q}_1
\end{aligned}
\right\}
\begin{aligned}
\ddot{q}_1 = \frac{1}{m_1}F_1 \Rightarrow \ddot{x}_1 = \frac{1}{m_1}F_1 \\
\ddot{q}_2 = -\ddot{q}_1 \Rightarrow \ddot{x}_2 - \ddot{x}_1 = -\ddot{x}_1 \\
\ddot{x}_2 = 0
\end{aligned}
\tag{2.21}
$$

- $b_1 = 0$, $b_2 \to \infty \Rightarrow \dot{q}_2 = \ddot{q}_2 = 0$ and $F_2 = 0$

$$
\left.
\begin{aligned}
m_1\ddot{q}_1 &= F_1 \\
0 &= F_2 - m_2\ddot{q}_1
\end{aligned}
\right\}
\begin{aligned}
\ddot{q}_1(m_1 + m_2) = F_1 + F_2 \\
\ddot{q}_1 = \frac{1}{m_1 + m_2}(F_1 + F_2) \xrightarrow[F_2=0]{\ddot{q}_1=\ddot{x}_1} \ddot{x}_1 = \frac{1}{m_1 + m_2}F_1 \qquad \ddot{x}_2 = \ddot{x}_1
\end{aligned}
\tag{2.22}
$$

- $b_1 = 0$, $b_2 \to \infty \Rightarrow \dot{q}_2 = \ddot{q}_2 = 0$ and $F_1 = 0$

$$
\left.
\begin{aligned}
m_1\ddot{q}_1 &= F_1 \\
0 &= F_2 - m_2\ddot{q}_1
\end{aligned}
\right\}
\begin{aligned}
\ddot{q}_1(m_1 + m_2) = F_1 + F_2 \\
\ddot{q}_1 = \frac{1}{m_1 + m_2}(F_1 + F_2) \xrightarrow[F_1=0]{\ddot{q}_1=\ddot{x}_1} \ddot{x}_1 = \frac{1}{m_1 + m_2}F_2 \qquad \ddot{x}_2 = \ddot{x}_1
\end{aligned}
\tag{2.23}
$$

The physical variables of the coupled linear motion equations obtained in Equation 2.19 are converted, by analogy, to the rotational motion parameters for the four-axis gimbal model, as shown in Table 2.2 below.

Table 2.2: Conversion of physical variables from linear to rotational motion.

Linear Motion		Rotational Motion for Couple EL-el Frames	
Physical Variables		Physical Variables	
Quantity	Symbol	Quantity	Symbol
Mass of block 1	m_1	Inertia of the outer elevation frame	J_E
Mass of block 2	m_2	Inertia of the inner elevation frame	J_e
Force applied to block 1	F_1	Torque applied to the outer elevation frame	τ_E
Force applied to block 2	F_2	Torque applied to the inner elevation frame	τ_e
Friction between ground and mass 1	b_1	Friction between outer azimuth and outer elevation frames	b_E
Friction between mass 1 and mass 2	b_2	Friction between outer elevation and inner elevation frames	b_e
Velocity and acceleration of block 1	$\dot{q}_1, \ddot{q}_1$	Angular vel. and acc. of the outer elevation frame	$\dot{\theta}_o, \ddot{\theta}_o$
Velocity and acceleration of block 2	$\dot{q}_2, \ddot{q}_2$	Angular vel. and acc. of the inner elevation frame	$\dot{\theta}_i, \ddot{\theta}_i$

The Equation 2.24 is obtained after applying the variable transformations to the Equation 2.19, as shown in table.

$$
\begin{aligned}
J_E\ddot{\theta}_o &= \tau_E - b_E\dot{\theta}_o + b_e\dot{\theta}_i \\
J_e\ddot{\theta}_i &= \tau_e - b_e\dot{\theta}_i - J_e\ddot{\theta}_o
\end{aligned}
\tag{2.24}
$$

The two equations mentioned before are significant because they explain the coupled condition between the outer and inner elevation frames. In Equation 2.24, the coupled rotational motion equations that we will use in the outer elevation and inner elevation dynamic block diagrams of the four axis gimbal platform are obtained. Based on these equations, the dynamic models are created.

Table 2.3: Conversion of physical variables from linear to rotational motion.

Linear Motion		Rotational Motion for Decoupled AZ-az Frames	
Physical Variables		Physical Variables	
Quantity	Symbol	Quantity	Symbol
Mass of block 1 and 2	m_1, m_2	Inertia of the outer and inner azimuth frame	J_A, J_a
Force applied to block 1 and 2	F_1, F_2	Torque applied to the outer and inner azimuth frame	τ_A, τ_a
Friction between ground and mass 1	b_1	Friction between base and outer azimuth frame	b_A
Friction between mass 1 and mass 2	b_2	Friction between inner elevation and inner azimuth frames	b_a
Velocity and acceleration of block 1 and 2	$\dot{x}_1, \ddot{x}_1, \dot{x}_2, \ddot{\psi}_i$	Angular vel. and acc. of the outer and inner azimuth frame	$\dot{\psi}_o, \ddot{\psi}_o, \dot{\psi}_i$,$\ddot{\psi}_i$

The physical variables of the decoupled linear motion equations obtained in Equation 2.17 are converted to the rotational motion physical variables for the four-axis gimbal model, as shown in Table 2.3 above.

Equation 2.25 is obtained after applying the variable transformations to Equation 2.17, as shown in table.

$$
\begin{aligned}
J_A\ddot{\psi}_o &= \tau_A - b_A\dot{\psi}_o \\
J_a\ddot{\psi}_i &= \tau_a
\end{aligned}
\tag{2.25}
$$

In Equation 2.25, the decoupled rotational motion equations that we will use in the outer azimuth and inner azimuth dynamic block diagrams of the four axis gimbal platform are obtained. Based on these equations, the dynamic models are created.

2.6 Dynamic Equations of 4-Axis Gimbal Platform

In this section, first, the dynamics and kinematics of the four-axis gimbal modelare combined and dynamic block diagrams are created for each axis, and then the dynamic equations are shown in detail. According to this model, the gimbal is perfectly balanced and rigid, spring effects are insignificant, and the motor dynamics are rapid enough to be ignored [9, 11].

2.6.1 Outer Azimuth Frame Dynamics

A block diagram of the outer azimuth frame dynamical model is given in Fig 2.6. The block diagram shows, J_A represents the outer azimuth frame inertia, b_A stands for the viscous friction constant, and τ_A is the torque exerted by the outer azimuth motor.

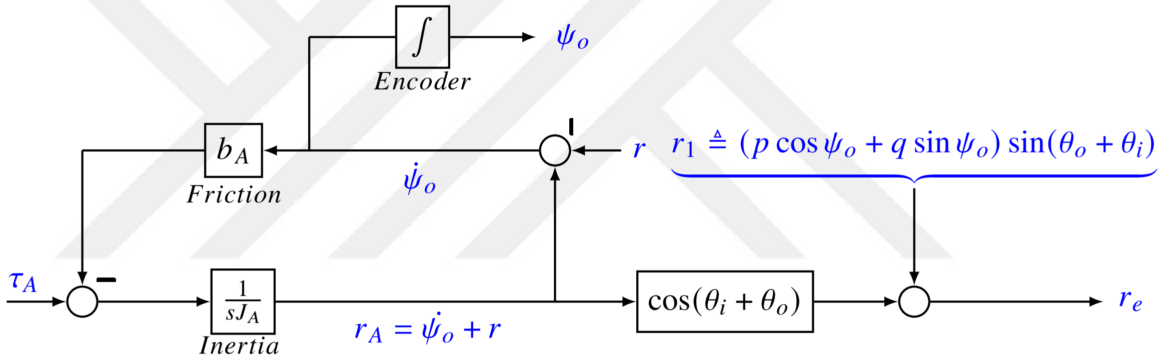

Figure 2.6: Outer azimuth frame dynamical model.

$\dot{\psi}_o$ can be obtained from Line 3 of Equation 2.8 as

$$\dot{\psi}_o = r_A - r \tag{2.26}$$

$\dot{r}_A$ can be obtained from outer azimuth frame dynamical model in Fig 2.6.

$$\begin{aligned} \dot{r}_A &= (\tau_A - b_A\dot{\psi}_o)\frac{1}{J_A} \\ &= \frac{1}{J_A}\tau_A - \frac{b_A}{J_A}r_A + \frac{b_A}{J_A}r \end{aligned} \tag{2.27}$$

r_e can be obtained from Line 3 of Equation 2.12 as

$$r_e = (p\cos\psi_o + q\sin\psi_o)\sin(\theta_o + \theta_i) + (\dot{\psi}_o + r)\cos(\theta_o + \theta_i) \tag{2.28}$$

2.6.2 Inner Azimuth Frame Dynamics

A block diagram of the inner azimuth frame dynamics are given in Fig 2.7. In the block diagram, J_a denotes the inner azimuth frame inertia. b_a denotes the viscous friction constants, and τ_a is the applied torque by the inner azimuth frame motor.

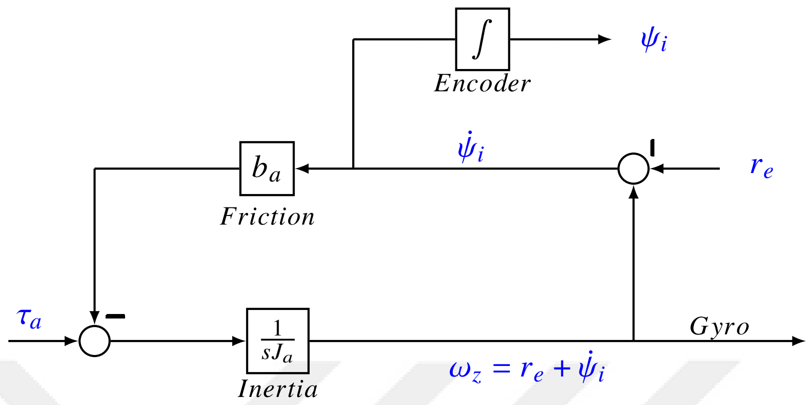

Figure 2.7: Inner azimuth frame dynamical model.

$\dot{\psi}_i$ can be obtained from Line 3 of 2.15 as

$$\begin{aligned}\dot{\psi}_i &= \omega_z - r_e \\ &= \omega_z - p\cos\psi_o\sin(\theta_o+\theta_i) - q\sin\psi_o\sin(\theta_o+\theta_i) - r_A\cos(\theta_o+\theta_i)\end{aligned} \tag{2.29}$$

$\dot{\omega}_z$ can be obtained from inner azimuth frame dynamical model in Figure 2.7.

$$\begin{aligned}\dot{\omega}_z &= (\tau_a - b_a\dot{\psi}_i)\frac{1}{J_a} \\ &= \frac{1}{J_a}\tau_a - \frac{b_a}{J_a}\omega_z + \frac{b_a\cos(\theta_o+\theta_i)}{J_a}r_A + \frac{b_a\sin(\theta_o+\theta_i)\cos\psi_o}{J_a}p + \frac{b_a\sin(\theta_o+\theta_i)\sin\psi_o}{J_a}q\end{aligned} \tag{2.30}$$

2.6.3 Outer and Inner Elevation Frame Dynamics

A block diagram of the outer and inner elevation frame dynamics are given in Fig 2.8. In the block diagram, J_E and J_e denote the outer elevation frame inertia and the inner elevation frame inertia, respectively. b_E and b_e denote the viscous friction constants. τ_E and τ_e are the applied torque by the outer elevation frame motor and the inner elevation frame motor, respectively.

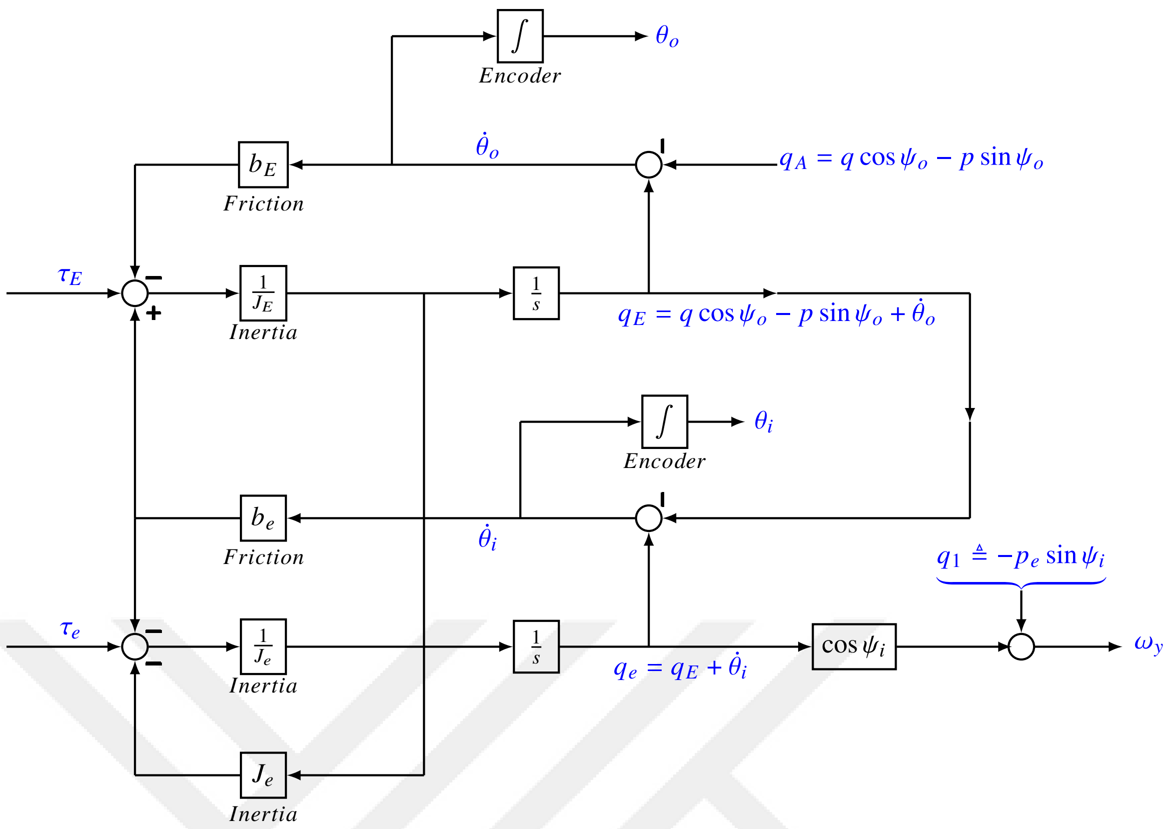

Figure 2.8: Outer and inner elevation frame dynamical models.

$\dot{\theta}_o$ can be obtained from Line 2 of Equation 2.10 as

$$\begin{aligned}\dot{\theta}_o &= q_E - q_A \\ &= q_E + p\sin\psi_o - q\cos\psi_o.\end{aligned} \tag{2.31}$$

and, $\dot{\theta}_i$ can be obtained from Line 2 of Equation 2.12 as

$$\dot{\theta}_i = q_e - q_E. \tag{2.32}$$

$\dot{q}_E$ and $\dot{q}_e$ can be obtained from outer and inner elevation frame dynamical models in Fig 2.8 as

$$\begin{aligned}\dot{q}_E &= (\tau_E - b_E\dot{\theta}_o + b_e\dot{\theta}_i)\frac{1}{J_E} \\ &= \frac{1}{J_E}\tau_E + \left(\frac{-b_E}{J_E} + \frac{-b_e}{J_E}\right)q_E + \frac{b_e}{J_E}q_e + \frac{-b_E\sin\psi_o}{J_E}p + \frac{b_E\cos\psi_o}{J_E}q\end{aligned} \tag{2.33}$$

$$\dot{q}_e = (\tau_e - b_e\dot{\theta}_i - J_e\dot{q}_E)\frac{1}{J_e}$$
$$= \frac{1}{J_e}\tau_e + \frac{-1}{J_E}\tau_E + \left(\frac{b_e}{J_e} + \frac{b_E}{J_E} + \frac{b_e}{J_E}\right)q_E + \left(\frac{-b_e}{J_e} + \frac{-b_e}{J_E}\right)q_e + \frac{b_E\sin\psi_o}{J_E}p + \frac{-b_E\cos\psi_o}{J_E}q. \quad (2.34)$$

ω_y can be obtained from Line 2 of Equation 2.15 as

$$\omega_y = q_e\cos\psi_i - p_e\sin\psi_i$$
$$= q_e\cos\psi_i - \sin\psi_i(p\cos\psi_o + q\sin\psi_o)\cos(\theta_o + \theta_i) + r_A\sin\psi_i\sin(\theta_o + \theta_i). \quad (2.35)$$

2.6.4 Four Axis Gimbal Platform Dynamical Model

In order to demonstrate the effects of kinematic and dynamic equations, the full dynamic model of the four axes is schematized in Fig 2.9. Thus, system inputs, outputs, system disturbances, and inner-frame coupling and decoupling situations have became clear. The effect of the output of the outer azimuth frame to the inner azimuth frame as a disturbance and the effect of the output of the outer elevation frame to the inner elevation frame as a disturbance are observed.

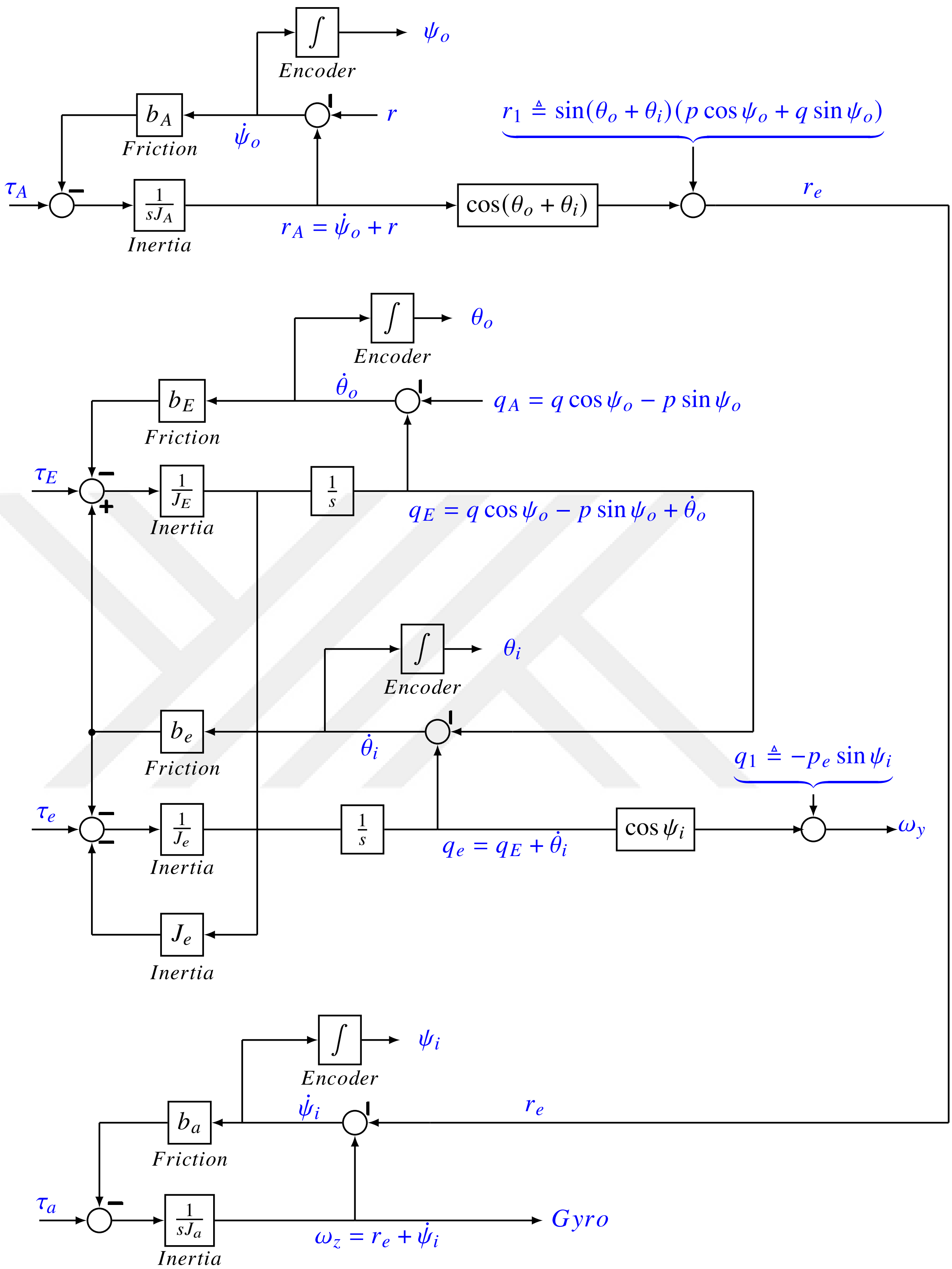

Figure 2.9: Four Axis Gimbal Platform Dynamical Model(AZ-EL-el-az).

2.7 State Space Representation of Four Axis Gimbal Platform

When the four axis gimbal model is considered, it can be seen that it is a multiple-input, multiple-output (MIMO) and non-linear system. In the case of MIMO systems, as an alternative to the classical control theory, modern control theory has an important role in the implement of high-order controller design strategies such as H_∞, linear quadratic gaussian (LQG) and linear quadratic regulator (LQR) in state space. This section examines the four axis gimbal system's state space representations before moving on to the control design studies. The four axis gimbal system's state and output equations have been generated using the system's kinematics and dynamics. All of the equations derived from system kinematics and dynamics and used in state and the output equations are detailed below.

Equation 2.36 are written from the four axis gimbal system's kinematic equations. (From Equation 2.8, Equation 2.10, Equation 2.12, Equation 2.15 respectively.)

$$\begin{aligned}
\dot{\psi}_o &= r_A - r \\
\dot{\theta}_o &= q_E + p \sin\psi_o - q \cos\psi_o \\
\dot{\theta}_i &= q_e - q_E \\
\dot{\psi}_i &= \omega_z - p \cos\psi_o \sin(\theta_o + \theta_i) - q \sin\psi_o \sin(\theta_o + \theta_i) - r_A \cos(\theta_o + \theta_i)
\end{aligned} \tag{2.36}$$

Equation 2.37 are written from the four axis gimbal system's dynamic equations. (From Equation 2.27, Equation 2.33, Equation 2.34 respectively.)

$$\begin{aligned}
\dot{r}_A &= (\tau_A - b_A\dot{\psi}_o)\frac{1}{J_A} \\
&= \frac{1}{J_A}\tau_A - \frac{b_A}{J_A}r_A + \frac{b_A}{J_A}r \\
\dot{q}_E &= (\tau_E - b_E\dot{\theta}_o + b_e\dot{\theta}_i)\frac{1}{J_E} \\
&= \left(\frac{1}{J_E}\right)\tau_E + \left(\frac{-b_E}{J_E} + \frac{-b_e}{J_E}\right)q_E + \left(\frac{b_e}{J_E}\right)q_e + \left(\frac{-b_E \sin\psi_o}{J_E}\right)p + \left(\frac{b_E \cos\psi_o}{J_E}\right)q \\
\dot{q}_e &= (\tau_e - b_e\dot{\theta}_i - J_e\dot{q}_E)\frac{1}{J_e} \\
&= \left(\frac{1}{J_e}\right)\tau_e + \left(\frac{-1}{J_E}\right)\tau_E + \left(\frac{b_e}{J_e} + \frac{b_E}{J_E} + \frac{b_e}{J_E}\right)q_E + \left(\frac{-b_e}{J_e} + \frac{-b_e}{J_E}\right)q_e + \left(\frac{b_E \sin\psi_o}{J_E}\right)p + \left(\frac{-b_E \cos\psi_o}{J_E}\right)q
\end{aligned} \tag{2.37}$$

Equation 2.38 are written from the four axis gimbal system's dynamic equations. (From Equation 2.30, Equation 2.35 respectively.)

$$
\begin{aligned}
\dot{\omega}_z &= (\tau_a - b_a\dot{\psi}_i)\frac{1}{J_a} \\
&= \frac{1}{J_a}\tau_a - \frac{b_a}{J_a}\omega_z + p\left(\frac{b_a}{J_a}\cos\psi_o\sin(\theta_o+\theta_i)\right) + q\left(\frac{b_a}{J_a}\sin\psi_o\sin(\theta_o+\theta_i)\right) + r_A\left(\frac{b_a}{J_a}\cos(\theta_o+\theta_i)\right) \\
\omega_y &= q_e\cos\psi_i - p_e\sin\psi_i \\
&= q_e\cos\psi_i - \sin\psi_i(p\cos\psi_o + q\sin\psi_o)\cos(\theta_o+\theta_i) + r_A\sin\psi_i\sin(\theta_o+\theta_i)
\end{aligned}
\tag{2.38}
$$

State variables are crucial in describing the system's behavior. Hence, the state variables of the four axis gimbal model are chosen as the outer azimuth angular position (ψ_o), the outer elevation angular position (θ_o), the inner elevation angular position (θ_i), and the inner azimuth angular position (ψ_i), respectively. Also, chosen state variables are r_A, q_E, and q_e measured from *virtual* gyros in outer azimuth, outer elevation, and inner elevation frames, respectively and ω_z angular velocity terms measured from inner azimuth gyro.

Output variables must be chosen as measurable quantities, but state variables are not required to be measurable. Therefore, the output variables are selected as the angular positions (ψ_o, θ_o, θ_i, ψ_i) measured by encoders on each axis and velocity responses (ω_y and ω_z) measured by the gyroscope in the inner azimuth frame. Motor torques refer to the control input variables (τ_A, τ_E, τ_e, τ_a). p, q and r are the platform motion's body *roll*, *pitch*, *yaw* rates, which are used to describe disturbance effects on the system.

The four axis gimbal system's nonlinear state space representation is in the following form:

$$
\begin{aligned}
\dot{x}(t) &= f(x(t), u(t), w(t)) \qquad x(0) = x_o \\
y(t) &= g(x(t), u(t), w(t))
\end{aligned}
\tag{2.39}
$$

$x(t) \in \mathbb{R}^n$; $x_o \in \mathbb{R}^n$; $u(t) \in \mathbb{R}^m$; $y(t) \in \mathbb{R}^p$; $f(x(t), u(t), w(t)) \in \mathbb{R}^n$; $g(x(t), u(t), w(t)) \in \mathbb{R}^p$; where the disturbance vector, the control input vector and the state vector, denoting platform motion applied to gimbal base, is represented by the symbols $w(t)$, $u(t)$, and $x(t)$, respectively. $f(x(t), u(t), w(t))$ is the state equation consisting of dynamic and kinematic equations of the four axis gimbal system. $\dot{x}(t)$ is the first order derivative of the state vector, $y(t)$ is the output vector, $g(x(t), u(t), w(t))$ is the output equation which indicate the system responses.

2.8 Linearization

State space representation of a linear time invariant (LTI) system is:

$$\begin{aligned} \dot{x}(t) &= Ax(t) + Bu(t) + Ew(t) \qquad x(0) = x_o \\ y(t) &= Cx(t) + Du(t) + Fw(t) \end{aligned} \tag{2.40}$$

where $\dot{x}$ is differential state vector, x is state vector, u is control input vector, y is output vector, w is disturbance input vector, A is state matrix, B is control input matrix, C is output matrix, D is feed-forward matrix, E is disturbance state matrix, F is disturbance output matrix.

State equation of the LTI system is written by Jacobian linearization method as follows:

$$\dot{\delta}_x(t) = A\delta_x(t) + B\delta_u(t) + E\delta_w(t) \qquad \delta_x(0) = \delta_{xo}$$

where A is the state matrix, B is the control input matrix, and E is the disturbance state matrix.

$$A = \left.\frac{\partial f}{\partial x}\right|_{x_e,u_e,w_e} = \begin{bmatrix} \frac{\partial f_1}{\partial x_1} & \frac{\partial f_1}{\partial x_2} & \cdots & \frac{\partial f_1}{\partial x_n} \\ \frac{\partial f_2}{\partial x_1} & \frac{\partial f_2}{\partial x_2} & \cdots & \frac{\partial f_2}{\partial x_n} \\ \vdots & \vdots & \ddots & \vdots \\ \frac{\partial f_n}{\partial x_1} & \frac{\partial f_n}{\partial x_2} & \cdots & \frac{\partial f_n}{\partial x_n} \end{bmatrix}_{(x_e,u_e,w_e)}$$

$$B = \left.\frac{\partial f}{\partial u}\right|_{x_e,u_e,w_e} = \begin{bmatrix} \frac{\partial f_1}{\partial u_1} & \frac{\partial f_1}{\partial u_2} & \cdots & \frac{\partial f_1}{\partial u_m} \\ \frac{\partial f_2}{\partial u_1} & \frac{\partial f_2}{\partial u_2} & \cdots & \frac{\partial f_2}{\partial u_m} \\ \vdots & \vdots & \ddots & \vdots \\ \frac{\partial f_n}{\partial u_1} & \frac{\partial f_n}{\partial u_2} & \cdots & \frac{\partial f_n}{\partial u_m} \end{bmatrix}_{(x_e,u_e,w_e)}$$

$$E = \left.\frac{\partial f}{\partial w}\right|_{x_e,u_e,w_e} = \begin{bmatrix} \frac{\partial f_1}{\partial w_1} & \frac{\partial f_1}{\partial w_2} & \cdots & \frac{\partial f_1}{\partial w_k} \\ \frac{\partial f_2}{\partial w_1} & \frac{\partial f_2}{\partial w_2} & \cdots & \frac{\partial f_2}{\partial w_k} \\ \vdots & \vdots & \ddots & \vdots \\ \frac{\partial f_n}{\partial w_1} & \frac{\partial f_n}{\partial w_2} & \cdots & \frac{\partial f_n}{\partial w_k} \end{bmatrix}_{(x_e,u_e,w_e)}$$

where n is the number of the state variables, m is the number of the control input variables and k is the number of the disturbance input variables.

The output equation is also linearized using the Jacobian method, as shown below:

$$\dot{\delta}_y(t) = C\delta_x(t) + D\delta_u(t) + F\delta_w(t)$$

where C is the output matrix, D is the feed forward matrix, F is the disturbance output matrix

$$C = \left.\frac{\partial g}{\partial x}\right|_{x_e,u_e,w_e} = \begin{bmatrix} \frac{\partial g_1}{\partial x_1} & \frac{\partial g_1}{\partial x_2} & \cdots & \frac{\partial g_1}{\partial x_n} \\ \frac{\partial g_2}{\partial x_1} & \frac{\partial g_2}{\partial x_2} & \cdots & \frac{\partial g_2}{\partial x_n} \\ \vdots & \vdots & \ddots & \vdots \\ \frac{\partial g_p}{\partial x_1} & \frac{\partial g_p}{\partial x_2} & \cdots & \frac{\partial g_p}{\partial x_n} \end{bmatrix}_{(x_e,u_e,w_e)}$$

$$D = \left.\frac{\partial g}{\partial u}\right|_{x_e,u_e,w_e} = \begin{bmatrix} \frac{\partial g_1}{\partial u_1} & \frac{\partial g_1}{\partial u_2} & \cdots & \frac{\partial g_1}{\partial u_m} \\ \frac{\partial g_2}{\partial u_1} & \frac{\partial g_2}{\partial u_2} & \cdots & \frac{\partial g_2}{\partial u_m} \\ \vdots & \vdots & \ddots & \vdots \\ \frac{\partial g_p}{\partial u_1} & \frac{\partial g_p}{\partial u_2} & \cdots & \frac{\partial g_p}{\partial u_m} \end{bmatrix}_{(x_e,u_e,w_e)}$$

$$F = \left.\frac{\partial g}{\partial w}\right|_{x_e,u_e,w_e} = \begin{bmatrix} \frac{\partial g_1}{\partial w_1} & \frac{\partial g_1}{\partial w_2} & \cdots & \frac{\partial g_1}{\partial w_k} \\ \frac{\partial g_2}{\partial w_1} & \frac{\partial g_2}{\partial w_2} & \cdots & \frac{\partial g_2}{\partial w_k} \\ \vdots & \vdots & \ddots & \vdots \\ \frac{\partial g_p}{\partial w_1} & \frac{\partial g_p}{\partial w_2} & \cdots & \frac{\partial g_p}{\partial w_k} \end{bmatrix}_{(x_e,u_e,w_e)}$$

where p is the number of output variables, n is the number of state variables, m is the number of control input variables, k is the number of disturbance input variables.

There are eight states, four control inputs, three disturbances and six outputs for the four axis gimbal model. The state vector contains the four angular positions measured in the outer azimuth (ψ_o), outer elevation (θ_o), inner elevation (θ_i), and inner azimuth (ψ_i) frames, as well as the relative angular velocities read from the virtual gyroscopes at the outer azimuth (r_A), outer elevation (q_E), and inner elevation (q_e) frames. It also includes the gyroscope's relative angular velocity in the inner azimuth (ω_z) frame. Control input vector involves four motor torques (τ_A, τ_E, τ_e, τ_a) and disturbance vector contains the p, q and r are the platform motion's body *roll*, *pitch*, *yaw* rates, which are used to describe disturbance effects on the system. Output vector includes four measurable angular positions (ψ_o, θ_o, θ_i, ψ_i) and two measurable relative angular velocities (ω_z, ω_y). The state vector, control input vector, disturbance input vector, and output vector are all shown below respectively.

$$
\begin{aligned}
x(t) &= \begin{bmatrix} \psi_o & \theta_o & \theta_i & \psi_i & r_A & q_E & q_e & \omega_z \end{bmatrix}^T \\
u(t) &= \begin{bmatrix} \tau_A & \tau_E & \tau_e & \tau_a \end{bmatrix}^T \\
w(t) &= \begin{bmatrix} p & q & r \end{bmatrix}^T \\
y(t) &= \begin{bmatrix} \psi_o & \theta_o & \theta_i & \psi_i & \omega_z & \omega_y \end{bmatrix}^T
\end{aligned}
$$

States are: $\psi_o, \theta_o, \theta_i, \psi_i, r_A, q_E, q_e, \omega_z$ Inputs are: $\tau_A, \tau_E, \tau_e, \tau_a, p, q, r$ Outputs are: $\psi_o, \theta_o, \theta_i, \psi_i, \omega_z, \omega_y$

State equation is given by

$$\begin{bmatrix} \dot{\psi}_o \\ \dot{\theta}_o \\ \dot{\theta}_i \\ \dot{\psi}_i \\ \dot{r}_A \\ \dot{q}_E \\ \dot{q}_e \\ \dot{\omega}_z \end{bmatrix} = \begin{bmatrix} 0 & 0 & 0 & 0 & 1 & 0 & 0 & 0 \\ p\cos\psi_o + q\sin\psi_o & 0 & 0 & 0 & 0 & 1 & 0 & 0 \\ 0 & 0 & 0 & 0 & 0 & -1 & 1 & 0 \\ p\sin(\theta_i+\theta_o)\sin\psi_o - q\sin(\theta_i+\theta_o)\cos\psi_o & r_A\sin(\theta_i+\theta_o) - p\cos(\theta_i+\theta_o)\cos\psi_o - q\cos(\theta_i+\theta_o)\sin\psi_o & r_A\sin(\theta_i+\theta_o) - p\cos(\theta_i+\theta_o)\cos\psi_o - q\cos(\theta_i+\theta_o)\sin\psi_o & 0 & -\cos(\theta_i+\theta_o) & 0 & 0 & 1 \\ 0 & 0 & 0 & 0 & -\frac{b_A}{J_A} & 0 & 0 & 0 \\ -\frac{b_E\,p\cos\psi_o}{J_E} - \frac{b_E\,q\sin\psi_o}{J_E} & 0 & 0 & 0 & 0 & -\frac{b_E}{J_E} - \frac{b_e}{J_E} & \frac{b_e}{J_E} & 0 \\ \frac{b_E\,p\cos\psi_o}{J_E} + \frac{b_E\,q\sin\psi_o}{J_E} & 0 & 0 & 0 & 0 & \frac{b_E}{J_E} + \frac{b_e}{J_E} + \frac{b_e}{J_e} & -\frac{b_e}{J_E} - \frac{b_e}{J_e} & 0 \\ \frac{b_a\,q\sin(\theta_i+\theta_o)\cos\psi_o}{J_a} - \frac{b_a\,p\sin(\theta_i+\theta_o)\sin\psi_o}{J_a} & \frac{b_a\,p\cos(\theta_i+\theta_o)\cos\psi_o}{J_a} - \frac{b_a\,r_A\sin(\theta_i+\theta_o)}{J_a} + \frac{b_a\,q\cos(\theta_i+\theta_o)\sin\psi_o}{J_a} & \frac{b_a\,p\cos(\theta_i+\theta_o)\cos\psi_o}{J_a} - \frac{b_a\,r_A\sin(\theta_i+\theta_o)}{J_a} + \frac{b_a\,q\cos(\theta_i+\theta_o)\sin\psi_o}{J_a} & 0 & \frac{b_a\cos(\theta_i+\theta_o)}{J_a} & 0 & 0 & -\frac{b_a}{J_a} \end{bmatrix} \begin{bmatrix} \psi_o \\ \theta_o \\ \theta_i \\ \psi_i \\ r_A \\ q_E \\ q_e \\ \omega_z \end{bmatrix}$$

$$+ \begin{bmatrix} 0 & 0 & 0 & 0 & 0 & 0 & -1 \\ 0 & 0 & 0 & 0 & \sin\psi_o & -\cos\psi_o & 0 \\ 0 & 0 & 0 & 0 & 0 & 0 & 0 \\ 0 & 0 & 0 & 0 & -\sin(\theta_i+\theta_o)\cos\psi_o & -\sin(\theta_i+\theta_o)\sin\psi_o & 0 \\ \frac{1}{J_A} & 0 & 0 & 0 & 0 & 0 & \frac{b_A}{J_A} \\ 0 & \frac{1}{J_E} & 0 & 0 & -\frac{b_E\sin\psi_o}{J_E} & \frac{b_E\cos\psi_o}{J_E} & 0 \\ 0 & -\frac{1}{J_E} & \frac{1}{J_e} & 0 & \frac{b_E\sin\psi_o}{J_E} & -\frac{b_E\cos\psi_o}{J_E} & 0 \\ 0 & 0 & 0 & \frac{1}{J_a} & \frac{b_a\sin(\theta_i+\theta_o)\cos\psi_o}{J_a} & \frac{b_a\sin(\theta_i+\theta_o)\sin\psi_o}{J_a} & 0 \end{bmatrix} \begin{bmatrix} \tau_A \\ \tau_E \\ \tau_e \\ \tau_a \\ p \\ q \\ r \end{bmatrix}$$

The output equation can be written as

$$
\begin{bmatrix} \psi_o \\ \theta_o \\ \theta_i \\ \psi_i \\ \omega_z \\ \omega_y \end{bmatrix}
=
\begin{bmatrix}
1 & 0 & 0 & 0 & 0 & 0 & 0 & 0 \\
0 & 1 & 0 & 0 & 0 & 0 & 0 & 0 \\
0 & 0 & 1 & 0 & 0 & 0 & 0 & 0 \\
0 & 0 & 0 & 1 & 0 & 0 & 0 & 0 \\
0 & 0 & 0 & 0 & 0 & 0 & 0 & 1 \\
-\cos(\theta_i+\theta_o)\sin\psi_i\,(q\cos\psi_o - p\sin\psi_o) & r_A\cos(\theta_i+\theta_o)\sin\psi_i + \sin(\theta_i+\theta_o)\sin\psi_i\,(p\cos\psi_o + q\sin\psi_o) & r_A\cos(\theta_i+\theta_o)\sin\psi_i + \sin(\theta_i+\theta_o)\sin\psi_i\,(p\cos\psi_o + q\sin\psi_o) & r_A\sin(\theta_i+\theta_o)\cos\psi_i - q_e\sin\psi_i - \cos(\theta_i+\theta_o)\cos\psi_i\,(p\cos\psi_o + q\sin\psi_o) & \sin(\theta_i+\theta_o)\sin\psi_i & 0 & \cos\psi_i & 0
\end{bmatrix}
\begin{bmatrix} \psi_o \\ \theta_o \\ \theta_i \\ \psi_i \\ r_A \\ q_E \\ q_e \\ \omega_z \end{bmatrix}
$$

$$
+
\begin{bmatrix}
0 & 0 & 0 & 0 & 0 & 0 & 0 \\
0 & 0 & 0 & 0 & 0 & 0 & 0 \\
0 & 0 & 0 & 0 & 0 & 0 & 0 \\
0 & 0 & 0 & 0 & 0 & 0 & 0 \\
0 & 0 & 0 & 0 & 0 & 0 & 0 \\
0 & 0 & 0 & 0 & -\cos(\theta_i+\theta_o)\cos\psi_o\sin\psi_i & -\cos(\theta_i+\theta_o)\sin\psi_i\sin\psi_o & 0
\end{bmatrix}
\begin{bmatrix} \tau_A \\ \tau_E \\ \tau_e \\ \tau_a \\ p \\ q \\ r \end{bmatrix}
$$

The four-axis gimbal system mechanical structure within the scope of this thesis was assumed to be a sphere made of the same material, with a radius of 25 cm, 24 cm, 23 cm and 22 cm, respectively, from the outside to the inside. Accordingly, the density values are integrated into the four axes. In addition, by considering that the outer azimuth, outer elevation and inner elevation axes are spheres(shell), and the inner azimuth axis is sphere(ball), inertia values are calculated accordingly and indicated in the table. Furthermore, friction values for each axis were included as one-tenth of the inertia values to the design processes.

Table 2.4: Parameter Description and Values.

Parameter	**Description**	**Value**
J_A	Outer azimuth frame inertia value	2.6180
J_E	Outer elevation frame inertia value	2.1346
J_e	Inner elevation frame inertia value	1.7255
J_a	Inner azimuth frame inertia value	0.9498
b_A	Friction between base and outer azimuth frame	0.2618
b_E	Friction between outer frame and outer elevation Frames	0.2135
b_e	Friction between outer elevation and inner elevation Frames	0.1725
b_a	Friction between inner elevation and inner azimuth Frames	0.0950
$\psi_o, \theta_o, \theta_i, \psi_i$	Gimbal angular position	0
r_A, q_e	Angular rates in outer azimuth and inner elevation	0
p, q	Disturbances from platform motion	0

Since the system has nonlinear equations, it was *linearized* around the values in the table. A state space model for the four axis gimbal system dynamics at the above condition is as follows.

$$\begin{aligned} \dot{x} &= Ax + Bu + Ew \\ y &= Cx + Du \end{aligned} \tag{2.41}$$

where

$$A=\begin{bmatrix}0&0&0&0&1&0&0&0\\0&0&0&0&0&1&0&0\\0&0&0&0&0&-1&1&0\\0&0&0&0&-1&0&0&1\\0&0&0&0&-0.1&0&0&0\\0&0&0&0&0&-0.1808&0.0808&0\\0&0&0&0&0&0.2808&-0.1808&0\\0&0&0&0&0.1&0&0&-0.1\end{bmatrix} \tag{2.42}$$

$$B=\begin{bmatrix}0&0&0&0&0&0&-1\\0&0&0&0&0&-1&0\\0&0&0&0&0&0&0\\0&0&0&0&0&0&0\\0.3820&0&0&0&0&0&0.1\\0&0.4685&0&0&0&0.1&0\\0&-0.4685&0.5796&0&0&-0.1&0\\0&0&0&1.0528&0&0&0\end{bmatrix} \tag{2.43}$$

$$C=\begin{bmatrix}1&0&0&0&0&0&0&0\\0&1&0&0&0&0&0&0\\0&0&1&0&0&0&0&0\\0&0&0&1&0&0&0&0\\0&0&0&0&0&0&0&1\\0&0&0&0&0&0&1&0\end{bmatrix} \qquad D=\begin{bmatrix}0&0&0&0&0&0&0\\0&0&0&0&0&0&0\\0&0&0&0&0&0&0\\0&0&0&0&0&0&0\\0&0&0&0&0&0&0\\0&0&0&0&0&0&0\end{bmatrix} \tag{2.44}$$

$$u=\begin{bmatrix}\tau_A - & \textit{Torque applied to the outer azimuth frame} & (N.m)\\ \tau_E - & \textit{Torque applied to the outer elevation frame} & (N.m)\\ \tau_e - & \textit{Torque applied to the inner elevation frame} & (N.m)\\ \tau_a - & \textit{Torque applied to the inner azimuth frame} & (N.m)\end{bmatrix} \tag{2.45}$$

$$w = \begin{bmatrix} p - & \textit{Disturbance from platform motion roll rates} & \textit{(rad/sec)} \\ q - & \textit{Disturbance from platform motion pitch rates} & \textit{(rad/sec)} \\ r - & \textit{Disturbance from platform motion yaw rates} & \textit{(rad/sec)} \end{bmatrix} \tag{2.46}$$

$$x = \begin{bmatrix} \psi_o - & \textit{Outer azimuth frame angular position} & \textit{(rad)} \\ \theta_o - & \textit{Outer elevation frame angular position} & \textit{(rad)} \\ \theta_i - & \textit{Inner elevation frame angular position} & \textit{(rad)} \\ \psi_i - & \textit{Inner azimuth frame angular position} & \textit{(rad)} \\ r_A - & \textit{Angular velocity from the virtual gyro at outer azimuth frame} & \textit{(rad/sec)} \\ q_E - & \textit{Angular velocity from the virtual gyro at outer elevation frame} & \textit{(rad/sec)} \\ q_e - & \textit{Angular velocity from the virtual gyro at inner azimuth frame} & \textit{(rad/sec)} \\ \omega_z - & \textit{Relative angular velocity in the inner azimuth frame} & \textit{(rad/sec)} \end{bmatrix} \tag{2.47}$$

$$y = \begin{bmatrix} \psi_o - & \textit{Outer azimuth frame angular position} & \textit{(rad)} \\ \theta_o - & \textit{Outer elevation frame angular position} & \textit{(rad)} \\ \theta_i - & \textit{Inner elevation frame angular position} & \textit{(rad)} \\ \psi_i - & \textit{Inner azimuth frame angular position} & \textit{(rad)} \\ \omega_z - & \textit{Relative angular velocity in the inner azimuth frame} & \textit{(rad/sec)} \\ \omega_y - & \textit{Relative angular velocity in the inner azimuth frame} & \textit{(rad/sec)} \end{bmatrix} \tag{2.48}$$

2.9 Transfer Function Matrix

The four axis gimbal system transfer function matrix from u to y is given by:

$$G(s) = C(sI - A)^{-1}B$$
$$= \begin{bmatrix} G_{\tau_A\psi_o} & G_{\tau_E\psi_o} & G_{\tau_e\psi_o} & G_{\tau_a\psi_o} \\ G_{\tau_A\theta_o} & G_{\tau_E\theta_o} & G_{\tau_e\theta_o} & G_{\tau_a\theta_o} \\ G_{\tau_A\theta_i} & G_{\tau_E\theta_i} & G_{\tau_e\theta_i} & G_{\tau_a\theta_i} \\ G_{\tau_A\psi_i} & G_{\tau_E\psi_i} & G_{\tau_e\psi_i} & G_{\tau_a\psi_i} \\ G_{\tau_A\omega_z} & G_{\tau_E\omega_z} & G_{\tau_e\omega_z} & G_{\tau_a\omega_z} \\ G_{\tau_A\omega_y} & G_{\tau_E\omega_y} & G_{\tau_e\omega_y} & G_{\tau_a\omega_y} \end{bmatrix} \tag{2.49}$$

where

$$G_{\tau_A\psi_o} = \frac{0.38197}{s(s+0.1)} \qquad G_{\tau_A\psi_i} = \frac{-0.38197s}{s(s+0.1)^2} \qquad G_{\tau_A\omega_z} = \frac{0.038197}{(s+0.1)^2} \tag{2.50}$$

$$\begin{aligned} G_{\tau_E\theta_o} &= \frac{0.46846(s+0.1)}{s(s+0.3315)(s+0.03017)} \\ G_{\tau_E\theta_i} &= \frac{-0.93693s}{s(s+0.3315)(s+0.03017)} \\ G_{\tau_E\omega_y} &= \frac{-0.46846(s-0.1)}{(s+0.3315)(s+0.03017)} \end{aligned} \tag{2.51}$$

$$\begin{aligned} G_{\tau_e\theta_o} &= \frac{0.046846}{s(s+0.3315)(s+0.03017)} \\ G_{\tau_e\theta_i} &= \frac{0.57955(s+0.1)}{s(s+0.3315)(s+0.03017)} \\ G_{\tau_e\omega_y} &= \frac{0.57955(s+0.1808)}{(s+0.3315)(s+0.03017)} \end{aligned} \tag{2.52}$$

$$G_{\tau_a\psi_i} = \frac{1.0528}{s(s+0.1)} \qquad G_{\tau_a\omega_z} = \frac{1.0528}{(s+0.1)} \tag{2.53}$$

Different transfer function matrices (TFM's) will be obtained if a different equlibrium point is assumed. The above is for $\psi_o = \theta_o = \theta_i = \psi_i = 0$ and $\dot{\psi}_o = \dot{\theta}_o = \dot{\theta}_o = \dot{\psi}_i = 0$.

CHAPTER 3

CONTROLLER DESIGN

In this section, the H^∞ mixed-sensitivity control design method, which is one of the robust control variants used for the four-axis gimbal model, is considered. Control system designs are obtained as solutions to weighted H^∞ mixed-sensitivity optimization problems possessing the form:

- *Weighted H^∞ Mixed Sensitivity Optimization Problem:* Find a stabilizing compensator K such that

$$\|T_{wz}\|_{H^\infty} = \left\| \begin{bmatrix} W_1 S \\ W_2 K S \\ W_3 T \end{bmatrix} \right\|_{H^\infty} < \gamma \tag{3.1}$$

where W_1, W_2 and W_3 are weighting functions and $\gamma > 0$ is parameter to be minimized.

3.1 Selection of Weighting Functions for Design Shaping

General rules (guidelines) for selecting the weighting functions W_1, W_2 and W_3 are now developed. Weighting functions are selected this way: [33]

- *Sensitivity Weighting*. In many applications, the weighting function W_1 on the sensitivity S is selected to have the form:

$$W_1(s) = \frac{1}{M_s}\left[\frac{s + M_s\omega_b}{s + \epsilon\omega_b}\right] \tag{3.2}$$

where $\epsilon > 0$, $\omega_b > 0$ and $M_s > 0$ are design parameters used to shape the sensitivity function.
Typically we have $0 < \epsilon << 1 < M_s < \infty$.

Using Bode approximation ideas, it follows the model

$$W_1 \approx \begin{cases} \frac{1}{\epsilon} & 0 \leq |s| << \epsilon\omega_b \\ \frac{\omega_b}{s} & \epsilon\omega_b << |s| << M_s\omega_b \\ \frac{1}{M_s} & M_s\omega_b << |s| < \infty \end{cases} \tag{3.3}$$

Sensitivity Design Parameter Interpretations. From this, we have the following interpretations for the design parameters ϵ, ω_b, M_s, and γ:

1. *Low Frequency Sensitivity Reduction.*
   ϵ is an upperbound for the desired low frequency sensitivity reduction; this sensitivity reduction is to take place for $\omega \leq \epsilon\omega_b$;

2. *Sensitivity Unity Gain Crossover Frequency.*
   ω_b is an upperbound for the desired sensitivity unity gain crossover frequency;

3. *Sensitivity High Frequency Upper Bound.* M_s is an upper bound for the sensitivity at frequencies $\omega \geq M_s\omega_b$.

By making γ smaller, the above upper bounds are improved; i.e. the effective sensitivity reduction is reduced, the effective sensitivity gain crossover frequency is increased, and the effective upper bound for the sensitivity at low frequencies is reduced. We therefore wish to make γ as small as possible.

- *Control Sensitivity Weighting.* The weighting function W_2 on KS imposes a penalty on the resulting controls. In this sense, W_2 is a control weighting function. In many applications, W_2 is selected to be a constant:

$$W_2(s) = M_u. \tag{3.4}$$

Since $|W_2KS| < \gamma$ for all frequencies, it follows that

$$|KS| < \gamma\frac{1}{M_u}. \tag{3.5}$$

Given this, it follows that

we increase (decrease) M_u in order to reduce (increase) the peak of $|KS|$.

Typically, $0 < M_u < 1$ so that $1 < \frac{1}{M_u} < \infty$ represents a nominal desired upper bound on $|KS|$. Given this, the parameter M_u is henceforth referred to as the control sensitivity peaking parameter or control penalty parameter. By making γ small, we make the peak even smaller than $\frac{1}{M_u}$. This is typically very desirable because it translates into less control action.

Dynamic Control Sensitivity Weighting. For some applications, it is important to control the bandwidth associated with KS as well as the peak. For such application, the following dynamic weighting function may be more appropriate:

$$\frac{1}{\epsilon}\left[\frac{s + \omega_{b_u}M_u}{s + \frac{\omega_{b_u}}{\epsilon}}\right] \tag{3.6}$$

where $M_u > 0$, $\omega_{b_u} > 0$, and $\epsilon > 0$ are design parameters used to shape the control sensitivity $|KS|$. The important parameters are M_u and ω_{b_u}. Typically, $0 < \epsilon << M_u < 1$. Here, $\epsilon > 0$ is typically very small - non-zero so that W_2 is proper.

Using Bode approximation ideas, it follows that

$$W_2 \approx \begin{cases} M_u & 0 \leq |s| << \omega_{b_u} M_u \\ \frac{s}{\omega_{b_u}} & \omega_{b_u} M_u << |s| << \frac{\omega_{b_u}}{\epsilon} \\ \frac{1}{\epsilon} & \frac{\omega_{b_u}}{\epsilon} << |s| < \infty \end{cases} \tag{3.7}$$

Control Sensitivity Design Parameter Interpretations. From this, we have the following interpretations for the design parameters M_u, ω_{b_u}, ϵ and γ:

1. *Bound on Peak Control Sensitivity.*
   $\frac{1}{M_u}$ is an upperbound for the desired peak control sensitivity $|KS|$ at low frequencies;

2. *Control Sensitivity Bandwidth and Roll-Off.*
   ω_{b_u} is an upperbound for the desired control sensitivity $|KS|$ bandwidth; i.e. high frequency unity gain crossover frequency;

3. *Control Sensitivity High Frequency Upper Bound.*
   ϵ is an upper bound for the control sensitivity $|KS|$ at frequencies $\omega \geq \frac{\omega_{b_u}}{\epsilon}$

By making γ smaller, the above upper bounds are all made smaller. We therefore wish to make γ as small as possible.

- *Complementary Sensitivity Weighting.* In many applications, the weighting function W_3 on the complementary sensitivity T is selected to have the following form:

$$W_3(s) = \frac{s + \frac{\omega_{b_c}}{M_y}}{\omega_{b_c}} \tag{3.8}$$

where $M_y > 0$ and $\omega_{b_c} > 0$ are design parameters used to shape the $|T|$. (Note that if the denominator is replaced by $\epsilon s + \omega_{b_c}$small, then the function W_3 becomes proper. This is sometimes required.)

Using Bode approximation ideas, it follows that

$$W_3 \approx \begin{cases} \frac{1}{M_y} & 0 \leq |s| << \frac{\omega_{b_c}}{M_y} \\ \frac{s}{\omega_{b_c}} & \frac{\omega_{b_c}}{M_y} << |s| < \infty \end{cases} \tag{3.9}$$

Complementary Sensitivity Design Parameter Interpretations. From this, we have the following interpretations for the design parameters M_y, ω_{b_c}, γ and γ:

1. *Bound on Peak Complementary Sensitivity.*
   M_y is an upperbound for the desired peak complementary sensitivity $|T|$ at low frequencies;

2. *Complementary Sensitivity Bandwidth and Roll-Off.*
   ω_{b_c} is an upperbound for the desired complementary sensitivity $|T|$ bandwidth; i.e. high frequency unity gain crossover frequency.

Typically, we have $1 < M_y << \infty$. By making γ smaller, the above upper bounds are made smaller. We therefore wish to make γ as small as possible.

Significance of γ Vis-a-Vis Design Specifications. One might use MATLAB's "hinfopt" command to find the minimum γ and a near-optimal controller K. (Caution: The command uses $\frac{1}{\gamma}$ instead of γ.) Given this, there are three cases worth noting.

- Non-demanding Design Specifications. A γ less than unity, implies that

$$|S(j\omega)| < |W_1^{-1}(j\omega)| \tag{3.10}$$

$$|K(j\omega)S(j\omega)| < |W_2^{-1}(j\omega)| \tag{3.11}$$

$$|T(j\omega)| < |W_3^{-1}(j\omega)| \tag{3.12}$$

for all ω. This suggests that weighting functions (design specifications) reflecting not very demanding (i.e. relaxed) were used. In such a case, one might then try to tighten the specifications by selecting more aggressive design parameters.

- *Demanding Design Specifications.* A γ greater than unity, suggests that weighting functions reflecting very demanding (i.e. aggressive) design specifications were used. In such a case, one might then try to loosen the specifications by selecting less aggressive design parameters.

- *Unrealistic Design Specifications.* If a controller does not exist (i.e. any one of the necessary and sufficient conditions for existence are violated), then this implies that the weighting functions (and the associated design specifications) used were unrealistic; i.e. far too aggressive. As a general rule, the design problem becomes more difficult as low and high frequency design specifications (reflected in the weighting functions) overlap.

  Why is this? Low frequency specifications typically call for a minimum bandwidth. High frequency specifications typically call for a maximum bandwidth. If the specifications are too demanding, a very high order (possibly infinite-dimensional) controller may be required to achieve the overlapping specifications. In such a case, a near optimal controller possessing dimension equal to that of the generalized plant may not exist.

3.2 H∞ Mixed Sensitivity Control System Design Structure: Four-Axis Gimbal Platform

In this section, the control system design structures for the four axis gimbal platform are explained. The gimbal platform's position and rate control structures have been investigated and schematized under separate titles. Furthermore, detailed analyses of controllers designed using the H∞ mixed sensitivity structure are presented.

3.3 Position Controller Design

The position control structure of the closed loop system is described in Fig 3.1. The models developed in Fig 2.9 are part of the four axis gimbal block. When the gimbal model is combined, it becomes a 5-input 4-output system. τ_A, τ_E, τ_e, and τ_a denote the torque inputs applied to the outer azimuth frame, outer elevation frame, inner elevation frame, and inner azimuth frame, respectively. $[p,q,r]$ is treated as a source of disturbance. K_{ψ_o}, K_{θ_o}, K_{θ_i} and K_{ψ_i} refers to SISO (1×1) position controllers designed to control ψ_o, θ_o, θ_i and ψ_i. Also, ${\psi_o}^c$, ${\theta_o}^c$, ${\theta_i}^c$ and ${\psi_i}^c$ are the command signal applied to the system.

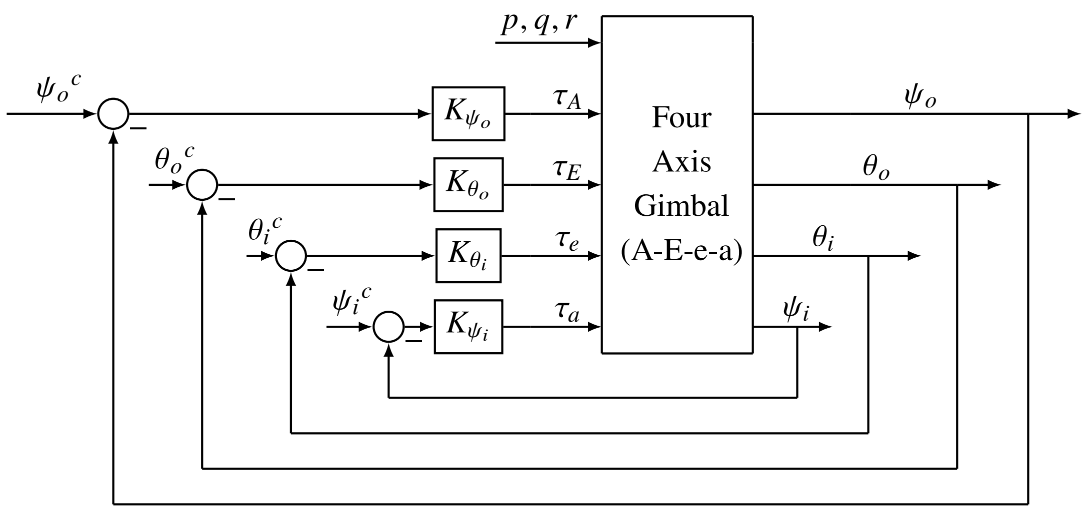

Figure 3.1: Gimbal Position Control (SISO) - Closed Loop Structure.

3.3.1 Outer Azimuth Position Controller Design (SISO)

The plant that was used in the design of the outer azimuth position controller was found in Equation 2.50 and is shown below.

$$Plant = P_{\psi_o} = G_{\tau_A \psi_o} = \frac{0.38197}{s(s+0.1)} \tag{3.13}$$

Each design was created by solving a standard weighted H_∞ *mixed-sensitivity control problem* using the weighting functions and design parameters shown in Table 3.1. It should be noted that little time was spent tuning the parameters.

Table 3.1: Weighting Functions and Design Parameters for ψ_o.

$W1_{\psi_o}$	$W2_{\psi_o}$	$W3_{\psi_o}$
$Ms_{\psi_o} = 10$ $\omega b_{\psi_o} = 2 * \pi * 0.5$ $\epsilon_{\psi_o} = 0.001$	$Mu_{\psi_o} = 0.01$	[]
$W1_{\psi_o}^{-1} = \frac{s + \epsilon \omega b_{\psi_o}}{\frac{s}{Ms_{\psi_o}} + \omega b_{\psi_o}}$ $= \frac{s + 0.003142}{0.1s + 3.142}$	$W2_{\psi_o}^{-1} = \frac{1}{Mu_{\psi_o}}$ $= 100$	$W3_{\psi_o}^{-1} = \frac{\omega bc_{\psi_o}}{s + \frac{\omega bc_{\psi_o}}{My_{\psi_o}}}$ $= []$

The *outer azimuth position controller* was designed using bilinear transformation. The following shows how the bilinear transformation is done.

$$s = \frac{\hat{s} + p_1}{\frac{\hat{s}}{p_2} + 1} \qquad \hat{s} = \frac{s - p_1}{1 - \frac{s}{p_2}} \tag{3.14}$$

where $p_1, p_2 \in \mathrm{R}$ may be used to influence the final control system design.

Bilinear Transformation Parameters Used. The *bilinear transformation parameters were selected as follows:*

$$\begin{aligned} p1_{\psi_o} &= -0.01 \\ p2_{\psi_o} &= -10^8. \end{aligned} \tag{3.15}$$

This selection yields

$$
\begin{aligned}
s &= \frac{\hat{s} + p_{1_{\psi_o}}}{\frac{\hat{s}}{p_{2_{\psi_o}}} + 1} = \frac{\hat{s} - 0.01}{\frac{\hat{s}}{-10^8} + 1} \approx \hat{s} - 0.01 \qquad \text{(inverse transformation)} \\
\hat{s} &\approx s + 0.01 \qquad\qquad\qquad\qquad\qquad \text{(transformation)}
\end{aligned} \tag{3.16}
$$

This selection of parameters results in a rightward shifting transformation $\hat{s} \approx s + 0.01$ and a leftward shifting transformation $s \approx \hat{s} - 0.01$. The selection thus shifts all plant poles and zeros 0.01 units to the right. The transformed plant is combined with the weighting functions to form the generalized plant G. (Note that the transformation is NOT applied to the weighting functions!). Designs are based on the resulting generalized plant G. After a design $\hat{K}$ is obtained, the inverse transform is applied to $\hat{K}$ - shifting its poles and zeros in the $\hat{s}$ plane toward the left to get poles and zeros in the s-plane. Since $\hat{K}$ internally stabilized $\hat{P}$, the resulting controller K is guaranteed to stabilize the original plant P.

The outer azimuth position controller design is obtained using

$$
P_{\psi_o} = \frac{0.38197}{s(s + 0.1)} \tag{3.17}
$$

as the plant model. The design process is initiated by transforming the generalized plant into the $\hat{s}$-plane using the above bilinear transformation. After this is done, a design is obtained. The resulting $\hat{s}$-plane design is then transformed back into the s-plane. The resulting minimum γ was found to be

$$
\gamma = 0.8650 \tag{3.18}
$$

The resulting s-domain controller is given by

$$
\begin{aligned}
K_{\psi_o} &= \frac{0.0005128(s + 10^8)(s + 0.1)(s + 0.01996)}{(s + 0.01314)(s + 9.005)(s + 596.8)} \\
&\approx \frac{0.0005128(s + 10^8)(s + 0.1)(s + 0.01996)}{s(s + 596.8)(s + 9.005)}
\end{aligned} \tag{3.19}
$$

The associated complementary sensitivity is given by

$$
\begin{aligned}
T_{\psi_o} &= \frac{0.00039175s(s + 10^8)(s + 596.8)(s + 9.005)(s + 0.1)^2(s + 0.01996)(s + 0.01314)}{s^2(s + 0.1)^2(s + 0.01314)^2(s + 9.005)^2(s + 596.8)^2} \\
&\approx \frac{0.00039175(s + 10^8)(s + 596.8)(s + 9.005)(s + 0.1)^2(s + 0.01996)(s + 10^{-7})(s - 10^{-7})}{s^4(s + 0.1)^2(s + 9.005)^2(s + 596.8)^2}
\end{aligned} \tag{3.20}
$$

Frequency Responses. Figures 3.2-3.8 contain relevant frequency responses for *outer azimuth position controller.*

The frequency response of the plant is given in Fig 3.2.

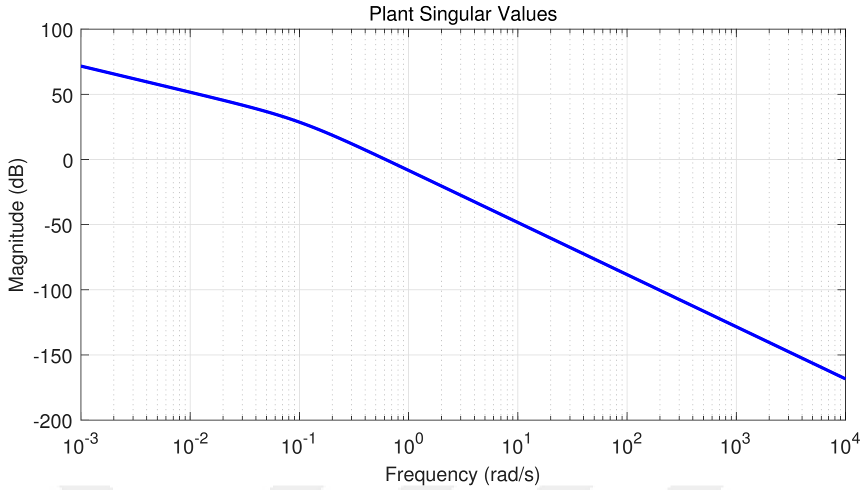

Figure 3.2: Plant Frequency Response - $P_{\psi_o} = \frac{0.38197}{s(s+0.1)}$.

The frequency response of the controller is given in Fig 3.3.

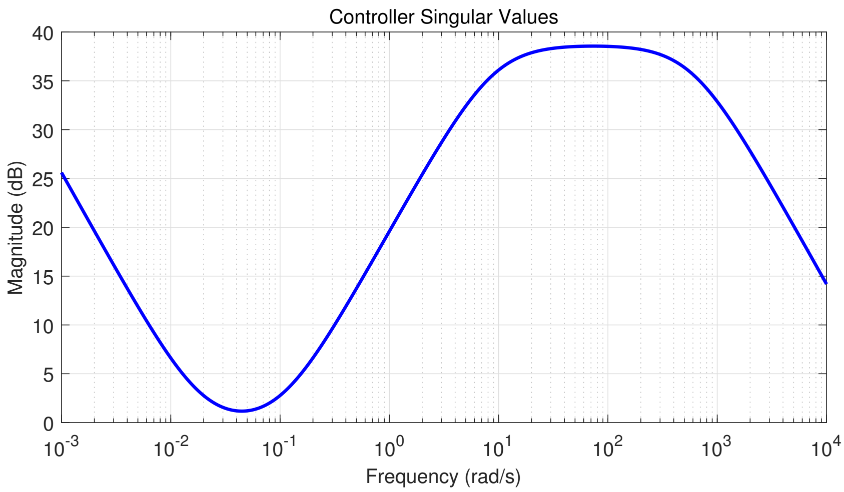

Figure 3.3: Controller Frequency Response - K_{ψ_o}.

The open loop transfer function is given in Fig 3.4. As can be seen from the figure the open loop bandwidth is about 3.5 rad/sec.

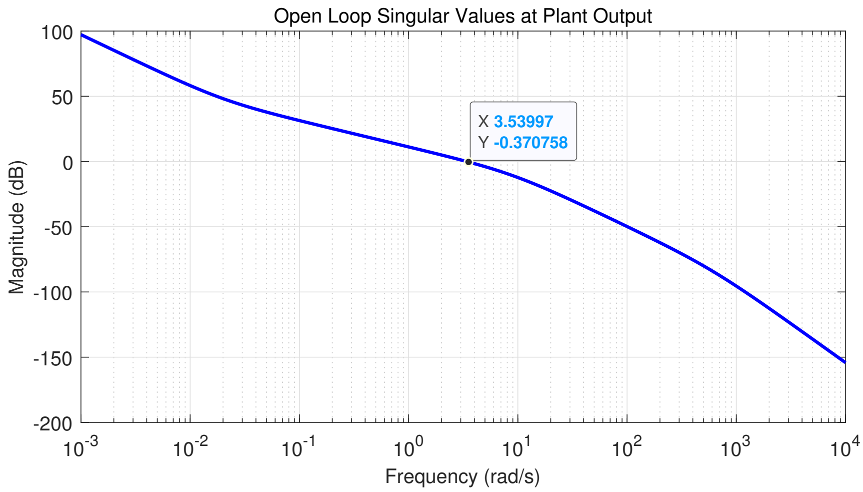

Figure 3.4: Open Loop Frequency Response - $L_{\psi_o} = P_{\psi_o} K_{\psi_o}$.

The frequency response of the sensitivity is given in Fig 3.5. Sensitivity frequency response is $|S|_\infty < |W_1^{-1}|_\infty$. The frequency response of sensitivity transfer function is as expected, i.e. small at low frequencies, and near unity (0 dB) at high frequencies.

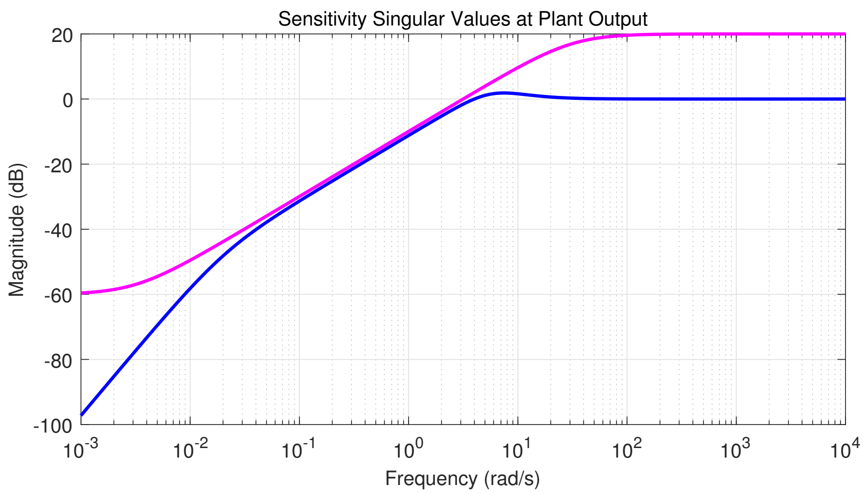

Figure 3.5: Sensitivity Frequency Response - $S_{\psi_o} = \frac{1}{1+P_{\psi_o} K_{\psi_o}} = (T_{doy})_{\psi_o}$.

The complementary sensitivity transfer function is given in Fig 3.6. As can be seen from the figure the complementary sensitivity bandwidth is approximately about 5 rad/sec. The frequency response of complementary sensitivity transfer function is as expected, i.e. small at high frequencies, and near unity (0 dB) at low frequencies.

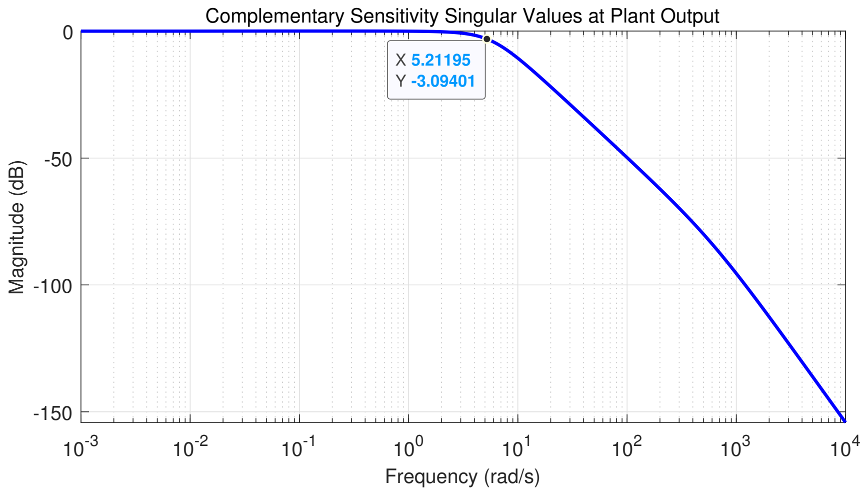

Figure 3.6: Complementary Sensitivity Frequency Response - $(T_o)_{\psi_o} = \frac{P_{\psi_o}K_{\psi_o}}{1+P_{\psi_o}K_{\psi_o}}$.

Control frequency response is given in Fig 3.7.

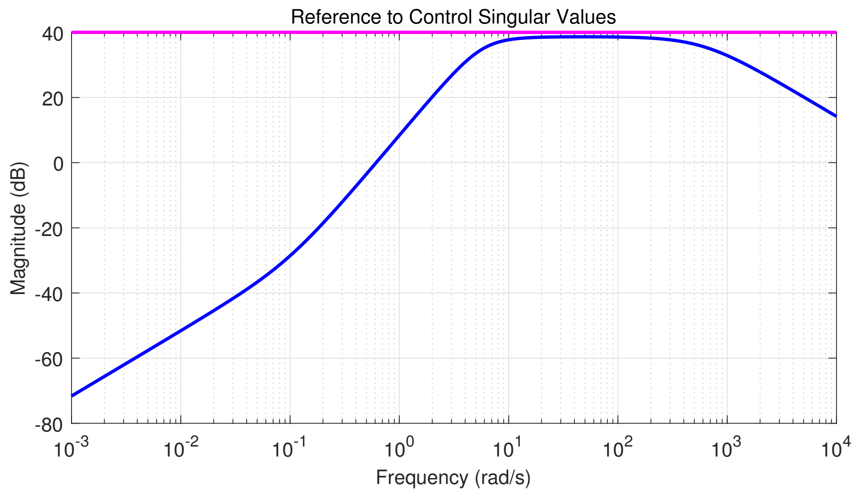

Figure 3.7: Reference to Control Frequency Response - $(T_{ru})_{\psi_o} = K_{\psi_o}S_{\psi_o}$.

Input disturbance to output frequency response is given in Fig 3.8. At very low frequencies, and high frequencies T_{diy} (Input disturbance singular value transfer function) is small as expected. For frequencies between 10^{-2} rad/sec and 0.3 rad/sec the disturbance rejection is poor.

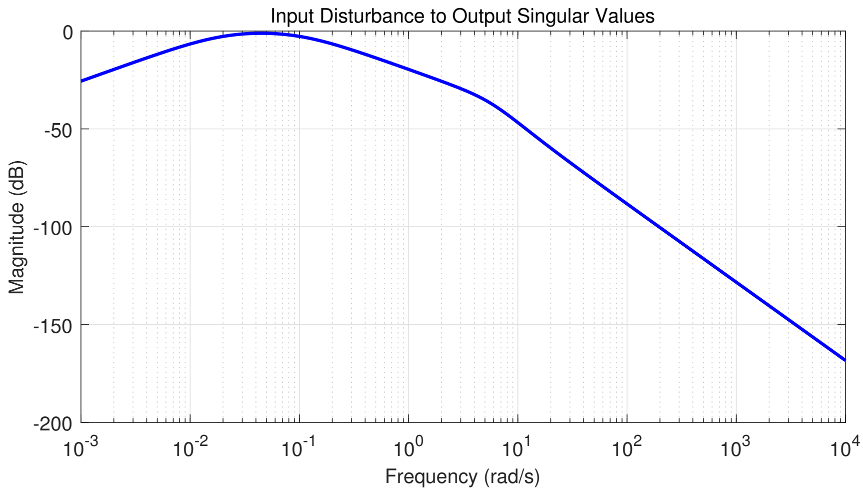

Figure 3.8: Input Disturbance to Output Frequency Response - $(T_{diy})_{\psi_o} = S_{\psi_o} P_{\psi_o}$.

Time Response Data: Step Command Following. We now address step command following for outer azimuth position controller.

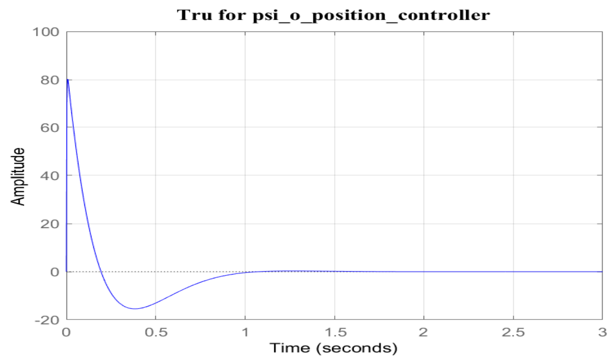

Figure 3.9: Control Response to Step Reference Command $(T_{ru})_{\psi_o}$.

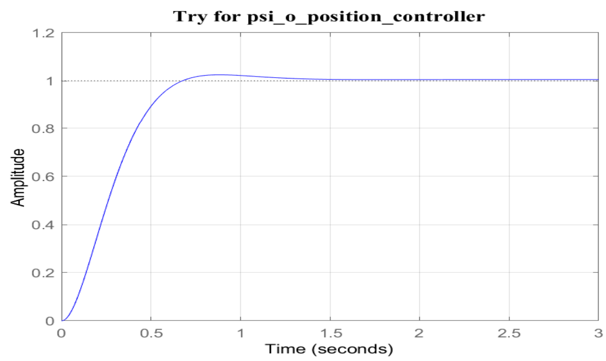

Figure 3.10: Output Response to Step Reference Command $(T_{ry})_{\psi_o}$.

Closed Loop Poles for Outer Azimuth Position Controller Design. The closed loop poles that result from our BLT (bilinear transformation) approach are as follows.

Table 3.2: Closed Loop Poles for Outer Azimuth Position Controller Design.

Poles	**Damping**	**Frequency(rad/sec)**
$-5.97e+02$	$1.00e+00$	$5.97e+02$
$-4.46e+00+3.56e+00i$	$7.81e-01$	$5.71e+00$
$-4.46e+00-3.56e+00i$	$7.81e-01$	$5.71e+00$
$-2.01e-02$	$1.00e+00$	$2.01e-02$
$-1.00e-01$	$1.00e+00$	$1.00e-01$

As expected, all closed loop poles associated with outer azimuth position controller design are at desirable locations - with damping $\zeta > 0.7$. Also it should be noted that, since $\gamma < 1$, this implies that our outer azimuth position controller design specifications (reflected within our weighting functions) *were not too aggressive.*

The output graph for ψ_o in the simulink block diagram after designing the outer azimuth position controller is shown below. When the system is given a *100*° position input, the response of the system with the designed controller is as in the Fig 3.11.

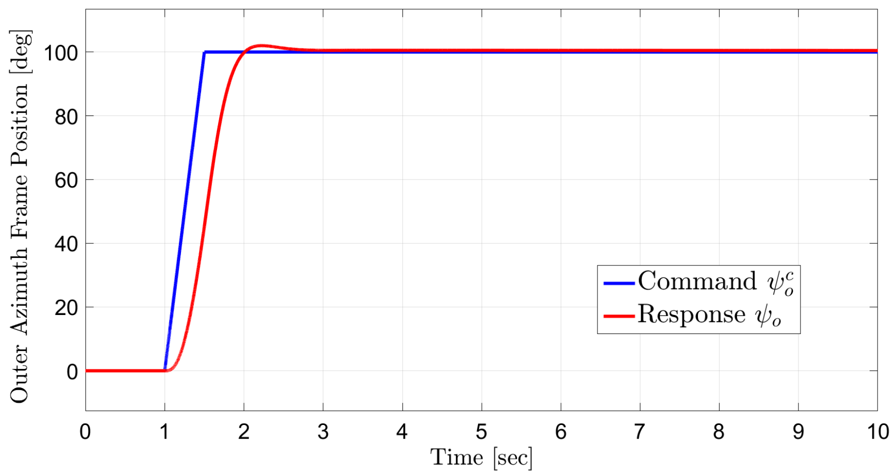

Figure 3.11: ψ_o - Output Response (SISO System).

3.3.2 Inner Azimuth Position Controller Design (SISO)

The plant that was used in the design of the inner azimuth position controller was found in Equation 2.53 and is shown below.

$$Plant = P_{\psi_i} = G_{\tau_a \psi_i} = \frac{1.0528}{s(s+0.1)} \tag{3.21}$$

Weighting Functions and Design Parameters. Weighting function parameters and weighting functions were selected as follows:

$$\begin{aligned} Ms_{\psi_i} &= 10 \\ \omega_{b\psi_i} &= 2*\pi*1.2 \\ \epsilon_{\psi_i} &= 0.001 \\ Mu_{\psi_i} &= 10^{-4} \\ \omega_{bc\psi_i} &= [] \\ My_{\psi_i} &= [] \end{aligned} \tag{3.22}$$

Table 3.3: Weighting Functions and Design Parameters for ψ_i.

$W1_{\psi_i}$	$W2_{\psi_i}$	$W3_{\psi_i}$
$Ms_{\psi_i} = 10$ $\omega_{b\psi_i} = 2*\pi*1.2$ $\epsilon_{\psi_i} = 0.001$	$Mu_{\psi_i} = 10^{-4}$	[]
$W1_{\psi_i}^{-1} = \dfrac{s+\epsilon\omega_{b\psi_i}}{\frac{s}{Ms_{\psi_i}}+\omega_{b\psi_i}}$ $= \dfrac{s+0.00754}{0.1s+7.54}$	$W2_{\psi_i}^{-1} = \dfrac{1}{Mu_{\psi_i}}$ $= 10^4$	$W3_{\psi_i}^{-1} = \dfrac{\omega_{bc\psi_i}}{s+\frac{\omega_{bc\psi_i}}{My_{\psi_i}}}$ $= []$

Very lightly damped closed loop poles, which are unacceptable in some design, have been observed. To prevent this undesirable plant pole inversion, we use the *bilinear transformation.*

Bilinear Transformation Parameters. The bilinear transformation (BLT) parameters selected were as follows:

$$\begin{aligned} p1_{\psi_i} &= -1 \\ p2_{\psi_i} &= -10^8 \end{aligned} \tag{3.23}$$

This selection results in

$$
\begin{aligned}
s &= \frac{\hat{s} + p_{1_{\psi_i}}}{\frac{\hat{s}}{p_{2_{\psi_i}}} + 1} = \frac{\hat{s} - 1}{\frac{\hat{s}}{-10^8} + 1} \approx \hat{s} - 1 \qquad \text{(inverse transformation)} \\
\hat{s} &\approx s + 1 \qquad\qquad\qquad\qquad\qquad \text{(transformation)}
\end{aligned} \tag{3.24}
$$

The transform performans a rightward ("destabilizing") shift. The inverse transform performs a leftward ("stabilizing") shift. The resulting minimum γ was found to be

$$\gamma = 0.2723 \tag{3.25}$$

Since $\gamma < 1$, this implies that our design specification were not too aggressive.

The resulting s-domain controller is given by

$$
\begin{aligned}
K_{\psi_i} &= \frac{0.075388(s+10^8)(s^2+3.675s+3.468)}{(s+1.008)(s+86)(s+2976)} \\
&\approx \frac{0.075388(s+10^8)(s^2+3.675s+3.468)}{s(s+86)(s+2976)}
\end{aligned} \tag{3.26}
$$

Frequency Responses. Figures 3.12-3.18 contain relevant frequency responses for *inner azimuth position controller.*

The frequency response of the plant is given in Fig 3.12.

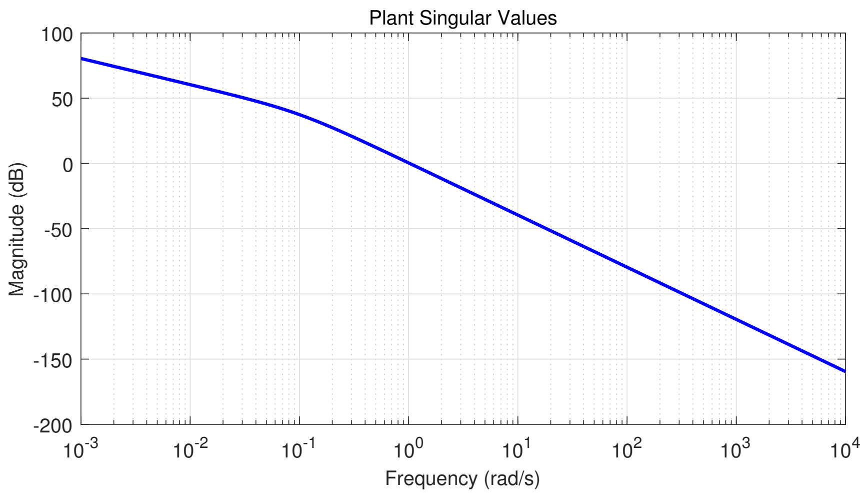

Figure 3.12: Plant Frequency Response - $P_{\psi_i} = \frac{1.0528}{s(s+0.1)}$.

The frequency response of the controller is given in Fig 3.13.

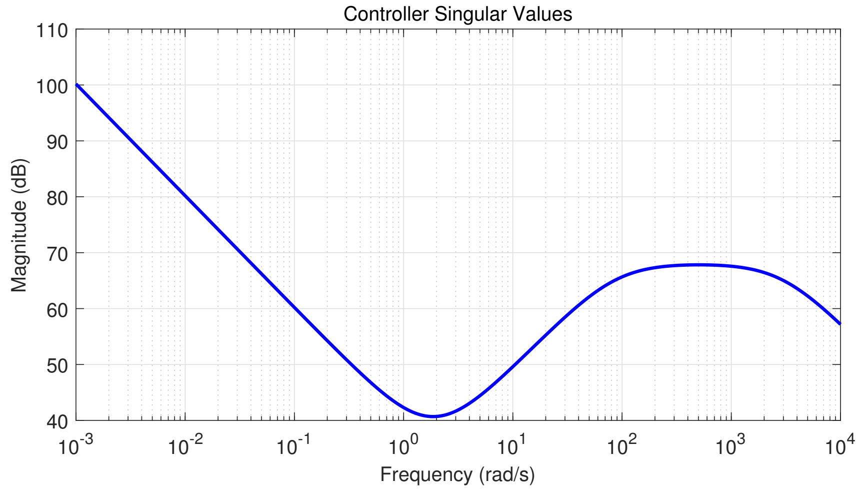

Figure 3.13: Controller Frequency Response - K_{ψ_i}.

The open loop transfer function is given in Fig 3.14. As can be seen from the figure the open loop bandwidth is about 32 rad/sec.

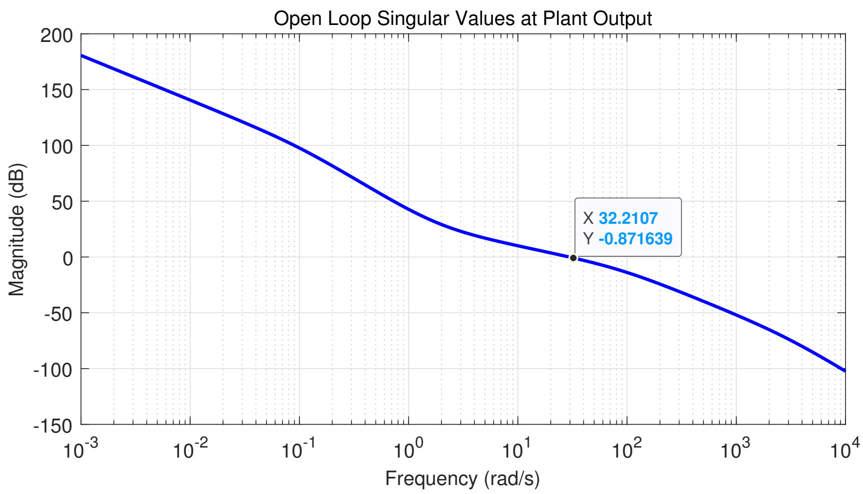

Figure 3.14: Open Loop Frequency Response - $L_{\psi_i} = P_{\psi_i} K_{\psi_i}$.

The frequency response of the sensitivity is given in Fig 3.15. Sensitivity frequency response is $|S|_\infty < |W_1^{-1}|_\infty$. The frequency response of sensitivity transfer function is as expected, i.e. small at low frequencies, and near unity (0 dB) at high frequencies.

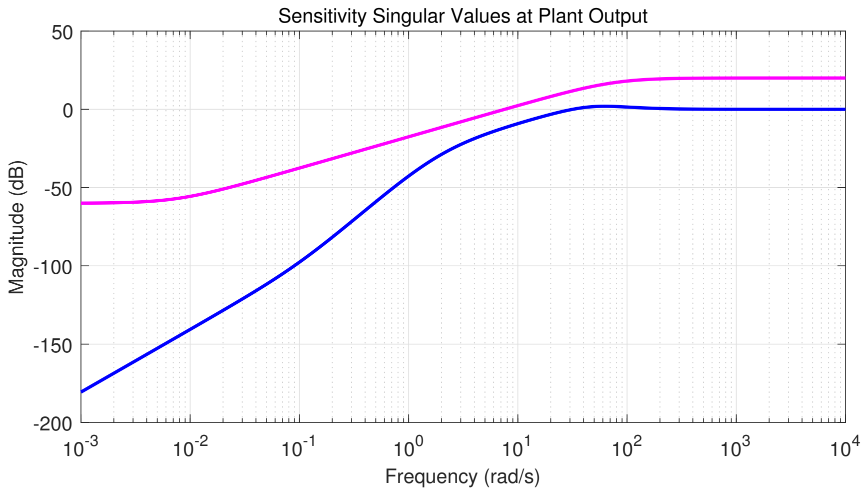

Figure 3.15: Sensitivity Frequency Response - $S_{\psi_i} = \frac{1}{1+P_{\psi_i}K_{\psi_i}} = (T_{doy})_{\psi_i}$.

The complementary sensitivity transfer function is given in Fig 3.16. As can be seen from the figure the complementary sensitivity bandwidth is approximately about 47 rad/sec. The frequency response of complementary sensitivity transfer function is as expected, i.e. small at high frequencies, and near unity (0 dB) at low frequencies.

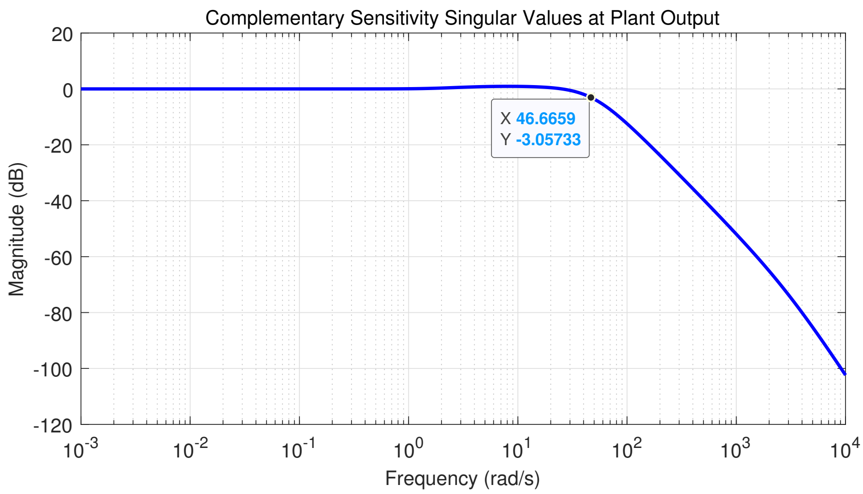

Figure 3.16: Complementary Sensitivity Frequency Response - $(T_o)_{\psi_i} = \frac{P_{\psi_i}K_{\psi_i}}{1+P_{\psi_i}K_{\psi_i}}$.

Control frequency response is given in Fig 3.17.

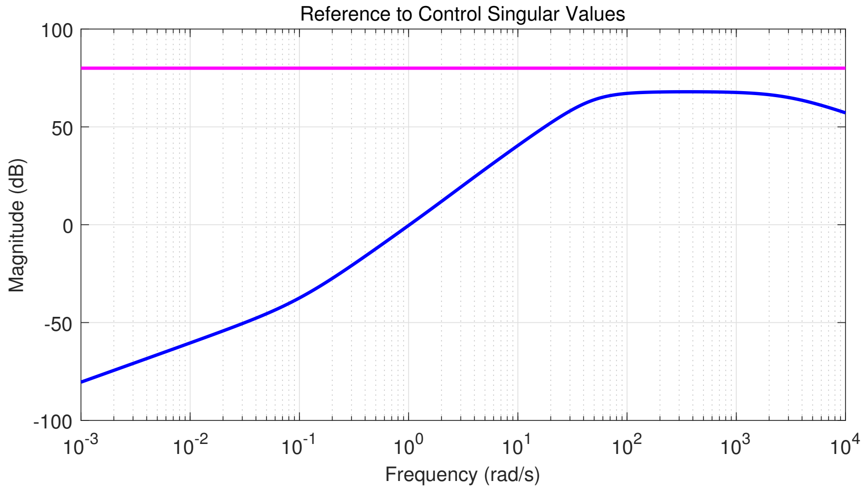

Figure 3.17: Reference to Control Frequency Response - $(T_{ru})_{\psi_i} = K_{\psi_i} S_{\psi_i}$.

Input disturbance to output frequency response is given in Fig 3.18. At very low frequencies, and high frequencies T_{diy} (Input disturbance singular value transfer function) is small as expected. For frequencies between 0.1 rad/sec and 10 rad/sec the disturbance rejection is poor.

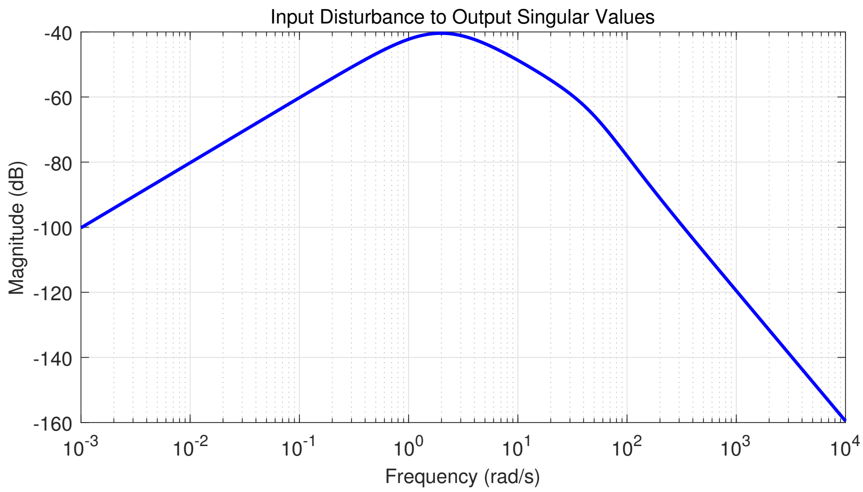

Figure 3.18: Input Disturbance to Output Frequency Response - $(T_{diy})_{\psi_i} = S_{\psi_i} P_{\psi_i}$.

Time Response Data: Step Command Following. We now address step command following for inner azimuth position controller.

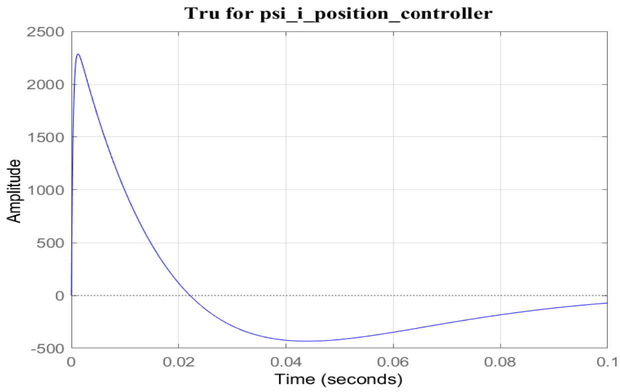

Figure 3.19: Control Response to Step Reference Command $(T_{ru})_{\psi_i}$.

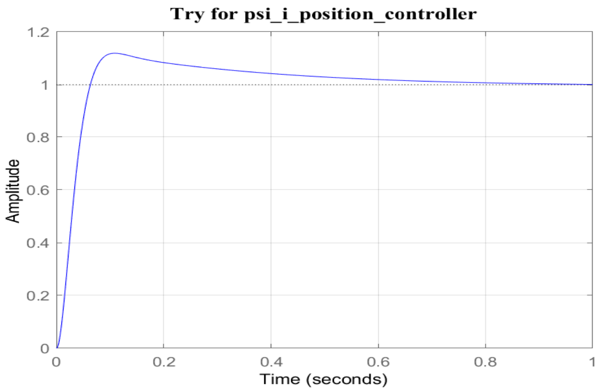

Figure 3.20: Output Response to Step Reference Command $(T_{ry})_{\psi_i}$.

Closed Loop Poles for Inner Azimuth Position Controller Design. The closed loop poles that result from our BLT (bilinear transformation) approach are as follows.

Table 3.4: Closed Loop Poles for Inner Azimuth Position Controller Design.

Poles	Damping	Frequency(rad/sec)
$-2.98e+03$	$1.00e+00$	$2.98e+03$
$-4.06e+01+2.63e+01i$	$8.39e-01$	$4.84e+01$
$-4.06e+01-2.63e+01i$	$8.39e-01$	$4.84e+01$
$-2.41e+00$	$1.00e+00$	$2.41e+00$
$-1.64e+00$	$1.00e+00$	$1.64e+00$

As expected, all closed loop poles associated with inner azimuth position controller design are at desirable locations - with damping $\zeta > 0.7$. Also it should be noted that, since $\gamma < 1$, this implies that our inner azimuth position controller design specifications (reflected within our weighting functions) *were not too aggressive.*

The output graph for ψ_i in the simulink block diagram after designing the inner azimuth position controller is shown below Fig 3.21. Given *100°* to the outer azimuth axis, it is desired that the inner azimuth axis stays at or around *1°* - *2°* . It is seen that this situation is achieved with the designed SISO position controller.

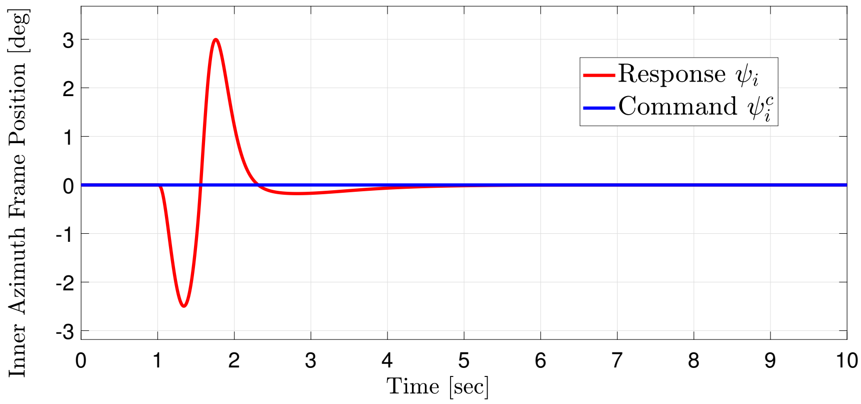

Figure 3.21: ψ_i - Output Response (SISO System).

3.3.3 Outer Elevation Position Controller Design(SISO)

The plant that was used in the design of the outer elevation position controller was found in Equation 2.51 and is shown below.

$$Plant = P_{\theta_o} = G_{\tau_E \theta_o} = \frac{0.46846(s+0.1)}{s(s+0.3315)(s+0.03017)} \tag{3.27}$$

Weighting Functions and Design Parameters. Weighting function parameters and weighting functions were selected as follows:

$$\begin{aligned} Ms_{\theta_o} &= 10 \\ \omega_{b\theta_o} &= 2 * \pi * 0.5 \\ \epsilon_{\theta_o} &= 0.001 \\ Mu_{\theta_o} &= 10^{-2} \\ \omega_{bc\theta_o} &= [] \\ My_{\theta_o} &= [] \end{aligned} \tag{3.28}$$

Table 3.5: Weighting Functions and Design Parameters for θ_o.

$W_{1\theta_o}$	$W_{2\theta_o}$	$W_{3\theta_o}$
$Ms_{\theta_o} = 10$ $\omega_{b\theta_o} = 2 * \pi * 0.5$ $\epsilon_{\theta_o} = 0.001$	$Mu_{\theta_o} = 10^{-2}$	[]
$W_{1\theta_o}^{-1} = \dfrac{s + \epsilon\omega_{b\theta_o}}{\frac{s}{Ms_{\theta_o}} + \omega_{b\theta_o}}$ $= \dfrac{s + 0.003142}{0.1s + 3.142}$	$W_{2\theta_o}^{-1} = \dfrac{1}{Mu_{\theta_o}}$ $= 10^2$	$W_{3\theta_o}^{-1} = \dfrac{\omega_{bc\theta_o}}{s + \frac{\omega_{bc\theta_o}}{My_{\theta_o}}}$ $= []$

Very lightly damped closed loop poles, which are unacceptable in some design, have been observed. To prevent this undesirable plant pole inversion, we use the *bilinear transformation.*

Bilinear Transformation Parameters. The bilinear transformation (BLT) parameters were selected as follows:

$$\begin{aligned} p_{1\theta_o} &= -0.01 \\ p_{2\theta_o} &= -10^8 \end{aligned} \tag{3.29}$$

This selection results in

$$\begin{aligned} s &= \frac{\hat{s} + p_{1\theta_o}}{\frac{\hat{s}}{p_{2\theta_o}} + 1} = \frac{\hat{s} - 0.01}{\frac{\hat{s}}{-10^8} + 1} \approx \hat{s} - 0.01 \qquad \text{(inverse transformation)} \\ \hat{s} &\approx s + 0.01 \qquad\qquad\qquad\qquad\qquad \text{(transformation)} \end{aligned} \tag{3.30}$$

The transform performance shifts a rightward ("destabilizing"). The inverse transform performance shifts a leftward ("stabilizing"). The resulting minimum γ was found to be

$$\gamma = 0.8072 \tag{3.31}$$

Since $\gamma < 1$, this implies that our design specification were not too aggressive.

The resulting s-domain controller is given by

$$
\begin{aligned}
K_{\theta_o} &= \frac{0.00041252(s+10^8)(s+0.3415)(s+0.04017)(s+0.01)}{(s+514.9)(s+9.661)(s+0.11)(s+0.01314)} \\
&\approx \frac{0.00041252(s+10^8)(s+0.3415)(s+0.04017)(s+0.01)}{s(s+514.9)(s+9.661)(s+0.11)}
\end{aligned}
\tag{3.32}
$$

Frequency Responses. Figures 3.22-3.28 contain relevant frequency responses for *outer elevation position controller.*

The frequency response of the plant is given in Fig 3.22.

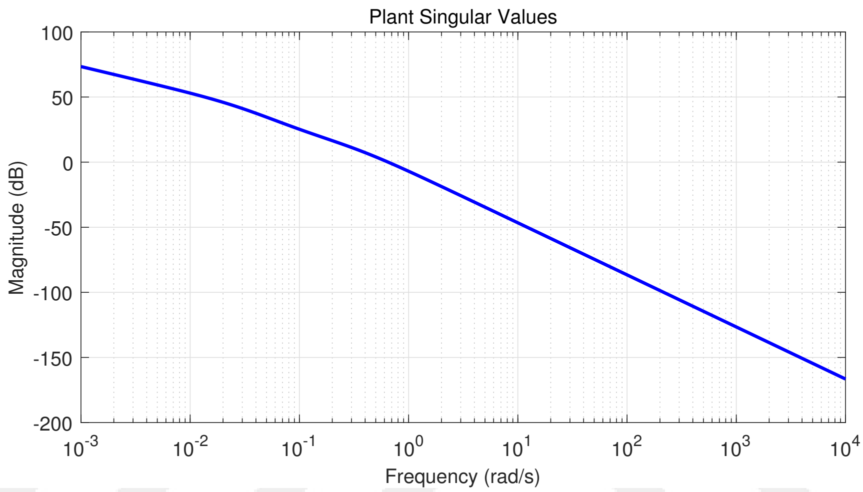

Figure 3.22: Plant Frequency Response - $P_{\theta_o} = \frac{0.46846(s+0.1)}{s(s+0.3315)(s+0.03017)}$.

The frequency response of the controller is given in Fig 3.23.

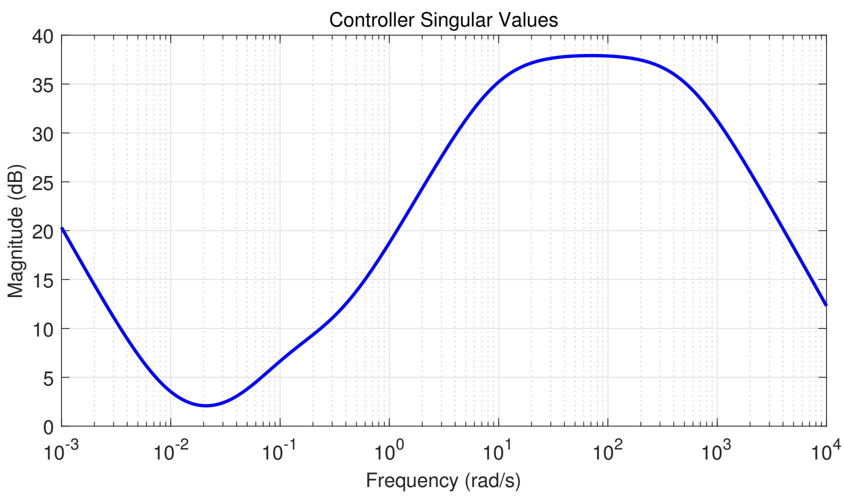

Figure 3.23: Controller Frequency Response - K_{θ_o}.

The open loop transfer function is given in Fig 3.24. As can be seen from the figure the open loop bandwidth is about 3.7 rad/sec.

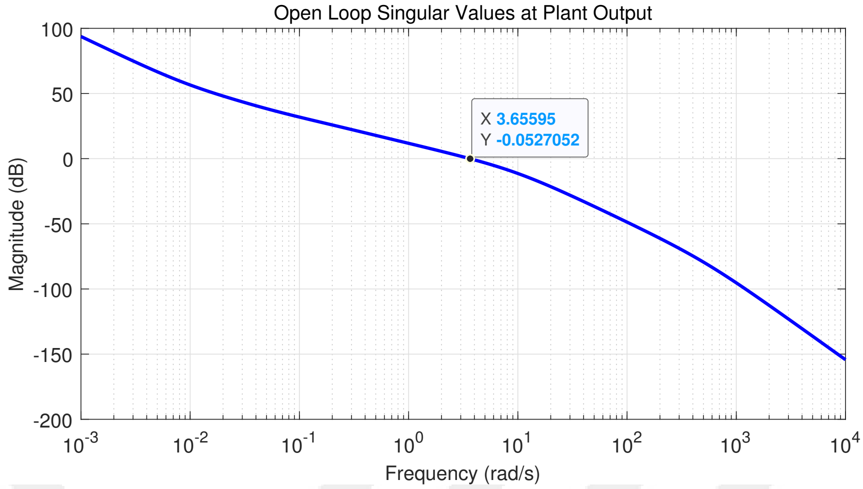

Figure 3.24: Open Loop Frequency Response - $L_{\theta_o} = P_{\theta_o} K_{\theta_o}$.

The frequency response of the sensitivity is given in Fig 3.25. Sensitivity frequency response is $|S|_\infty < |W_1^{-1}|_\infty$. The frequency response of sensitivity transfer function is as expected, i.e. small at low frequencies, and near unity (0 dB) at high frequencies.

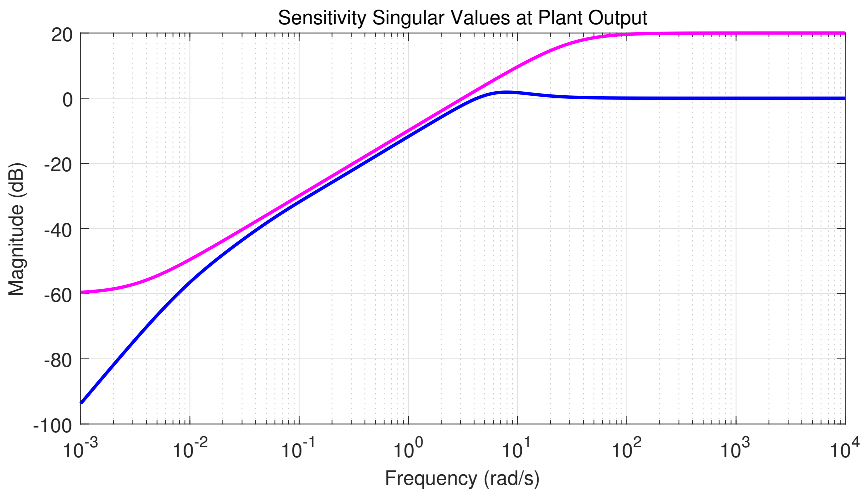

Figure 3.25: Sensitivity Frequency Response - $S_{\theta_o} = \frac{1}{1+P_{\theta_o} K_{\theta_o}} = (T_{doy})_{\theta_o}$.

The complementary sensitivity transfer function is given in Fig 3.26. As can be seen from the figure the complementary sensitivity bandwidth is approximately about 5.5 rad/sec. The frequency response of complementary sensitivity transfer function is as expected, i.e. small at high frequencies, and near unity (0 dB) at low frequencies.

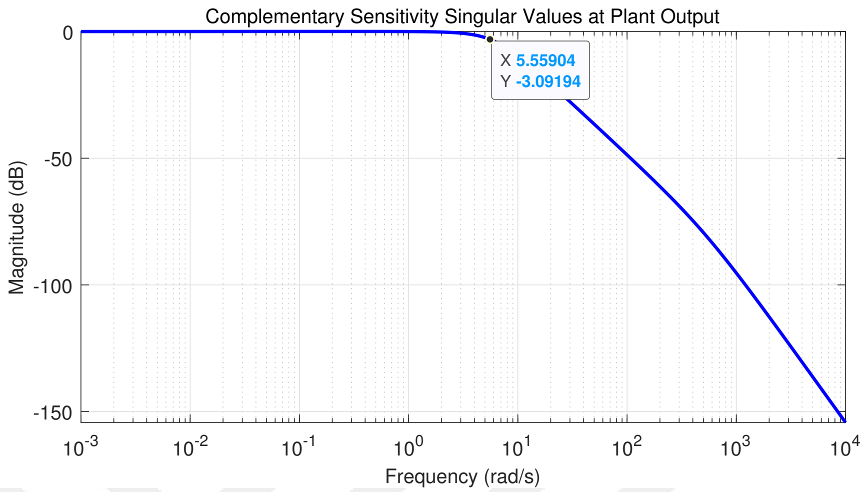

Figure 3.26: Complementary Sensitivity Frequency Response - $(T_o)_{\theta_o} = \frac{P_{\theta_o} K_{\theta_o}}{1+P_{\theta_o} K_{\theta_o}}$.

Control frequency response is given in Fig 3.27.

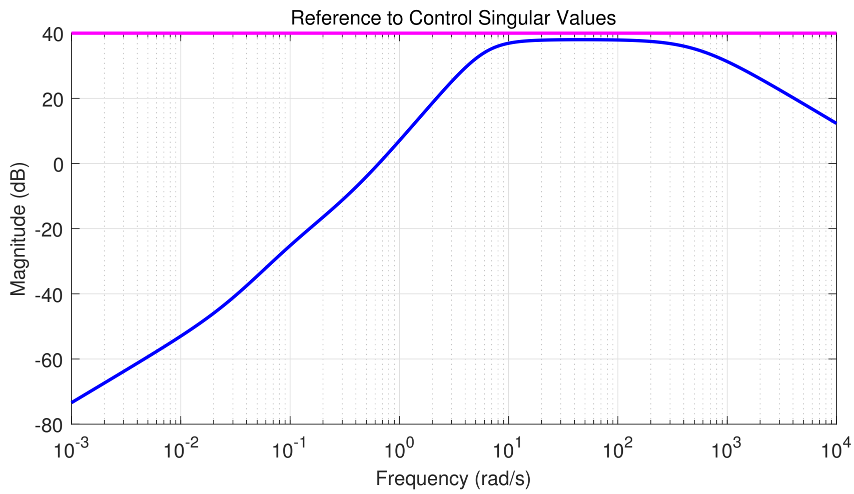

Figure 3.27: Reference to Control Frequency Response - $(T_{ru})_{\theta_o} = K_{\theta_o} S_{\theta_o}$.

Input disturbance to output frequency response is given in Fig 3.28. At very low frequencies, and high frequencies T_{diy} (Input disturbance singular value transfer function) is small as expected. For frequencies between 0.04 rad/sec and 0.2 rad/sec the disturbance rejection is poor.

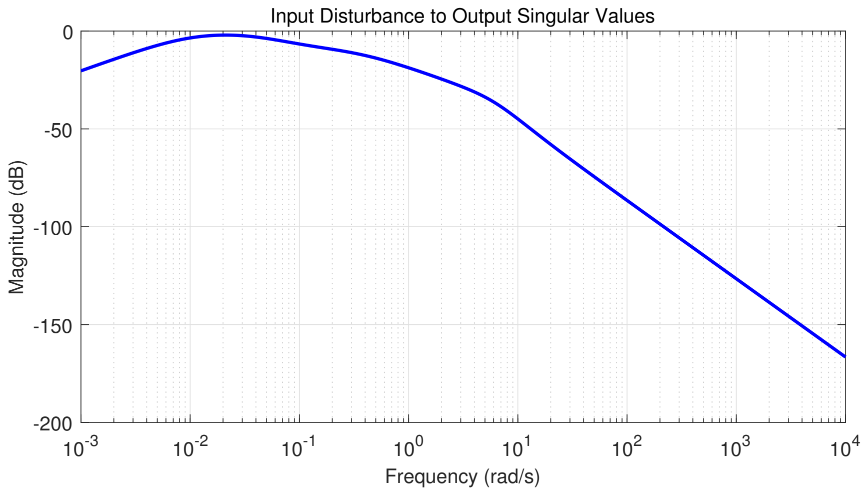

Figure 3.28: Input Disturbance to Output Frequency Response - $(T_{diy})_{\theta_o} = S_{\theta_o} P_{\theta_o}$.

Time Response Data: Step Command Following. We now address step command following for outer elevation position controller.

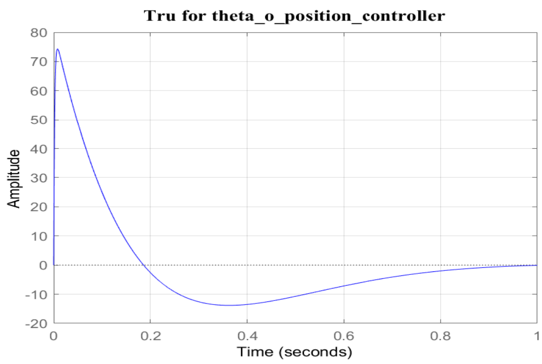

Figure 3.29: Control Response to Step Reference Command $(T_{ru})_{\theta_o}$.

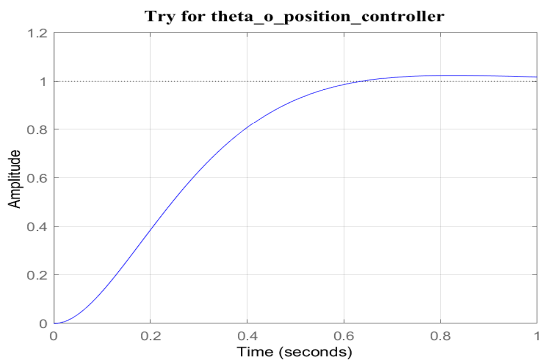

Figure 3.30: Output Response to Step Reference Command $(T_{ry})_{\theta_o}$.

Closed Loop Poles for Outer Elevation Position Controller Design. The closed loop poles that result from our BLT (bilinear transformation) approach are as follows.

Table 3.6: Closed Loop Poles for Outer Elevation Position Controller Design.

Poles	**Damping**	**Frequency(rad/sec)**
$-5.15e+02$	$1.00e+00$	$5.15e+02$
$-4.78e+00+3.80e+00i$	$7.83e-01$	$6.11e+00$
$-4.78e+00-3.80e+00i$	$7.83e-01$	$6.11e+00$
$-3.42e-01$	$1.00e+00$	$3.42e-01$
$-9.97e-02$	$1.00e+00$	$9.97e-02$
$-4.03e-02$	$1.00e+00$	$4.03e-02$
$-1.00e-02$	$1.00e+00$	$1.00e-02$

As expected, all closed loop poles associated with outer elevation position controller design are at desirable locations - with damping $\zeta > 0.7$. Also it should be noted that, since $\gamma < 1$, this implies that our outer elevation position controller design specifications (reflected within our weighting functions) *were not too aggressive.*

The output graph for θ_o in the simulink block diagram after designing the outer elevation position controller is shown below. When the system is given a *100*° position input, the response of the system with the designed controller is as in the Fig 3.31.

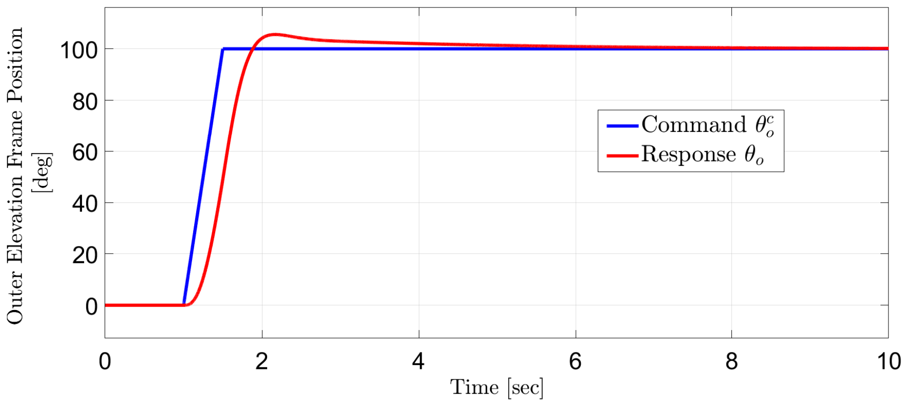

Figure 3.31: θ_o - Output Response (SISO System).

3.3.4 Inner Elevation Position Controller Design (SISO)

The plant that was used in the design of the inner elevation position controller was found in Equation 2.52 and is shown below.

$$Plant = P_{\theta_i} = G_{\tau_e \theta_i} = \frac{0.57955(s+0.1)}{s(s+0.3315)(s+0.03017)} \tag{3.33}$$

Weighting Functions and Design Parameters. Weighting function parameters and weighting functions were selected as follows:

$$\begin{aligned} Ms_{\theta_i} &= 10 \\ \omega_{b\theta_i} &= 2 * \pi * 0.7 \\ \epsilon_{\theta_i} &= 0.001 \\ Mu_{\theta_i} &= 10^{-6} \\ \omega_{bc\theta_i} &= [] \\ My_{\theta_i} &= [] \end{aligned} \tag{3.34}$$

Table 3.7: Weighting Functions and Design Parameters for θ_i.

$W1_{\theta_i}$	$W2_{\theta_i}$	$W3_{\theta_i}$
$Ms_{\theta_i} = 10$, $\omega_{b\theta_i} = 2 * \pi * 0.7$, $\epsilon_{\theta_i} = 0.001$	$Mu_{\theta_i} = 10^{-6}$	[]
$W1_{\theta_i}^{-1} = \frac{s + \epsilon\omega_{b\theta_i}}{\frac{s}{Ms_{\theta_i}} + \omega_{b\theta_i}} = \frac{s+0.004398}{0.1s+4.398}$	$W2_{\theta_i}^{-1} = \frac{1}{Mu_{\theta_i}} = 10^6$	$W3_{\theta_i}^{-1} = \frac{\omega_{bc\theta_i}}{s + \frac{\omega_{bc\theta_i}}{My_{\theta_i}}} = []$

Very lightly damped closed loop poles, which are unacceptable in some design, have been observed. To prevent this undesirable plant pole inversion, we use the *bilinear transformation.*

Bilinear Transformation Parameters. The bilinear transformation (BLT) parameters were selected as follows:

$$\begin{aligned} p_{1\theta_i} &= -2 \\ p_{2\theta_i} &= -10^8 \end{aligned} \tag{3.35}$$

This selection results in

$$\begin{aligned} s &= \frac{\hat{s} + p_{1\theta_i}}{\frac{\hat{s}}{p_{2\theta_i}} + 1} = \frac{\hat{s} - 2}{\frac{\hat{s}}{-10^8} + 1} \approx \hat{s} - 2 \qquad \text{(inverse transformation)} \\ \hat{s} &\approx s + 2 \qquad \text{(transformation)} \end{aligned} \tag{3.36}$$

The transform performans a rightward ("destabilizing") shift. The inverse transform performs a leftward ("stabilizing") shift. The resulting minimum γ was found to be

$$\gamma = 0.1284 \tag{3.37}$$

Since $\gamma < 1$, this implies that our design specification were not too aggressive.

The resulting s-domain controller is given by

$$\begin{aligned} K_{\theta_i} &= \frac{0.60836(s + 10^8)(s + 2.331)(s + 2.03)(s + 2)}{(s + 5253)(s + 198)(s + 2.1)(s + 2.004)} \\ &\approx \frac{0.60836(s + 10^8)(s + 2.331)(s + 2.03)(s + 2)}{s(s + 5253)(s + 198)(s + 2.1)} \end{aligned} \tag{3.38}$$

Frequency Responses. Figures 3.32-3.38 contains relevant frequency responses for *inner elevation position controller.*

The frequency response of the plant is given in Fig 3.32.

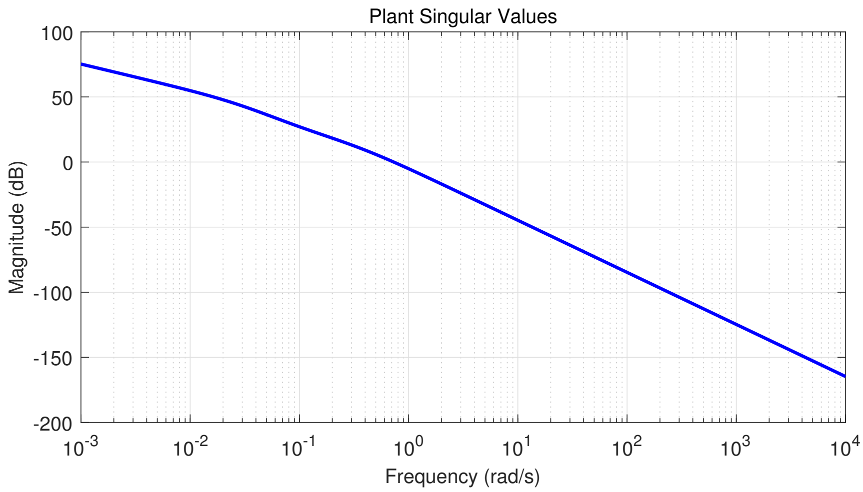

Figure 3.32: Plant Frequency Response - $P_{\theta_i} = \frac{0.57955(s+0.1)}{s(s+0.3315)(s+0.03017)}$.

The frequency response of the controller is given in Fig 3.33.

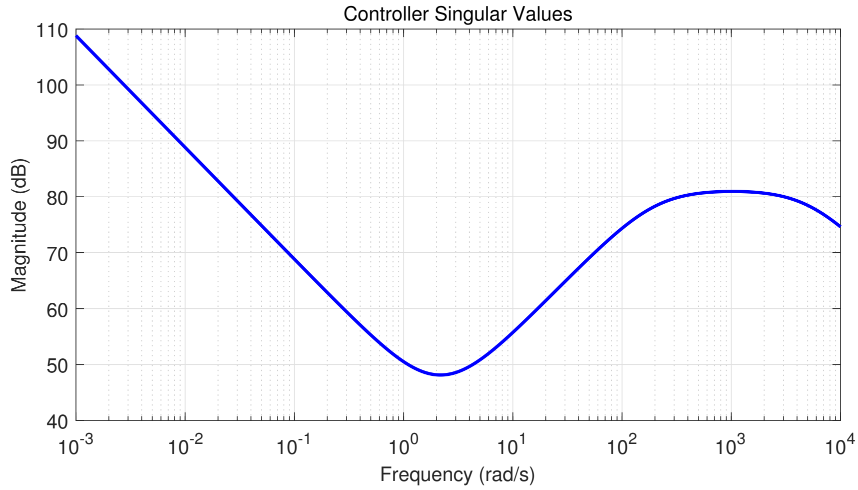

Figure 3.33: Controller Frequency Response - K_{θ_i}.

The open loop transfer function is given in Fig 3.34. As can be seen from the figure the open loop bandwidth is about 34 rad/sec.

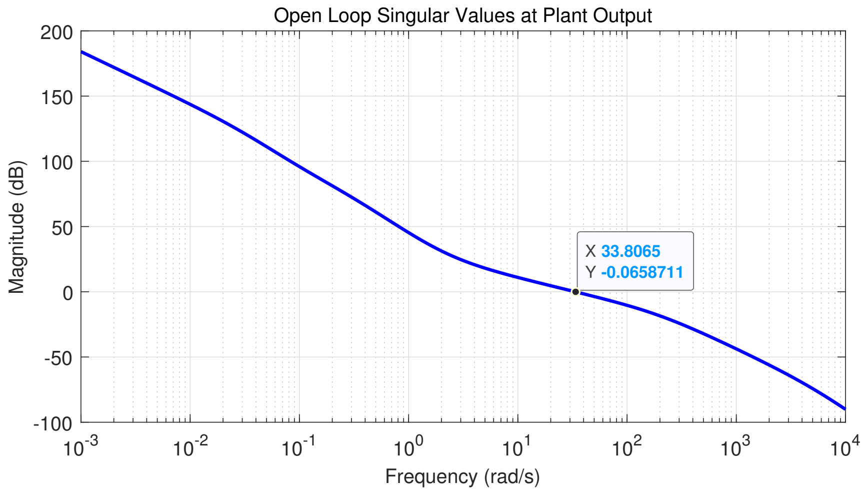

Figure 3.34: Open Loop Frequency Response - $L_{\theta_i} = P_{\theta_i} K_{\theta_i}$.

The frequency response of the sensitivity is given in Fig 3.35. Sensitivity frequency response is $|S|_\infty < |W_1^{-1}|_\infty$. The frequency response of sensitivity transfer function is as expected, i.e. small at low frequencies, and near unity (0 dB) at high frequencies.

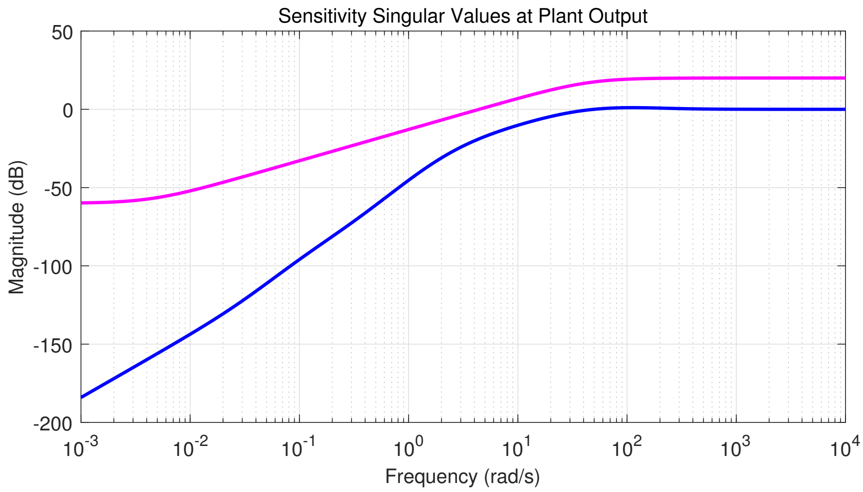

Figure 3.35: Sensitivity Frequency Response - $S_{\theta_i} = \frac{1}{1+P_{\theta_i}K_{\theta_i}} = (T_{doy})_{\theta_i}$.

The complementary sensitivity transfer function is given in Fig 3.36. As can be seen from the figure the complementary sensitivity bandwidth is approximately about 46 rad/sec. The frequency response of complementary sensitivity transfer function is as expected, i.e. small at high frequencies, and near unity (0 dB) at low frequencies.

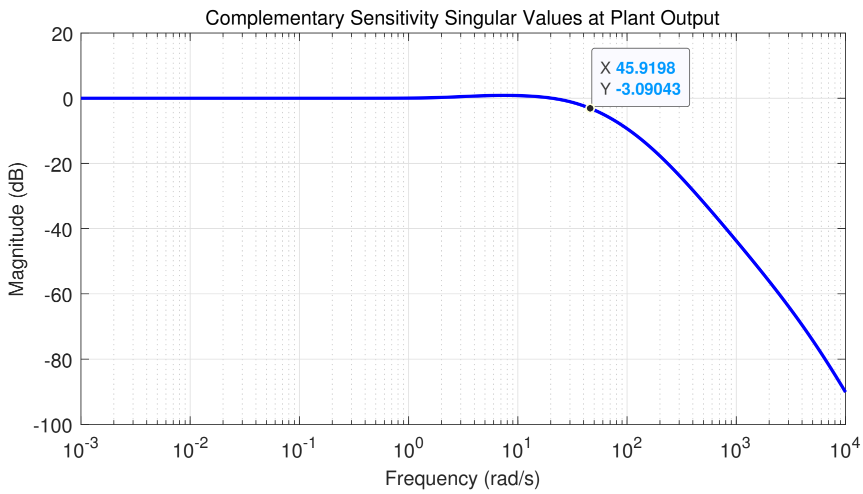

Figure 3.36: Complementary Sensitivity Frequency Response - $(T_o)_{\theta_i} = \frac{P_{\theta_i}K_{\theta_i}}{1+P_{\theta_i}K_{\theta_i}}$.

Control frequency response is given in Fig 3.37.

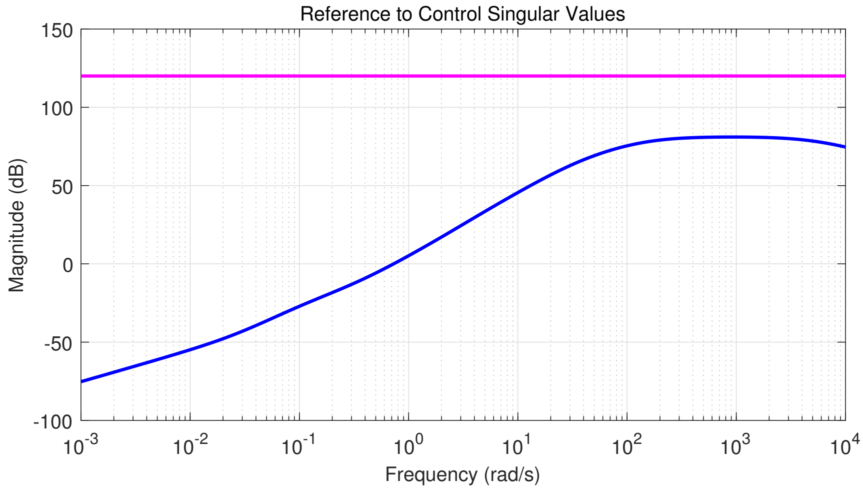

Figure 3.37: Reference to Control Frequency Response - $(T_{ru})_{\theta_i} = K_{\theta_i} S_{\theta_i}$.

Input disturbance to output frequency response is given in Fig 3.38. At very low frequencies, and high frequencies T_{diy} (Input disturbance singular value transfer function) is small as expected. For frequencies between 0.2 rad/sec and 18 rad/sec the disturbance rejection is poor.

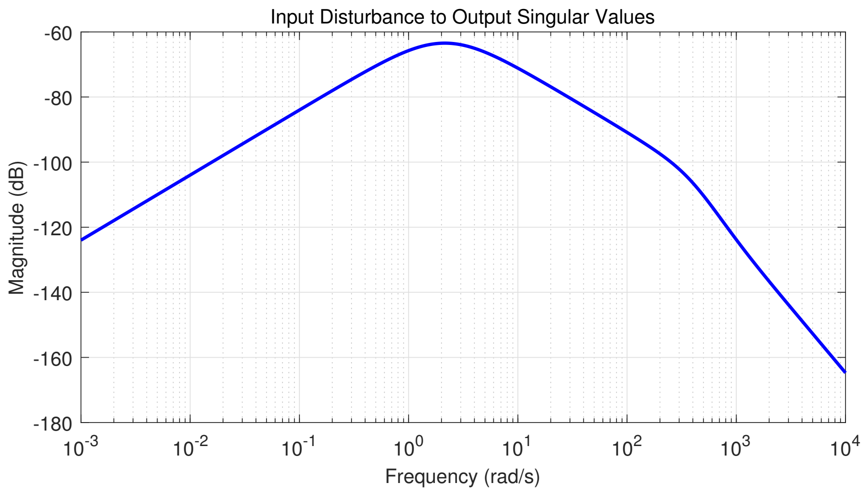

Figure 3.38: Input Disturbance to Output Frequency Response - $(T_{diy})_{\theta_i} = S_{\theta_i} P_{\theta_i}$.

Time Response Data: Step Command Following. We now address step command following for inner elevation position controller.

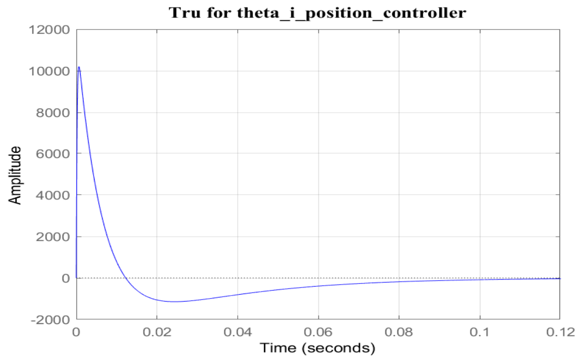

Figure 3.39: Control Response to Step Reference Command $(T_{ru})_{\theta_i}$.

Figure 3.40: Output Response to Step Reference Command $(T_{ry})_{\theta_i}$.

Closed Loop Poles for Inner Elevation Position Controller Design. The closed loop poles that result from our BLT (bilinear transformation) approach are as follows.

Table 3.8: Closed Loop Poles for Inner Elevation Position Controller Design.

Poles	**Damping**	**Frequency(rad/sec)**
$-5.25e+03$	$1.00e+00$	$5.25e+03$
$-1.54e+02$	$1.00e+00$	$1.54e+02$
$-3.77e+01$	$1.00e+00$	$3.77e+01$
$-1.00e-01$	$1.00e+00$	$1.00e-01$
$-3.07e+00$	$1.00e+00$	$3.07e+00$
$-1.78e+00$	$1.00e+00$	$1.78e+00$
$-2.00e+00$	$1.00e+00$	$2.00e+00$

As expected, all closed loop poles associated with inner elevation position controller design are at desirable locations - with damping $\zeta > 0.7$. Also it should be noted that, since $\gamma < 1$, this implies that our inner elevation position controller design specifications (reflected within our weighting functions) *were not too aggressive.*

The output graph for θ_i in the simulink block diagram after designing the inner elevation position controller is shown below Fig 3.41. Given *100*° to the outer elevation axis, it is expected that the inner elevation axis stays at or around *1*° - *2* °. It is seen that this situation is achieved with the designed SISO position controller.

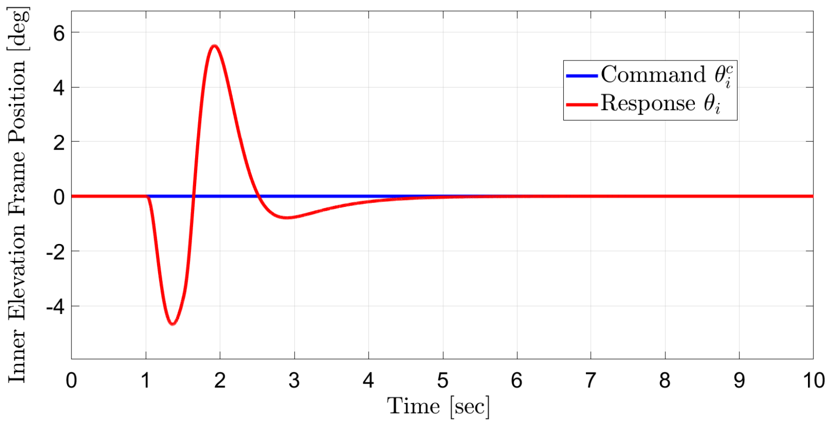

Figure 3.41: θ_i - Output Response (SISO System).

3.3.5 Outer-Inner Elevation Position Controller Design (MIMO)

The MIMO structure was created and analyzed only for the outer elevation and inner elevation frames.

Weighting Function Parameters. Weighting function parameters were selected as follows:

$$\begin{aligned}
(\omega_{b_1})_{\theta_o\theta_i} &= 2*\pi*0.1 & (\omega_{b_2})_{\theta_o\theta_i} &= 2*\pi*0.5 \\
(M_{s_1})_{\theta_o\theta_i} &= 10 & (M_{s_2})_{\theta_o\theta_i} &= 10 \\
(M_{u_1})_{\theta_o\theta_i} &= 10^{-3} & (M_{u_2})_{\theta_o\theta_i} &= 10^{-6} \\
(\omega_{bc_1})_{\theta_o\theta_i} &= [] & (\omega_{bc_2})_{\theta_o\theta_i} &= [] \\
(M_{y_1})_{\theta_o\theta_i} &= [] & (M_{y_2})_{\theta_o\theta_i} &= [] \\
\epsilon_{\theta_o\theta_i} &= 0.001
\end{aligned} \tag{3.39}$$

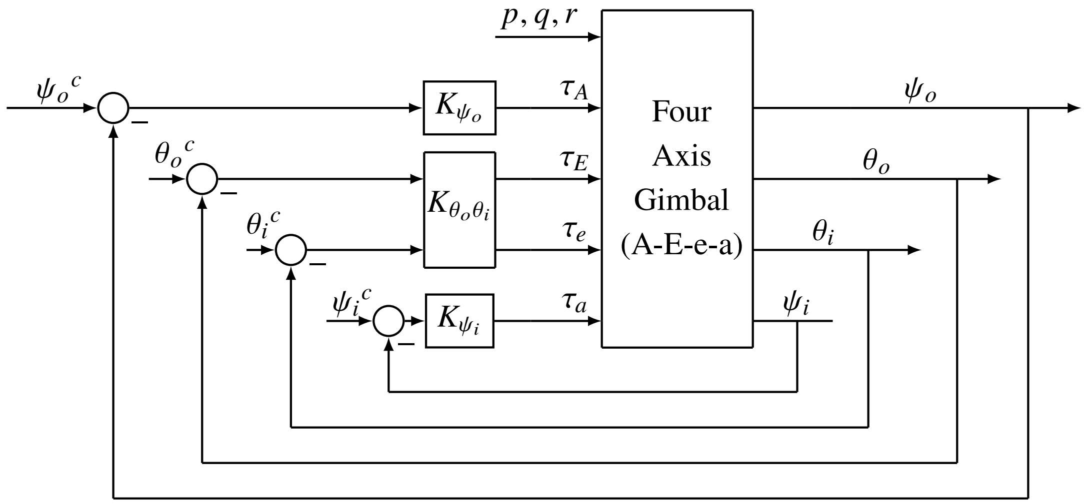

Figure 3.42: Gimbal Position Control (MIMO) - Closed Loop Structure.

Weighting Functions. Weighting functions were selected as follows:

$$
\begin{aligned}
{W_1}^{-1} &= \begin{bmatrix} \frac{s/(M_{s_1})_{\theta_o\theta_i}+(\omega_{b_1})_{\theta_o\theta_i}}{s+(\omega_{b_1})_{\theta_o\theta_i}\epsilon_{\theta_o\theta_i}} & 0 \\ 0 & \frac{s/(M_{s_2})_{\theta_o\theta_i}+(\omega_{b_2})_{\theta_o\theta_i}}{s+(\omega_{b_2})_{\theta_o\theta_i}\epsilon_{\theta_o\theta_i}} \end{bmatrix}^{-1} \\
&= \begin{bmatrix} \frac{s+0.0006283}{0.1s+0.6283} & 0 \\ 0 & \frac{s+0.003142}{0.1s+3.142} \end{bmatrix}
\end{aligned}
\tag{3.40}
$$

$$
\begin{aligned}
{W_2}^{-1} &= \begin{bmatrix} \frac{1}{(M_{u_1})_{\theta_o\theta_i}} & 0 \\ 0 & \frac{1}{(M_{u_2})_{\theta_o\theta_i}} \end{bmatrix}^{-1} \\
&= \begin{bmatrix} 10^3 & 0 \\ 0 & 10^6 \end{bmatrix}
\end{aligned}
\tag{3.41}
$$

$$
{W_3}^{-1} = \begin{bmatrix} [] & [] \\ [] & [] \end{bmatrix}^{-1} = [] \tag{3.42}
$$

Very lightly damped closed loop poles, which are unacceptable in some design, have been observed. To prevent this undesirable plant pole inversion, we use the *bilinear transformation.*

Bilinear Transformation Parameters. The bilinear transformation (BLT) parameters were selected as follows:

$$
\begin{aligned}
p_{1_{\theta_o\theta_i}} &= -0.8 \\
p_{2_{\theta_o\theta_i}} &= -10^8
\end{aligned}
\tag{3.43}
$$

This selection results in

$$
\begin{aligned}
s &= \frac{\hat{s} + p_{1_{\theta_o\theta_i}}}{\frac{\hat{s}}{p_{2_{\theta_o\theta_i}}} + 1} = \frac{\hat{s} - 0.8}{\frac{\hat{s}}{-10^8} + 1} \approx \hat{s} - 1.8 \qquad \text{(inverse transformation)} \\
\hat{s} &\approx s + 0.8 \qquad \text{(transformation)}
\end{aligned}
\tag{3.44}
$$

The plant was transformed using the above bilinear transformation. The transformation essentially moves all poles and zeros to the right 0.8 unit. A design was obtained using the generalized plant (including the transformed plant and weighting functions).The resulting minimum γ was found to be

$$\gamma = 0.1602 \tag{3.45}$$

Since $\gamma < 1$, this implies that our design specification were not too aggressive.

Frequency Responses. Figures 3.43-3.49 contain relevant frequency responses for *outer elevation- inner elevation (MIMO) position controller.*

The frequency response of the plant is given in Fig 3.43.

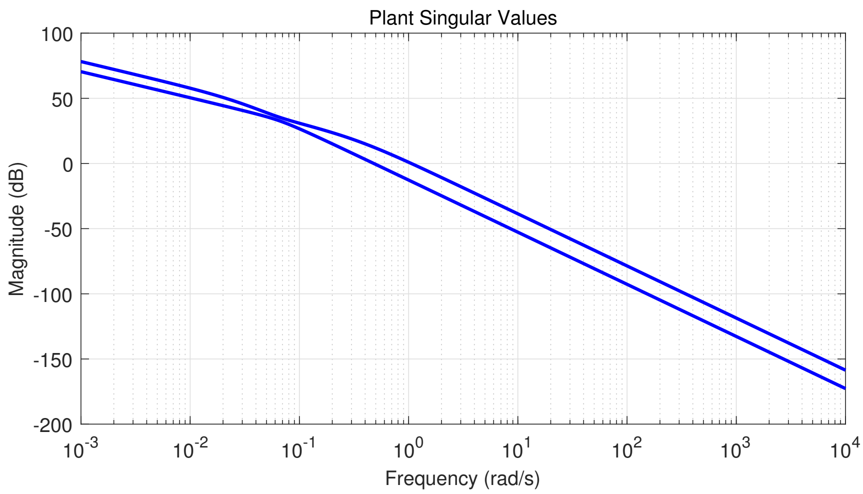

Figure 3.43: Plant Singular Values - $P_{\theta_o\theta_i}$.

The frequency response of the controller is given in Fig 3.44.

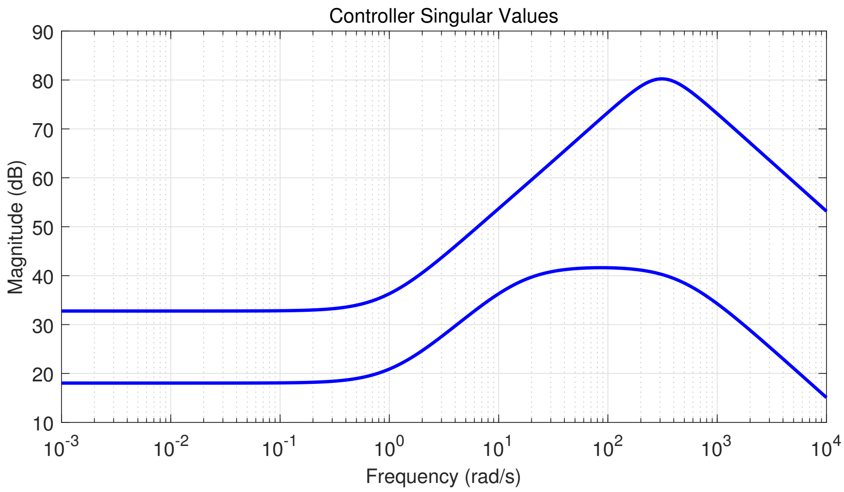

Figure 3.44: Controller Singular Values - $K_{\theta_o \theta_i}$.

The open loop transfer function is given in Fig 3.45. As can be seen from the figure the open loop bandwidts are about 3.4 rad/sec and 30.2 rad/sec.

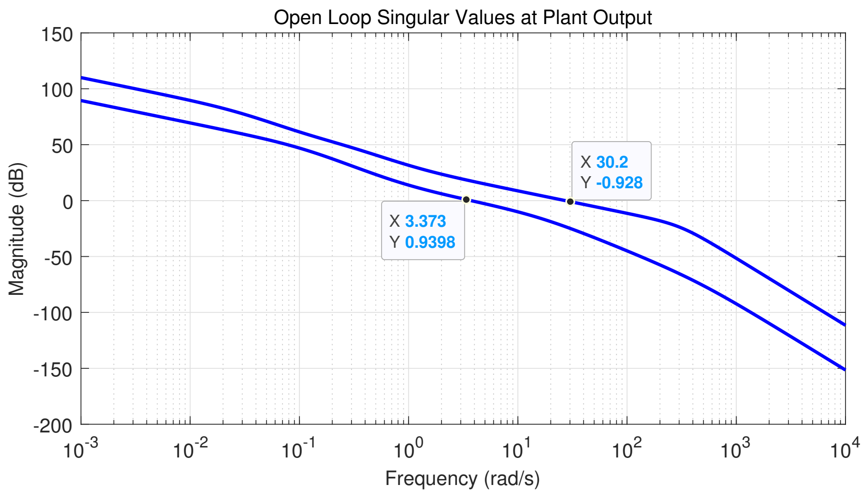

Figure 3.45: Open Loop Singular Values at Plant Output - $(L_o)_{\theta_o \theta_i} = P_{\theta_o \theta_i} K_{\theta_o \theta_i}$.

The frequency response of the sensitivity is given in Fig 3.46. Sensitivity frequency response is $|S|_\infty < |W_1^{-1}|_\infty$. The frequency response of sensitivity transfer function is as expected, i.e. small at low frequencies, and near unity (0 dB) at high frequencies.

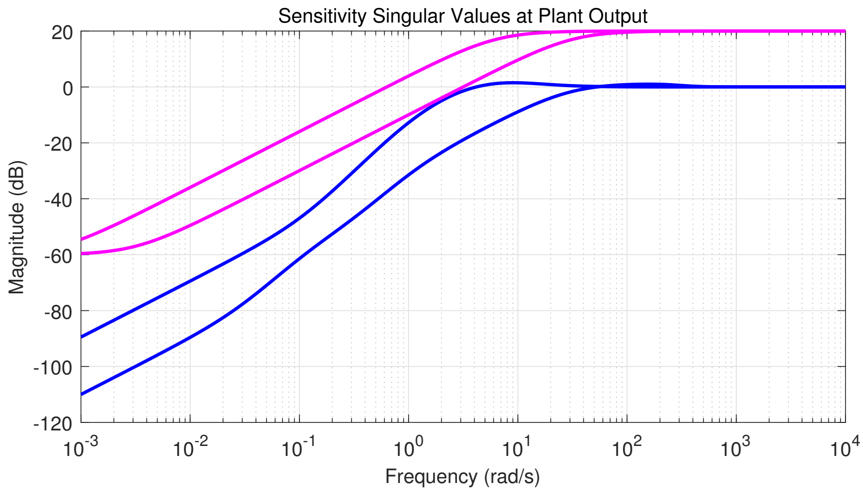

Figure 3.46: Sensitivity Singular Values at Plant Output - $(S_o)_{\theta_o\theta_i} = [I + P_{\theta_o\theta_i}K_{\theta_o\theta_i}]^{-1}$.

The complementary sensitivity transfer function is given in Fig 3.47. As can be seen from the figure the complementary sensitivity bandwidths are approximately about 6 rad/sec and 33 rad/sec. The frequency response of complementary sensitivity transfer function is as expected, i.e. small at high frequencies, and near unity (0 dB) at low frequencies.

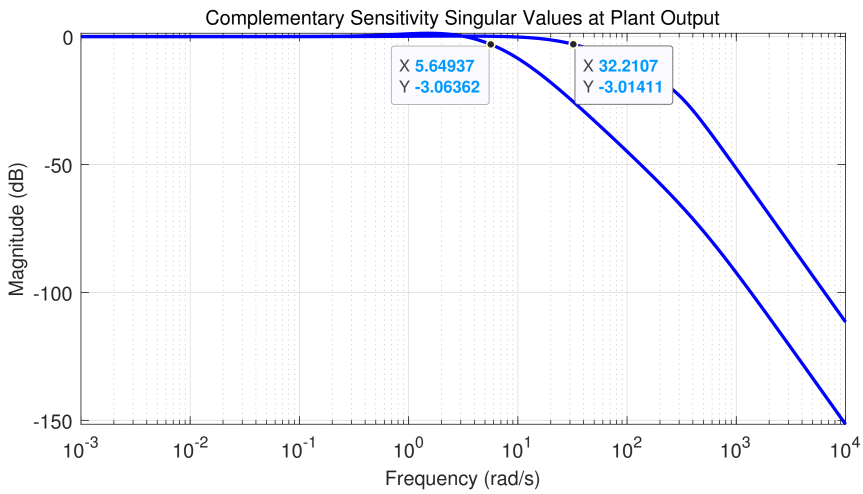

Figure 3.47: Complementary Sensitivity Singular Values at Plant Output $(T_o)_{\theta_o\theta_i} = P_{\theta_o\theta_i}K_{\theta_o\theta_i}[I + P_{\theta_o\theta_i}K_{\theta_o\theta_i}]^{-1}$.

Control frequency response is given in Fig 3.48.

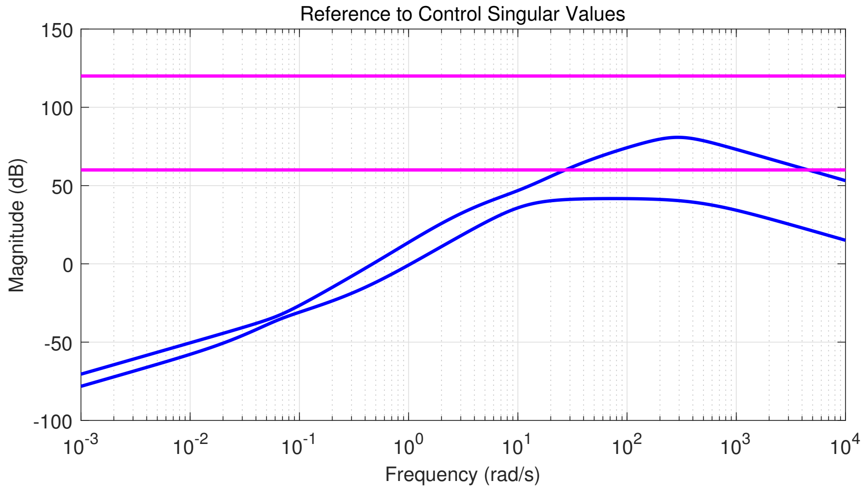

Figure 3.48: Reference to Control Frequency Response - $(T_{ru})_{\theta_o \theta_i} = K_{\theta_o \theta_i} S_{\theta_o \theta_i}$.

Input disturbance to output frequency response is given in Fig 3.49. At very low frequencies, and high frequencies T_{diy} (Input disturbance singular value transfer function) is small as expected. For frequencies between 10^{-3} and 1 the disturbance rejection is poor.

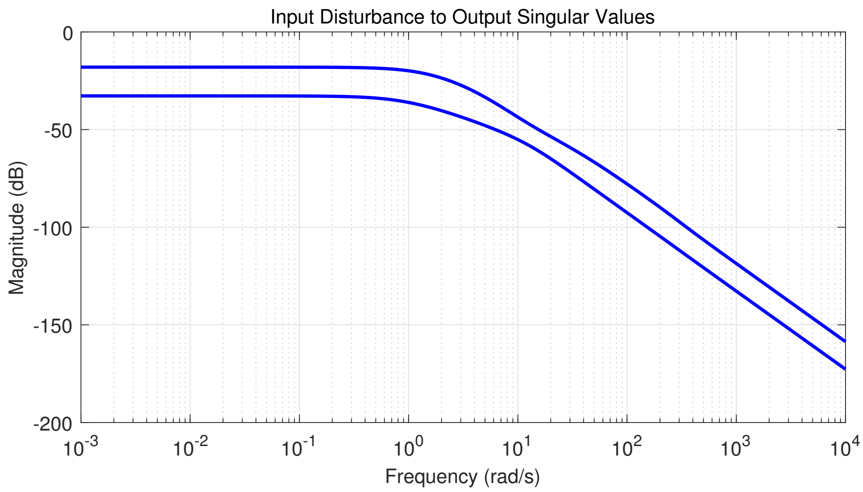

Figure 3.49: Input Disturbance to Output Frequency Response - $(T_{diy})_{\theta_o \theta_i} = S_{\theta_o \theta_i} P_{\theta_o \theta_i}$.

Time Response Data: Step Command Following. We now address step command following for outer elevation-inner elevation (MIMO) position controller.

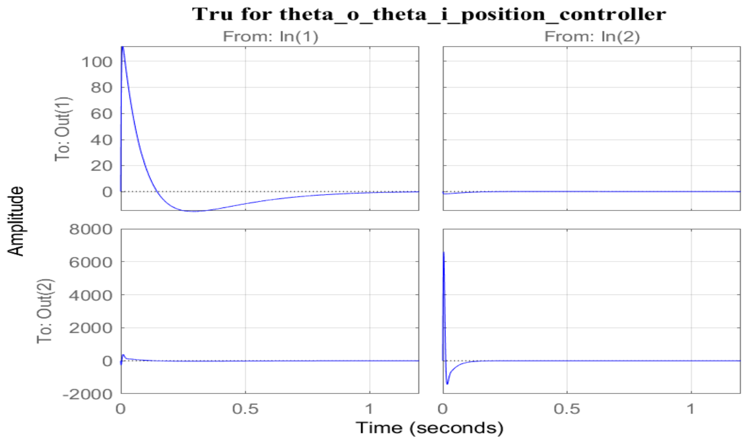

Figure 3.50: Control Response to Step Reference Command $(T_{ru})_{\theta_o\theta_i}$.

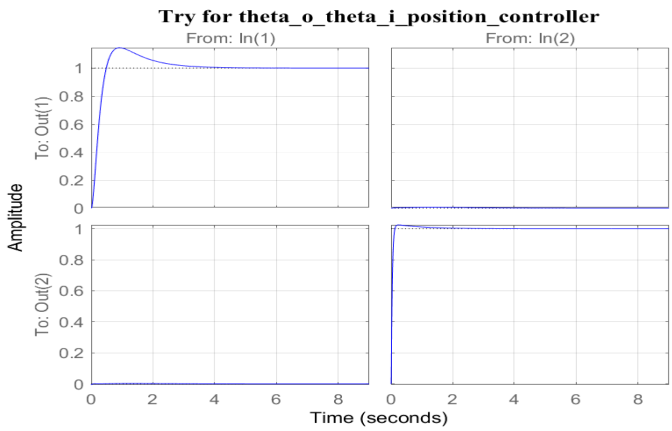

Figure 3.51: Output Response to Step Reference Command $(T_{ry})_{\theta_o\theta_i}$.

Closed Loop Poles for Outer Elevation Inner Elevation (MIMO) Position Controller Design. The closed loop poles that result from our BLT (bilinear transformation) approach are as follows.

Table 3.9: Closed Loop Poles for Outer Elevation-Inner Elevation (MIMO) Position Controller Design.

Poles	Damping	Frequency(rad/sec)
$-4.57e+02$	$1.00e+00$	$4.57e+02$
$-2.06e+02+2.04e+02i$	$7.09e-01$	$2.90e+02$
$-2.06e+02-2.04e+02i$	$7.09e-01$	$2.90e+02$
$-3.03e+01$	$1.00e+00$	$3.03e+01$
$-1.05e+01$	$1.00e+00$	$1.05e+01$
$-3.98e+00$	$1.00e+00$	$3.98e+00$
$-3.02e-02$	$1.00e+00$	$3.02e-02$
$-3.31e-01$	$1.00e+00$	$3.31e-01$
$-1.36e+00$	$1.00e+00$	$1.36e+00$
$-1.13e+00$	$1.00e+00$	$1.13e+00$
$-9.96e-01$	$1.00e+00$	$9.96e-01$
$-8.30e-01$	$1.00e+00$	$8.30e-01$
$-8.01e-01$	$1.00e+00$	$8.01e-01$
$-8.00e-01$	$1.00e+00$	$8.00e-01$

The output graphs for θ_o and θ_i in the simulink block diagram after designing the outer and inner elevation position controller (MIMO) is shown below Fig 3.52 and Fig 3.53. Given *100*° to the outer elevation axis, it is expected that the inner elevation axis stays at or around *0*° It is seen that this situation is achieved with the designed MIMO position controller.

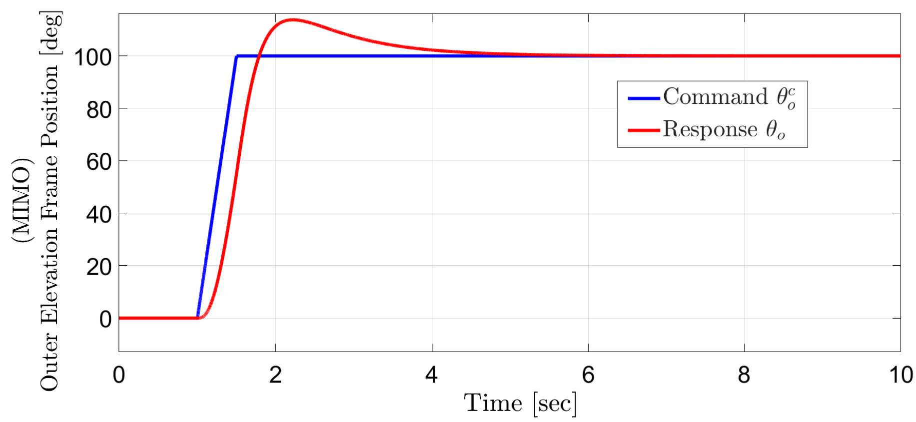

Figure 3.52: θ_o - Output Response (MIMO System).

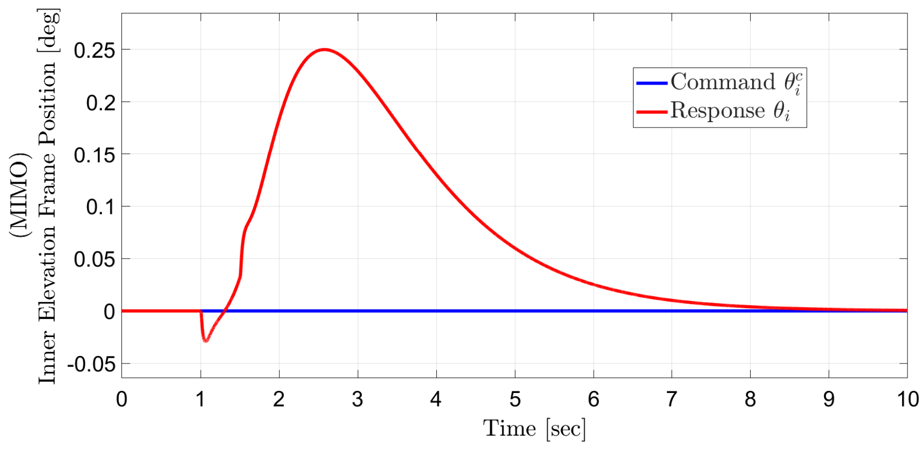

Figure 3.53: θ_i - Output Response (MIMO System).

The system responses against the position controllers designed for the four axis gimbal model are shown in a single figure below, with each axis seperately. In Fig 3.54 SISO controllers are designed for all axes and their responses are given.

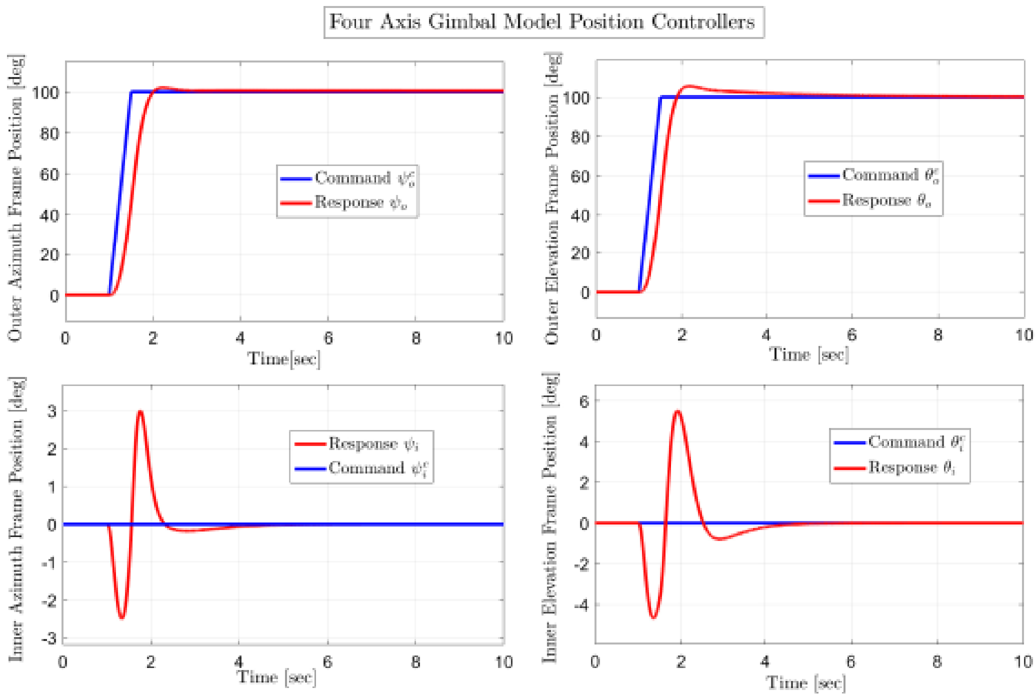

Figure 3.54: Four Axis Gimbal Model Position Controllers.

In Fig 3.55, the MIMO controllers were designed only for the outer and inner elevation frames, and the other frames remained as SISO controllers.

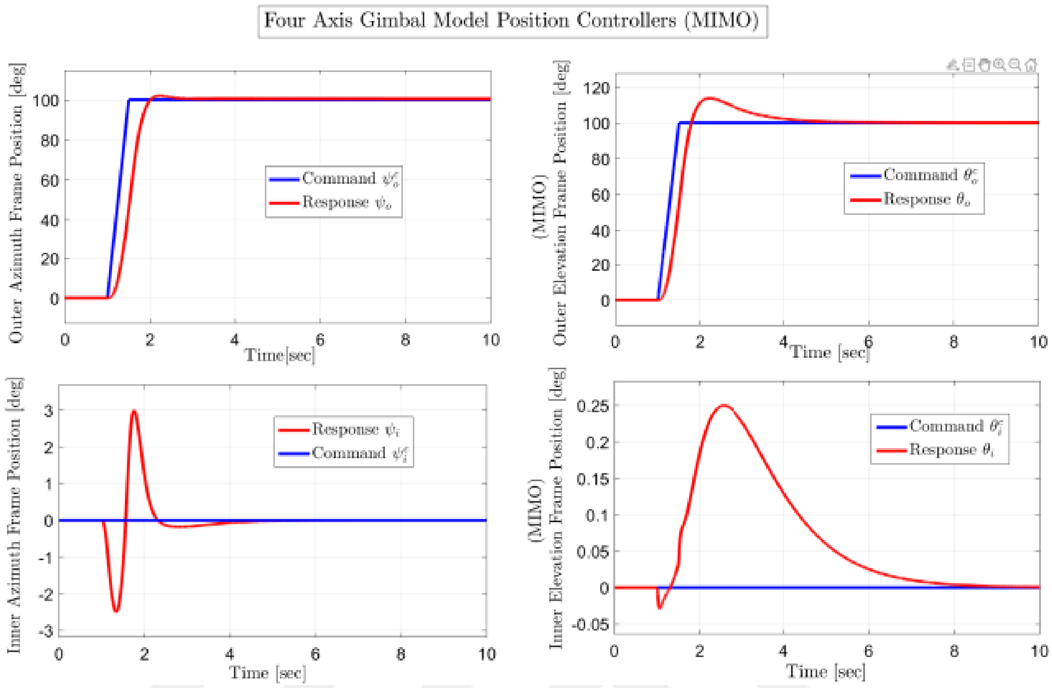

Figure 3.55: Four Axis Gimbal Model Position Controllers .

When Fig 3.54 and Fig 3.55 are compared, it is clear that the responses in Fig 3.55 are better. Because it has been seen that at a position of *100°* given to the outer elevation, the inner elevation moves much closer to *0°*. In other words, it is understood that the performance of H_∞ MIMO controllers designed for outer elevation and inner elevation is better.

3.4 Rate Controller Design

The rate control structure of the closed loop system is described in Fig 3.56. Four axis gimbal block includes the models developed in Fig 2.9. When the gimbal model is combined, it becomes a 5-input 6-output system. τ_A, τ_E, τ_e, and τ_a denote to the torque inputs applied to the outer azimuth frame, outer elevation frame, inner elevation frame, and inner azimuth frame, respectively. As previously stated, the platform's angular rate vector, $[pqr]^T$, is regarded as a source of disturbance. K_{ω_z} and K_{ω_y} are rate controllers to control ω_z and ω_y. ${\omega_z}^c$, ${\omega_y}^c$ are the command signal applied to the system.

The first of the important points in the rate controller is that the system is following the reference signal. The other is the values of ψ_o, θ_o, θ_i and ψ_i angles measured at the output after ${\omega_z}^c$ and ${\omega_y}^c$ given to the system. It is critical that the inner axis angle values (θ_i and ψ_i) are not too large in here.

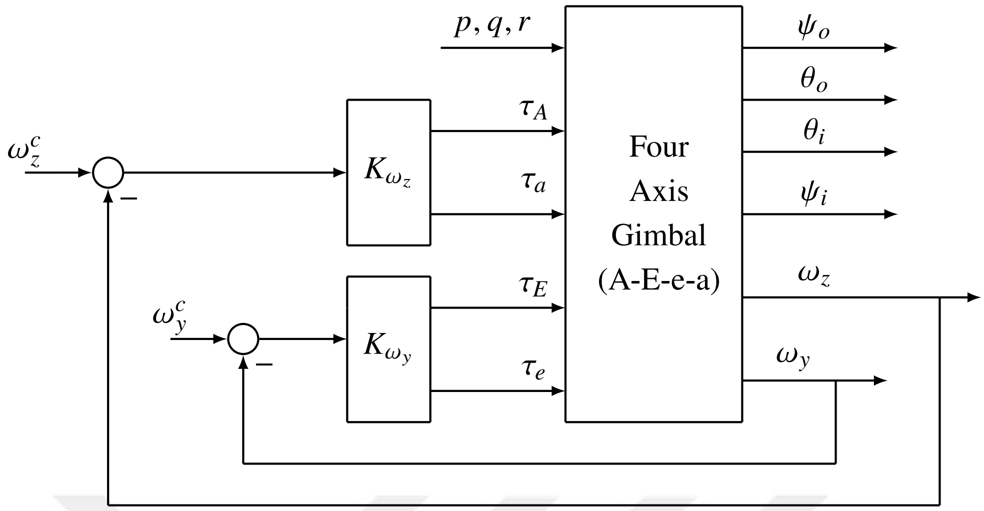

Figure 3.56: Gimbal Rate Control - Closed Loop Structure.

3.4.1 ω_z Rate Controller Design

The internal structure of the K_{ω_z} rate controller is depicted in Fig 3.57. The goal here is to ensure that the outer axis makes low-frequency movements and the inner axis makes high-frequency movements. A low pass filter is placed on the outer axis in the upper channel and a high pass filter is placed on the inner axis in the lower channel for this purpose. The parameters, frequency, and time responses of the controllers designed in MATLAB with this structure are detailed below.

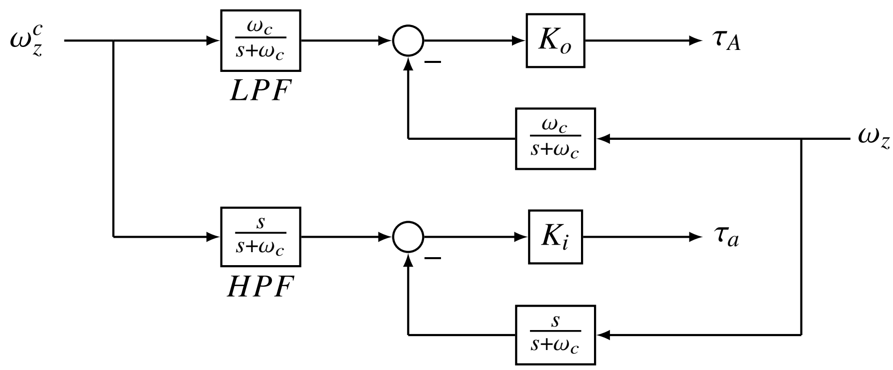

Figure 3.57: Controller K_{ω_z}'s Internal Structure.

In the system expressed by Fig 3.57 the upper canal plant from τ_A to ω_z is the

$$P_o = G_{\tau_A \omega_z} = \frac{0.038197}{(s+0.1)^2}. \tag{3.46}$$

The controller designed using the H_∞ methodology for this plant is K_o. LPF (low pass filter) and HPF (high pass filter) are designed to be complementary with each other. ω_c is the system's cut off frequency, which was set to 0.5 Hz.

$$P_i = G_{\tau_a \omega_z} = \frac{1.0528}{(s+0.1)} \tag{3.47}$$

is the lower channel plant from τ_a to ω_z. K_i is the controller designed to the plant. The designed controllers' frequency responses are shown below.

Frequency Responses. Figures 3.58-3.64 contain relevant frequency responses for w_z *outer rate controller.* (K_o)

The frequency response of the plant is given in Fig 3.58.

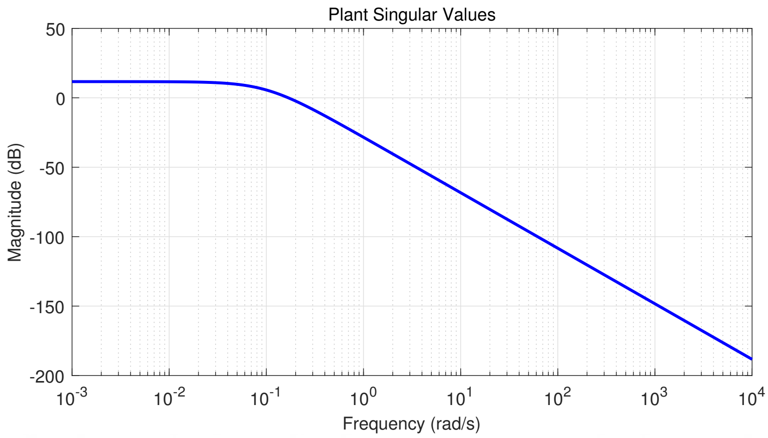

Figure 3.58: Plant Frequency Response - $P_{\tau_A \omega_z} = \frac{0.038197}{(s+0.1)^2}$.

The frequency response of the controller is given in Fig 3.59.

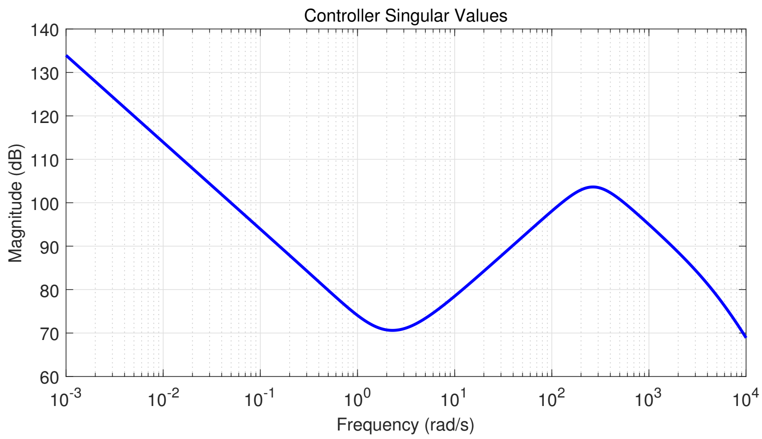

Figure 3.59: Controller Frequency Response - $K_{\tau_A \omega_z} = K_o$.

The open loop transfer function is given in Fig 3.60. As can be seen from the figure the open loop bandwidth is about 33 rad/sec.

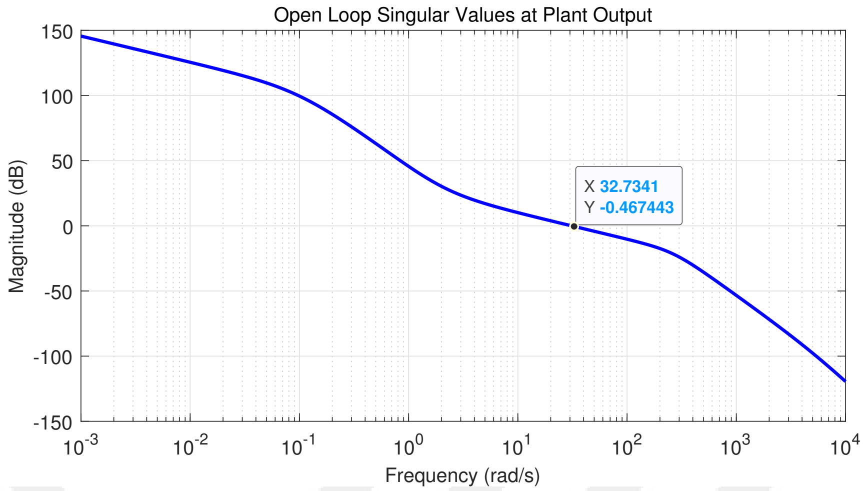

Figure 3.60: Open Loop Frequency Response - $L = PK$.

The frequency response of the sensitivity is given in Fig 3.61. Sensitivity frequency response is $|S|_\infty < |W_1^{-1}|_\infty$. The frequency response of sensitivity transfer function is as expected, i.e. small at low frequencies, and near unity (0 dB) at high frequencies.

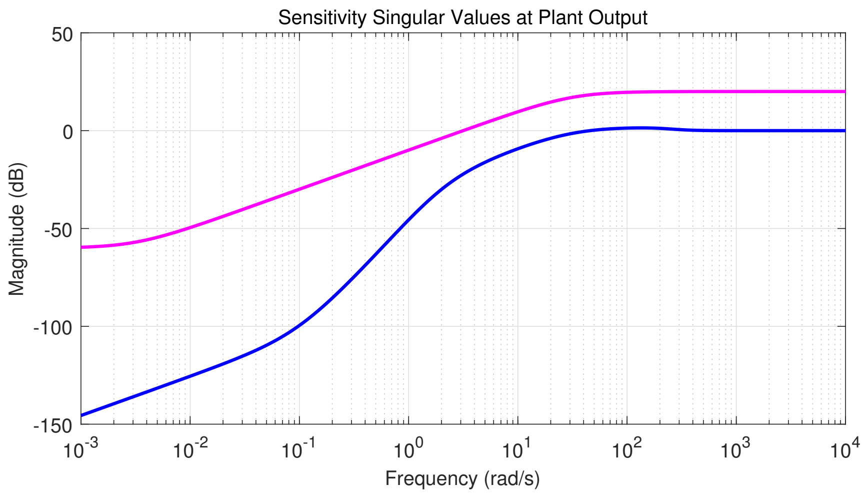

Figure 3.61: Sensitivity Frequency Response - $S = \frac{1}{1+PK} = T_{doy}$.

The complementary sensitivity transfer function is given in Fig 3.62. As can be seen from the figure the complementary sensitivity bandwidth is approximately about 43 rad/sec. The frequency response of complementary sensitivity transfer function is as expected, i.e. small at high frequencies, and near unity (0dB) at low frequencies.

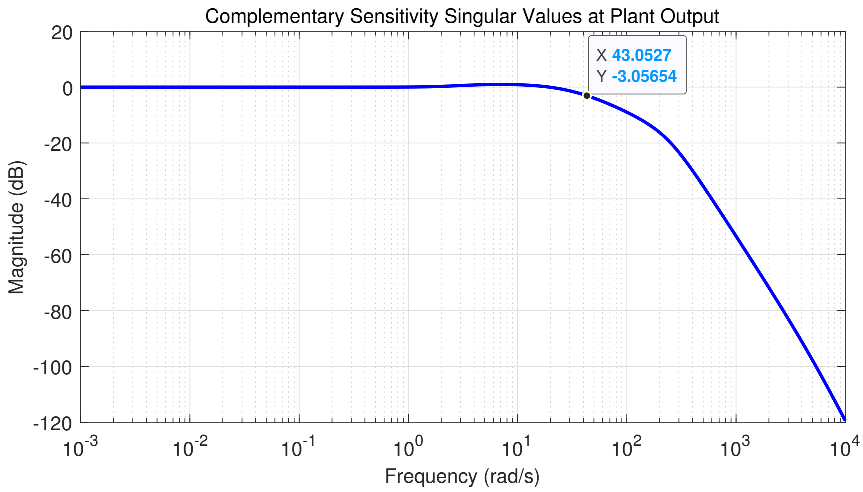

Figure 3.62: Complementary Sensitivity Frequency Response - $T_o = \frac{PK}{1+PK}$.

Control frequency response is given in Fig 3.63.

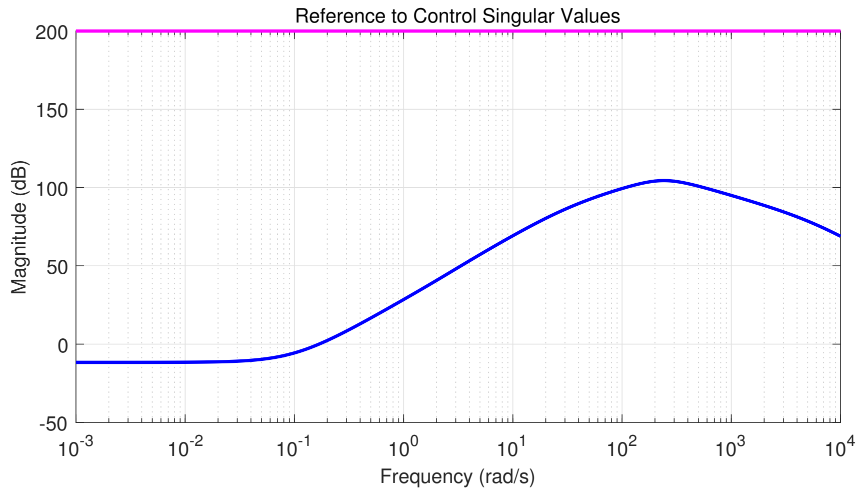

Figure 3.63: Reference to Control Frequency Response - $T_{ru} = KS$.

Input disturbance to output frequency response is given in Fig 3.64. At very low frequencies, and high frequencies T_{diy} (Input disturbance singular value transfer function) is small as expected. For frequencies between 0.5 rad/sec and 13 rad/sec the disturbance rejection is poor.

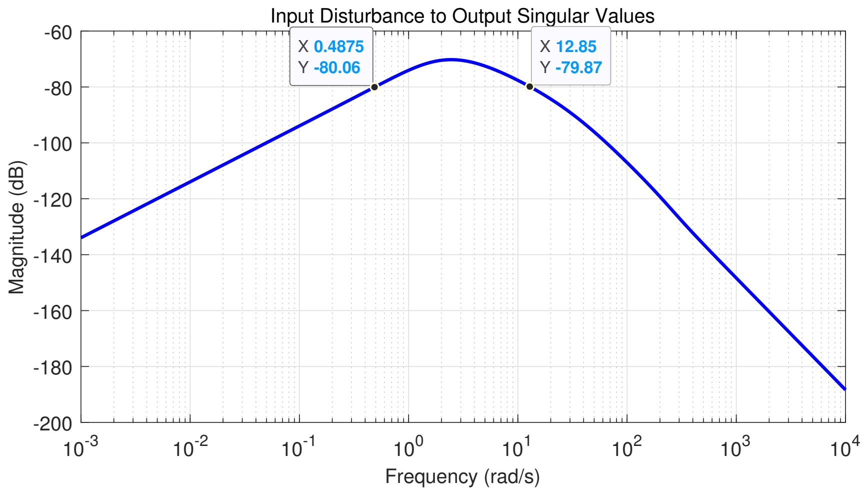

Figure 3.64: Input Disturbance to Output Frequency Response - $T_{diy} = SP$.

Frequency Responses. Figures 3.65-3.71 contain relevant frequency responses for w_z *inner rate controller.* (K_i)

The frequency response of the plant is given in Fig 3.65.

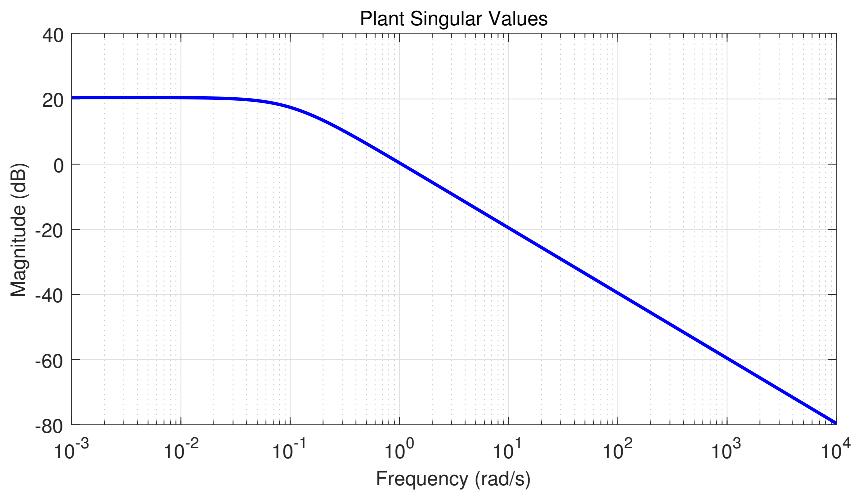

Figure 3.65: Plant Frequency Response - $P_{\tau_a \omega_z} = \frac{1.0528}{(s+0.1)}$.

The frequency response of the controller is given in Fig 3.66.

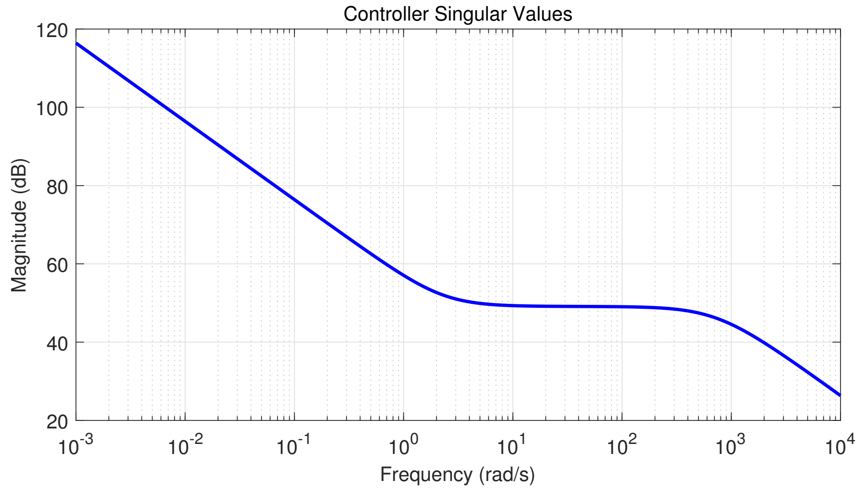

Figure 3.66: Controller Frequency Response - $K_{\tau_a \omega_z} = K_i$.

The open loop transfer function is given in Fig 3.67. As can be seen from the figure the open loop bandwidth is about 300 rad/sec.

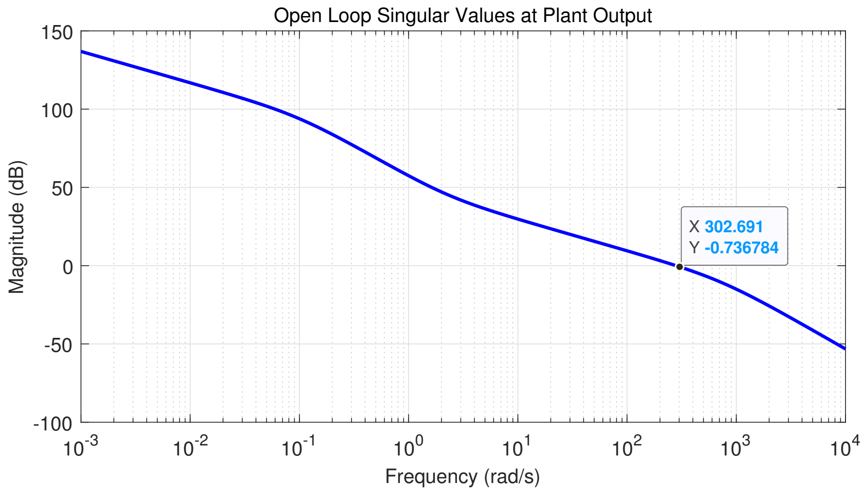

Figure 3.67: Open Loop Frequency Response - $L = PK$.

The frequency response of the sensitivity is given in Fig 3.68. Sensitivity frequency response is $|S|_\infty < |W_1^{-1}|_\infty$. The frequency response of sensitivity transfer function is as expected, i.e. small at low frequencies, and near unity (0 dB) at high frequencies.

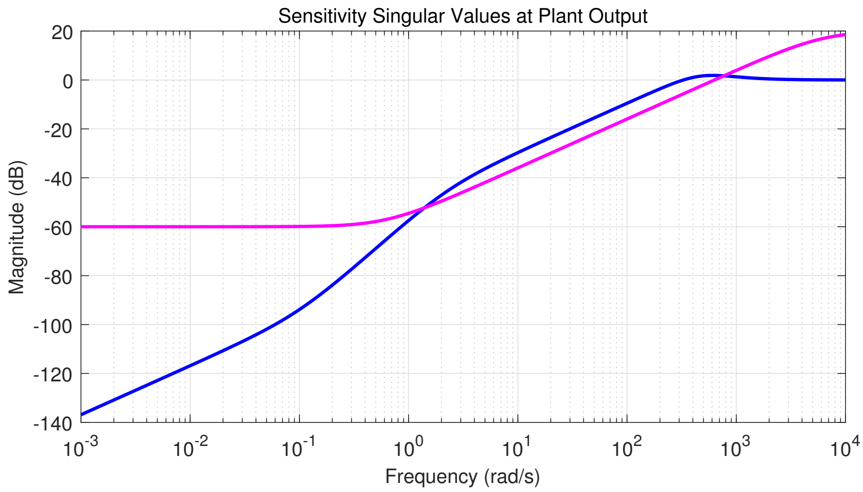

Figure 3.68: Sensitivity Frequency Response - $S = \frac{1}{1+PK} = T_{doy}$.

The complementary sensitivity transfer function is given in Fig 3.69. As can be seen from the figure the complementary sensitivity bandwidth is approximately about 420 rad/sec. The frequency response of complementary sensitivity transfer function is as expected, i.e. small at high frequencies, and near unity (0 dB) at low frequencies.

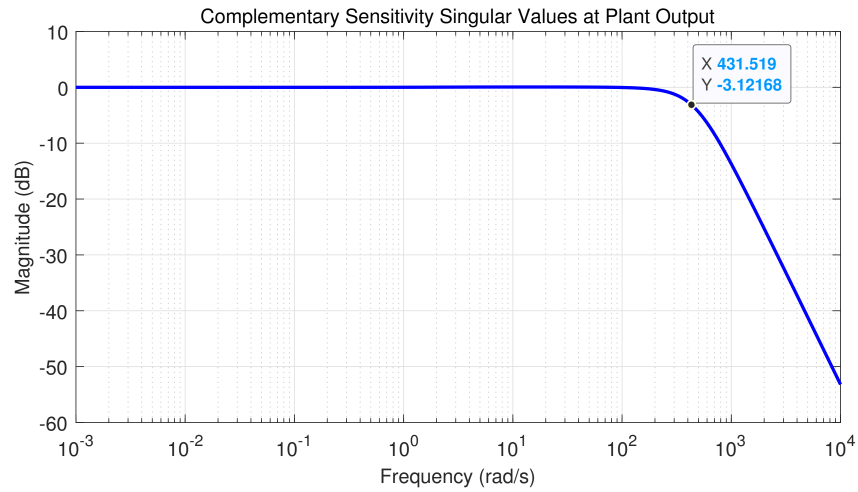

Figure 3.69: Complementary Sensitivity Frequency Response - $T_o = \frac{PK}{1+PK}$.

Control frequency response is given in Fig 3.70.

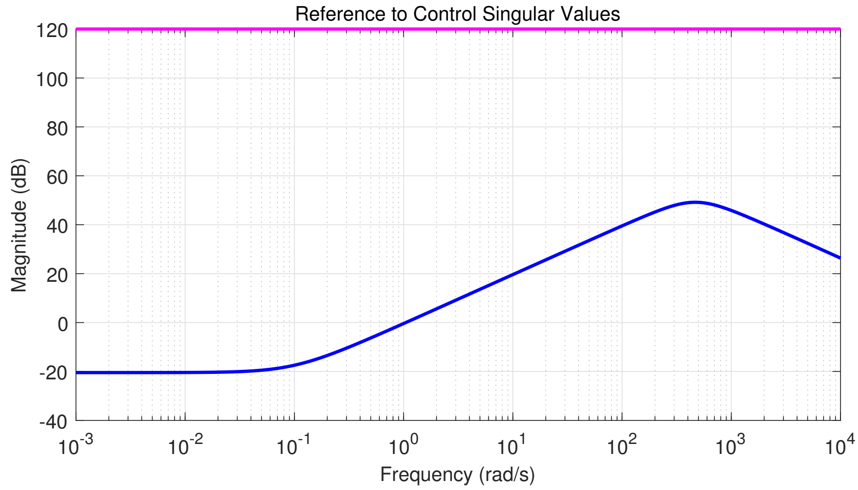

Figure 3.70: Reference to Control Frequency Response - $T_{ru} = KS$.

Input disturbance to output frequency response is given in Fig 3.71. At very low frequencies, and high frequencies T_{diy} (Input disturbance singular value transfer function) is small as expected. For frequencies between 2 rad/sec and 400 rad/sec the disturbance rejection is poor.

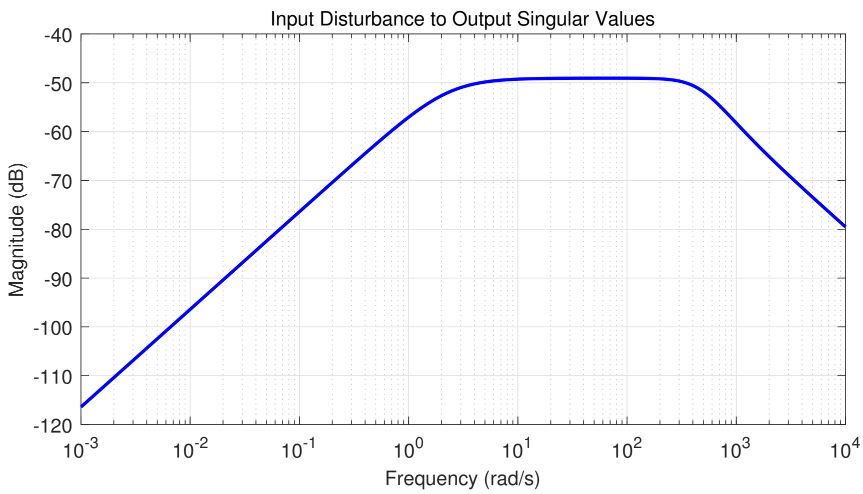

Figure 3.71: Input Disturbance to Output Frequency Response - $T_{diy} = SP$.

When the disturbance movements from the platform are 0 ($pqr = 0$), the effects of the ω_z rate controller designed for the four-axis gimbal system on command following, outer azimuth frame, and inner azimuth frame position are as Fig 3.72. While the rate command given to ω_z rotates the outer axis to any position, its effect on the inner axis is small.

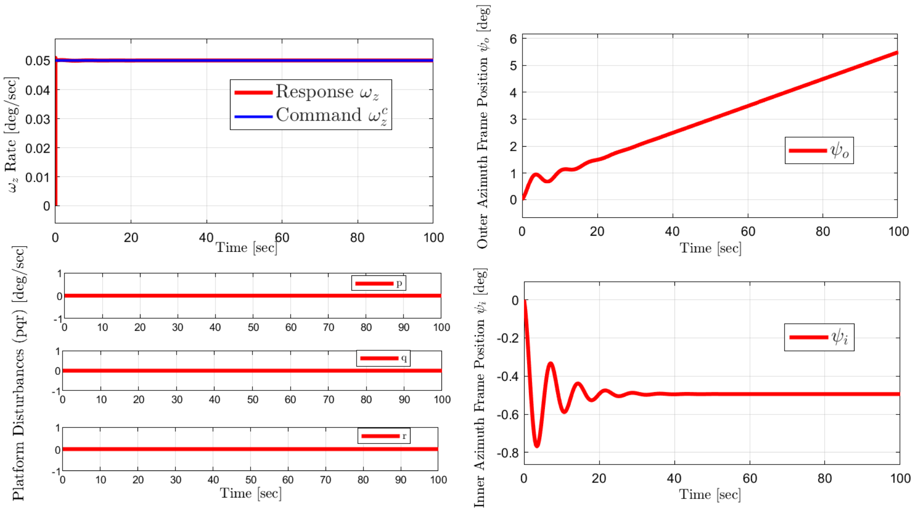

Figure 3.72: ω_z Rate Control Design .

When the disturbance from the platform is 100 deg/sec, the response of outer azimuth frame position and inner azimuth frame position is as follows. Inner azimuth frame movement of 1-2 degrees is acceptable.

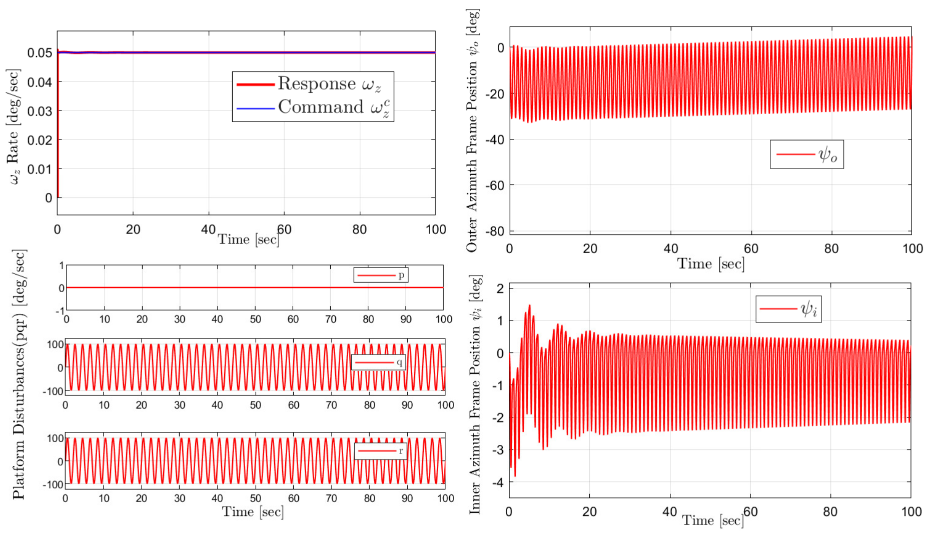

Figure 3.73: ω_z Rate Control Design via Platform Movement.

3.4.2 ω_y Rate Controller Design

The same structure in ω_z was used in the design of the ω_y rate controller.

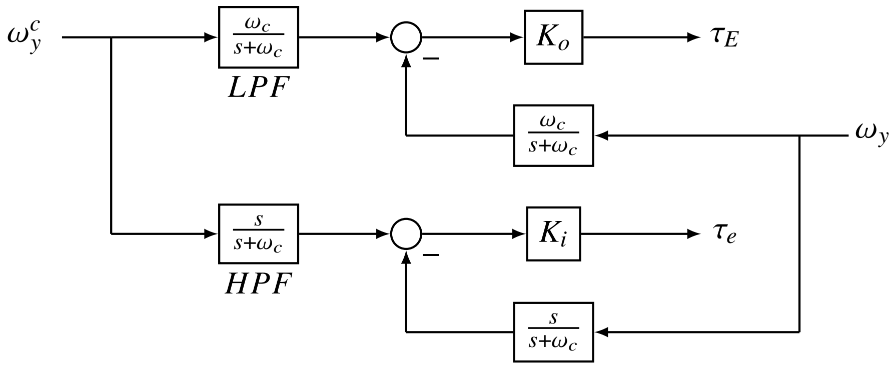

Figure 3.74: Controller K_{ω_y}'s Internal Structure.

In the system illustrated by Fig 3.74 the upper canal plant from τ_E to ω_y is

$$P_o = G_{\tau_E \omega_y} = \frac{-0.46846(s-0.1)}{(s+0.3315)(s+0.03017)}. \tag{3.48}$$

The controller designed using the H_∞ methodology for this plant is K_o. LPF (low pass filter) and HPF (high pass filter) are designed to be complementary with each other. ω_c is the system's cut off frequency, which was set to 0.5 Hz.

$$P_i = G_{\tau_e \omega_y} = \frac{0.57955(s+0.1808)}{(s+0.3315)(s+0.03017)} \tag{3.49}$$

is the lower channel plant from τ_e to ω_y. K_i is the controller designed to the plant. The designed controllers' frequency responses are shown below.

Frequency Responses. Figures 3.75-3.81 contain relevant frequency responses for w_y *inner rate controller. (K_i)*

The frequency response of the plant is given in Fig 3.75.

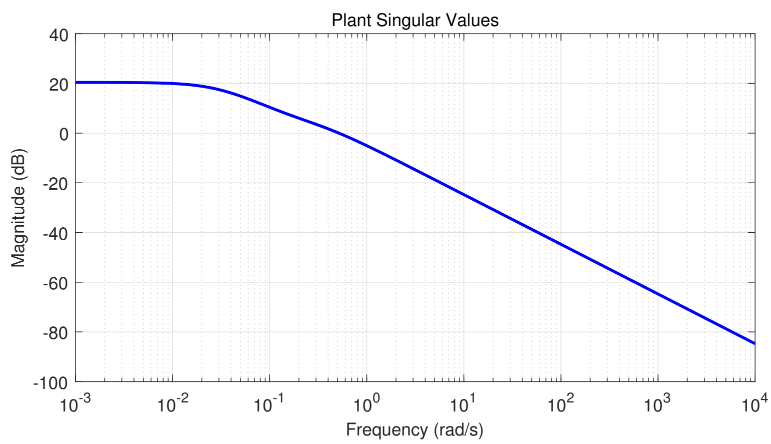

Figure 3.75: Plant Frequency Response - $P_{\tau_A \omega_z} = \frac{0.57955(s+0.1808)}{(s+0.3315)(s+0.03017)}$.

The frequency response of the controller is given in Fig 3.76.

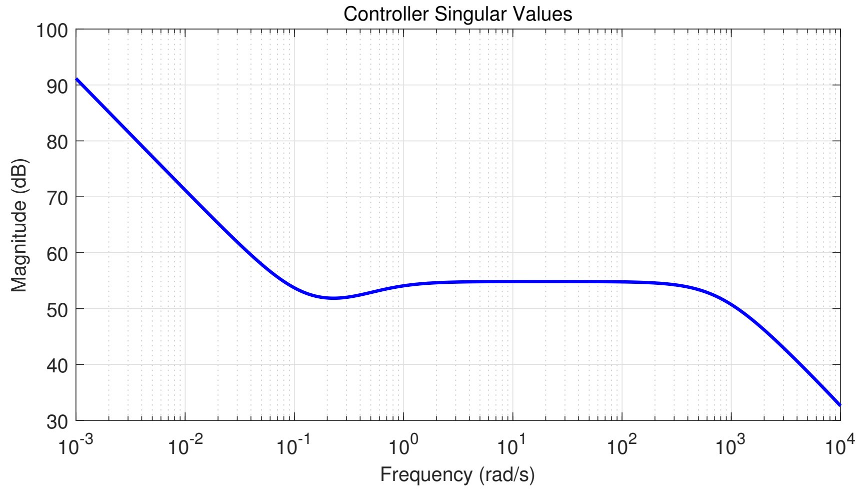

Figure 3.76: Controller Frequency Response - $K_{\tau_e \omega_y} = K_i$.

The open loop transfer function is given in Fig 3.77. As can be seen from the figure the open loop bandwidth is about 300 rad/sec.

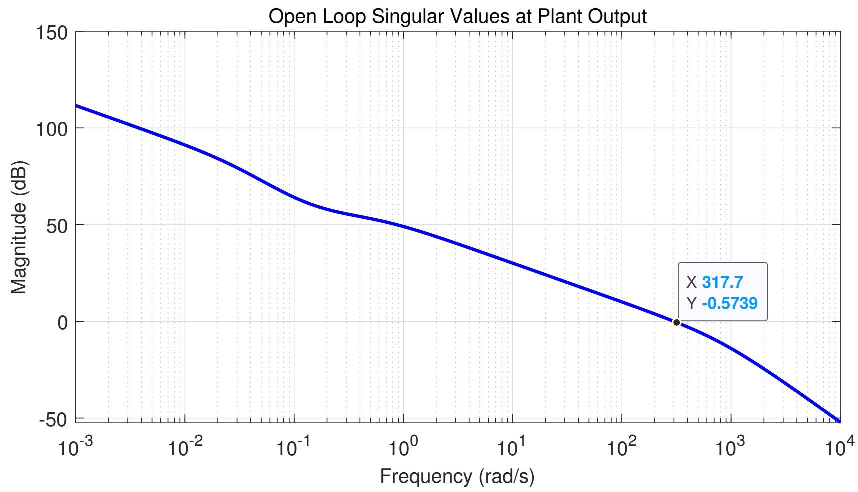

Figure 3.77: Open Loop Frequency Response - $L = PK$.

The frequency response of the sensitivity is given in Fig 3.78. Sensitivity frequency response is $|S|_\infty < |W_1^{-1}|_\infty$. The frequency response of sensitivity transfer function is as expected, i.e. small at low frequencies, and near unity (0dB) at high frequencies.

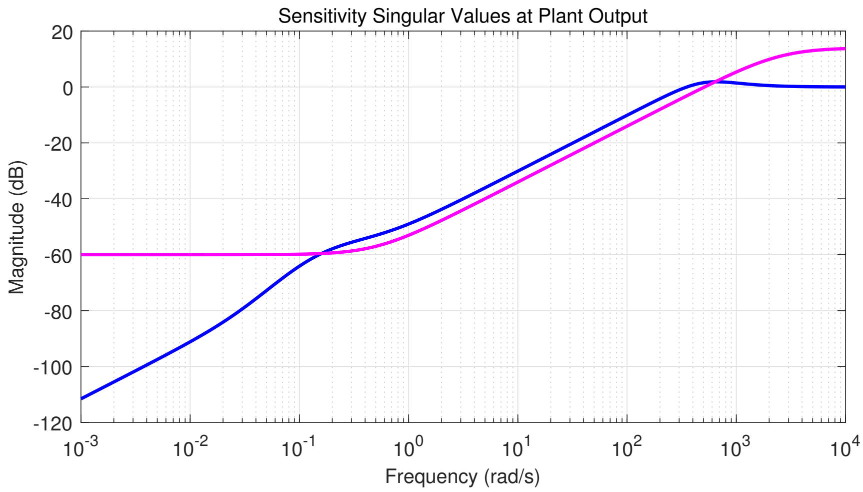

Figure 3.78: Sensitivity Frequency Response - $S = \frac{1}{1+PK} = T_{doy}$.

The complementary sensitivity transfer function is given in Fig 3.79. As can be seen from the figure the complementary sensitivity bandwidth is approximately about 450 rad/sec. The frequency response of complementary sensitivity transfer function is as expected, i.e. small at high frequencies, and near unity (0 dB) at low frequencies.

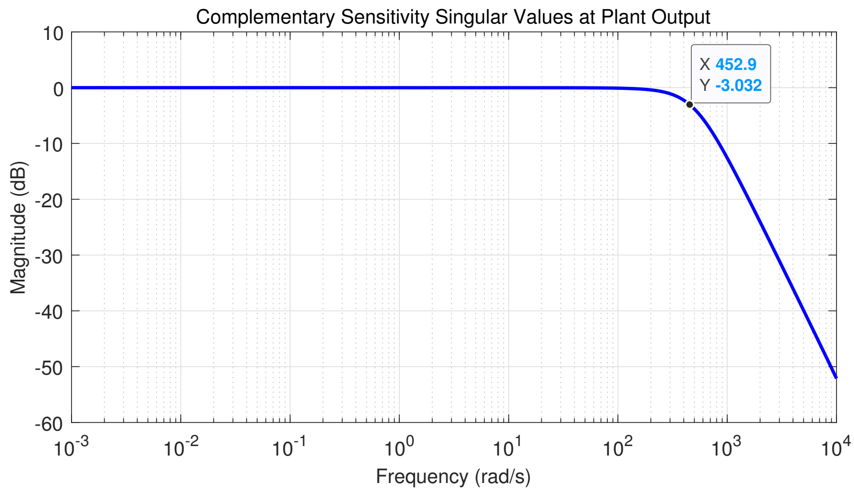

Figure 3.79: Complementary Sensitivity Frequency Response - $T_o = \frac{PK}{1+PK}$.

Control frequency response is given in Fig 3.80.

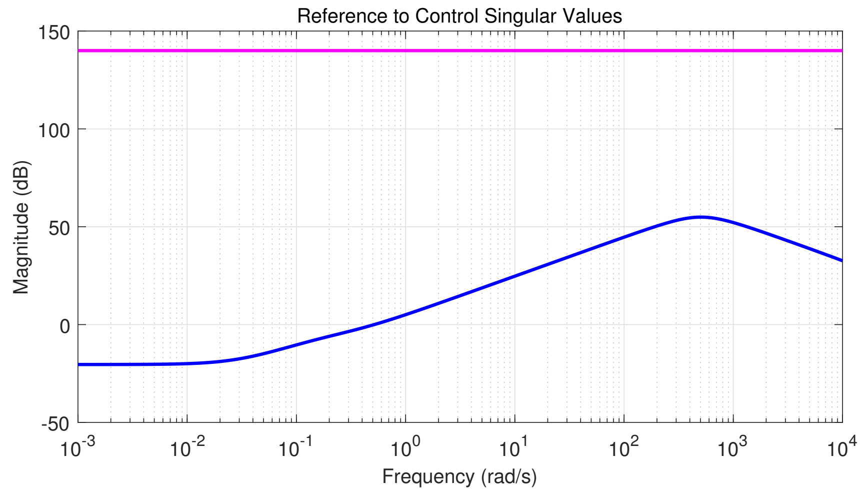

Figure 3.80: Reference to Control Frequency Response - $T_{ru} = KS$.

Input disturbance to output frequency response is given in Fig 3.81. At very low frequencies, and high frequencies T_{diy} (Input disturbance singular value transfer function) is small as expected. For frequencies between 0.2 rad/sec and 300 rad/sec the disturbance rejection is poor.

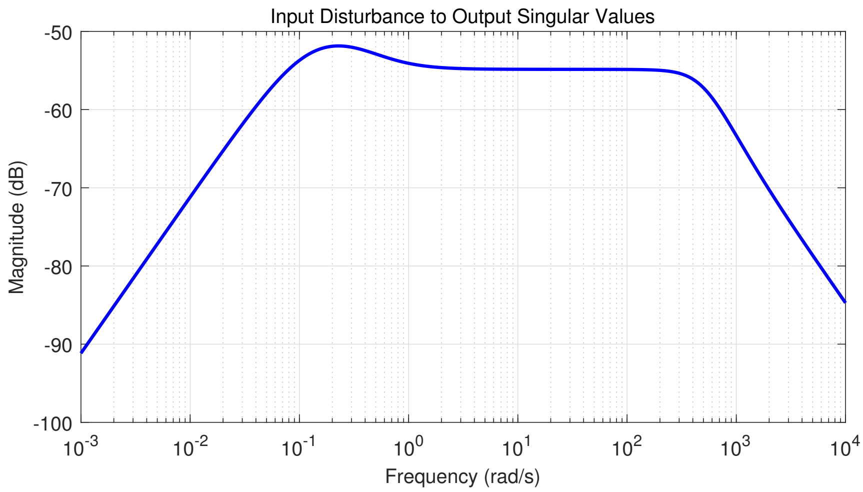

Figure 3.81: Input Disturbance to Output Frequency Response - $T_{diy} = SP$.

When the disturbance from the platform is 100 deg/sec, the response of outer elevation frame position (θ_o) and inner elevation frame position (θ_i) is as follows. The movement in inner elevation frame is at an acceptable level as it is within the limit limits.

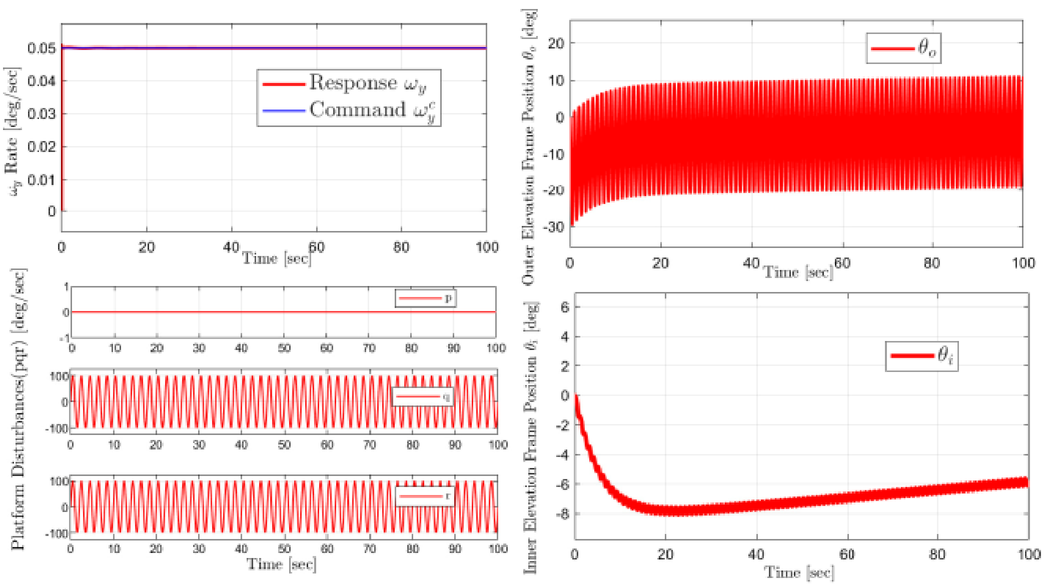

Figure 3.82: ω_y Rate Control Design via Platform Movement.

CHAPTER 4

CONCLUSION AND FUTURE WORKS

Within the scope of this thesis, a detailed mathematical modeling of the four axis gimbal system was made and controllers in different configurations were designed for each axis with the H_∞ mixed sensitivity method, which is one of the robust control methods.

The designed controllers are discussed under two titles as position and rate controllers. In position and rate controllers, outer axes are selected in low bandwidth, and inner axes are selected in high bandwidth. In addition, the designed position controllers are examined in two ways: SISO and MIMO. We have found that the MIMO configuration gives better results since the two inner axes of the four axis gimbal system are coupled to each other.

Generally, it is clear that the H_∞ mixed sensitivity controllers designed for the four axis gimbal system, which has been mathematically modeled in explicit detail, give good performance results. We aim to compare the results that were found in this thesis with the different robust controller types of the four axis gimbal system in future studies. Moreover, simulating these results with a target tracking scenario is also one of the goals of future.

REFERENCES

[1] ABDO Maher, VALI Ahmad Reza, TOLOEI Alireza and ARVAN Mohammad Reza (2013), "Research on the cross-coupling of a two axes gimbal system with dynamic unbalance", *International Journal of advanced robotic systems*, 10(10):357.

[2] ASHOK Kumar M. and KANTHALAKSHMI S. (2022), "H∞ control law for line of sight stabilization in two-axis gimbal system", *Journal of Vibration and Control*, 28(1-2):182–191.

[3] BAI Changrui and ZHANG Zhou (2018), "A least mean square based active disturbance rejection control for an inertially stabilized platform", *Optik*, 174:609–622.

[4] BASKIN Mehmet (2015), *Lqg/ltr, h-infinity and mu robust controllers design for line of sight stabilization* (Master's thesis), Middle East Technical University, Ankara.

[5] BASKIN Mehmet and LEBLEBİCİOĞLU Kemal M. (2016), "Robust stabilization loop design for gimbaled electro-optical imaging system", *arXiv preprint arXiv:1602.06832.*

[6] BASKIN Mehmet and LEBLEBİCİOĞLU Kemal M. (2017), "Robust control for line-of-sight stabilization of a two-axis gimbal system", *Turkish Journal of Electrical Engineering and Computer Sciences*, 25(5):3839–3853.

[7] BATTISTEL Andrei, LIZARRALDE Fernando and HSU Liu (2012) "Inertially stabilized platforms using only two gyroscopic measures and sensitivity analysis to unmodeled motion", *In 2012 American Control Conference (ACC) IEEE*, pp. 4582-4587.

[8] ÇİFDALÖZ Oğuzhan (2021), "Line-of-sight rate construction for a roll-pitch gimbal via a virtual pitch-yaw gimbal", *Turkish Journal of Electrical Engineering and Computer Sciences*, 29(5):2502–2519.

[9] EKSTRAND Bertil (2001), "Equations of motion for a two-axes gimbal system", *IEEE Transactions on Aerospace and Electronic Systems*, 37(3):1083–1091.

[10] HALLIDAY David, RESNICK Robert and WALKER Jearl (2013), *Fundamentals of physics*, John Wiley & Sons.

[11] HILKERT J. M. (2008), "Inertially stabilized platform technology concepts and principles", *IEEE control systems magazine*, 28(1):26–46.

[12] HILKERT J. M. and JONAS Matthew (2008), "A unique three-axis gimbal mechanism", *In Acquisition, Tracking, Pointing, and Laser Systems Technologies XXII, SPIE*, vol. 6971, pp. 83-90.

[13] JIA Ruting, NANDIKOLLA Vidya K., HAGGART Gary, VOLK Charles and TAZARTES Daniel (2017), "System performance of an inertially stabilized gimbal platform with friction, resonance, and vibration effects", *Journal of Nonlinear Dynamics*.

[14] JIE Ma and QINBEI Xu (2015), "Four-axis gimbal system application based on gimbal self-adaptation adjustment", *In 2015 34th Chinese Control Conference (CCC), IEEE*, pp. 8866-8871.

[15] KENNEDY Peter J. and KENNEDY Rhonda L. (2003), "Direct versus indirect line of sight (LOS) stabilization", *IEEE Transactions on control systems technology*, 11(1):3–15.

[16] KHODADADI Hamed, MOTLAGH Mohammad Reza Jahed and GORJI Mohammad (2011), "Robust control and modeling a 2-dof inertial stabilized platform", *In International Conference on Electrical, Control and Computer Engineering 2011 (InECCE), IEEE*, pages 223–228.

[17] KRISHNAMOORTY J. A. R., MARATHE Rajeey and SULE V. R. (2002), "H_∞ control law for line-of-sight stabilization for mobile land vehicles", *Optical engineering*, 41(11):2935–2944.

[18] LEBLEBICIOGLU Damla, ATESOGLU Ozgur and CAKMAKCI Melih (2021), "Nn based active disturbance rejection controller for a multi-axis gimbal system", *arXiv preprint*, arXiv:2112.02130.

[19] LEBLEBICIOGLU Damla, ATESOGLU Ozgur, DERINOZ Anıl E. and CAKMAKCI Melih (2021), "Learning-Based Control Compensation for Multi-Axis Gimbal Systems Using Inverse and Forward Dynamics", *arXiv preprint*, arXiv:2112.02561.

[20] LEE Dong Hun, TRAN Duc Quan, KIM Young Bok and CHAKIR Soumayya (2020), "A robust double active control system design for disturbance suppression of a two-axis gimbal system", *Electronics*, 9(10):1638.

[21] LEGHMIZI Said, LIU Sheng, FRAGA Ramzi and BOUGHELALA Adel (2012), "Dynamics modeling for satellite antenna dish stabilized platform", *In Advanced Materials Research*, vol. 566, pages 187–196. Trans Tech Publ.

[22] LIU Xuancen, YANG Yueneng, MA Chenxiang, LI Jie and ZHANG Shifeng (2020), "Real-time visual tracking of moving targets using a low-cost unmanned aerial vehicle with a 3-axis stabilized gimbal system", *Applied Sciences*, 10(15):5064.

[23] MASTEN Michael K. (2008), "Inertially stabilized platforms for optical imaging systems", *IEEE Control Systems Magazine*, 28(1):47–64.

[24] ÖZTÜRK Taha (2010), *Angular acceleration assisted stabilization of a-2 dof gimbal platform* (Master's thesis), Middle East Technical University, Ankara.

[25] PAIK Sanjoy, NANDAKUMAR M. P. and ASHOK S. (2015) "Model development and adaptive control implementation of a 3-axis platform stabilization system", *In 2015 International Conference on Smart Technologies and Management for Computing, Communication, Controls, Energy and Materials (ICSTM), IEEE*, pages 526–531.

[26] POYRAZOĞLU Erhan (2017), *Detailed modeling and control of a 2-dof gimbal system* (Master's thesis), Middle East Technical University, Ankara.

[27] RZASA J. R. (2007), *Design and application of pan and tilt servo gimbals in pointing, acquisition, and tracking*, University of Maryland, College Park.

[28] ŞENER Irmak Ece (2015), *Stabilization of an image based tracking system* (Master's thesis), Middle East Technical University, Ankara.

[29] SEONG Ki Jun, KANG Ho Gyun, YEO Bo Yeon and LEE Ho Pyeong (2006), "The stabilization loop design for a two-axis gimbal system using lqg/ltr controller", *In 2006 SICE-ICASE International Joint Conference, IEEE*, pages 755–759.

[30] TEZGELEN Oğuzhan (2020), *İki eksen gimbal sistemleri için gürbüz kontrol yöntemlerinin karşılaştırılması* (Master's thesis), TOBB ETÜ Fen Bilimleri Enstitüsü.

[31] TITTERTON David, WESTON John L. and WESTON John (2004), *Strapdown inertial navigation technology*, vol. 17. IET.

[32] WENLIANG Bao, XIANLIN Huang and XIAOJUN Ban (2010), "Control system design of multi- gimbal electro-optical platform by the technique of μ-synthesis", *In Proceedings of the 29th Chinese Control Conference.*

[33] ZHOU Kemin and DOYLE John C. (1998), *Essentials of robust control*, vol 104. Prentice hall Upper Saddle River, NJ.

APPENDIX A

MATLAB MACROS

psi-o-position-controller.m (SISO)

```
% % % % % % % % % % % % %
% designed by @ezelyalcinkaya %
% % % % % % % % % % % % %
% % 2022  A p r i l  29 % %
% % % % % % % % % % % % %

clc
clearvars
close all

equilibrium_point

bode_plot_opts = bodeoptions;
bode_plot_opts.FreqUnits = 'rad/s';
bode_plot_opts.Title.FontSize = 14;
bode_plot_opts.XLabel.FontSize = 14;
bode_plot_opts.YLabel.FontSize = 14;
bode_plot_opts.TickLabel.FontSize = 14;
bode_plot_opts.Grid = 'on';


wvec = logspace(-3, 4, 1001);

%% Outer Azimuth Axis Position Controller Design (
   psi_o_position_controller)
%% 1) psi_o_position_controller (1*1 SISO System)
%%%%% The position controllers are designed with
   H_infinity controller methodology
```

```
disp('Plant from tA to psi_o = P_psi_o')
P_psi_o = zpk(H(1,1))

%%

n_y_psi_o = size(P_psi_o,1);          % Number of Outputs for Plant tA to psi_o
n_u_psi_o = size(P_psi_o,2);          % Number of Inputs for Plant tA to psi_o
n_s_psi_o = size(P_psi_o,'order');    % Number of States for Plant tA to psi_o


%% Weighting Functions for psi_o_position controller
%% W1  (sensitivity)
Ms_psi_o = 10;                   %% 'Ms' helps adjust overshoot in sensitivity graph.
wb_psi_o = 2*pi*0.5 ;            %% 'wb' helps adjust bandwith range.
Eps_psi_o = 0.001;               %% Eps is a minimum value in sensitivity function.
k_psi_o = 1;                     %% 'k' provides steeper transition .
W1_psi_o = tf([1/(Ms_psi_o)^(1/k_psi_o) wb_psi_o], [1 wb_psi_o*(Eps_psi_o)^(1/k_psi_o)])^k_psi_o; %%general form.

%% W2  (control sensitivity)
Eps_psi_o = 0.01;
wbu_psi_o = 1e4;
Mu_psi_o = 10^-2;
k_psi_o=1;
% W2_psi_o = tf([1 wbu_psi_o/(Mu_psi_o^(1/k_psi_o))],[Eps_psi_o^(1/k_psi_o) wbu_psi_o])^k_psi_o   %% general form.
% W2_psi_o = tf([1 wbu_psi_o/Mu_psi_o], [Eps_psi_o wbu_psi_o]);
```

```
W2_psi_o = tf(Mu_psi_o, 1);             %% any fixed
   function.
%%%W2_psi_o = tf(1/Mu_psi_o, 1);   %%inverse  W2_psi_o
%% W3  (complemantary sensitivity)
 %My_psi_o = 10^(20/20) ;
 %wbc_psi_o= 2*pi*50;
 %Eps_psi_o = 0.01;
 %W3_psi_o = tf([1 wbc_psi_o/My_psi_o], [Eps_psi_o
    wbc_psi_o]);
W3_psi_o=[];

%%
aug = false;
blt = true;

%% Augment with Integrators at the Input for
   psi_o_position_controller

if aug
    Paug_psi_o = f_Augment_at_Input(P_psi_o);
else
    Paug_psi_o =ss(P_psi_o);
end

%% Bilinear Transformation for psi_o_position_controller

if blt
    p2_psi_o = -1e8; p1_psi_o = -0.01;
    Pt_psi_o=bilin(Paug_psi_o, 1,'Sft_jw',[p2_psi_o
       p1_psi_o]);
else
    Pt_psi_o=Paug_psi_o;
end

%% Augmented Plant for psi_o_position_controller
G_psi_o = augw(Pt_psi_o,W1_psi_o,W2_psi_o,W3_psi_o); %%
   augmented plant
```

```
%% Hinf Controller Design Methodology for
    psi_o_position_controller
design_opts = hinfsynOptions;
design_opts.Method='RIC';%'LMI';%'MAXE';
design_opts.Display='on';
[Kt_psi_o,CL,GAM,INFO] = hinfsyn(G_psi_o,n_y_psi_o,
    n_u_psi_o,design_opts);

%% Inverse Bilinear Transformation for
    psi_o_position_controller
if blt
    K_psi_o=bilin(Kt_psi_o,-1,'Sft_jw',[p2_psi_o p1_psi_o
       ]);
else
    K_psi_o = Kt_psi_o;
end
n_k_psi_o = size(K_psi_o,'order'); % Number of States

%% Augment with Integrators for psi_o_position_controller
if aug
    K_psi_o = f_Augment_at_Output(K_psi_o);
end
disp('Outer Azimuth Position Controller = K_psi_o')
zpk(K_psi_o)

%% Controller Design (rule of thumb) for
    psi_o_position_controller
figure(1)
bode(K_psi_o, 'r', bode_plot_opts)
hold on

[zz, pp, kk] = zpkdata(K_psi_o,'v')

K_psi_o_rot=zpk(zz,[pp([2 3]);0 ],kk);%choose zz, pp, kk

zpk(K_psi_o_rot)
```

```
clearvars zz pp kk

disp('Rule of Thumb Outer Azimuth Position Controller =
    K_psi_o_rot')
bode (K_psi_o_rot,'b',bode_plot_opts)
set(findall(gcf, 'Type', 'line'), 'LineWidth', 2)
set(gcf, 'Position', [100 100 800 600])

% K_psi_o_rot=K_psi_o;
[num den] = tfdata(K_psi_o_rot, 'v');

% str = ['test_pdf.pdf']
% set(gcf,'PaperPosition', [0 0 800 600])
% set(gcf,'PaperPositionMode','Auto',...
%          'PaperUnits','centimeters',...
%          'PaperSize',[10 10])
% print(gcf,str,'-dpdf','-r600', '-loose', '-fillpage')
% disp('DONE')

%% Model Reduction for psi_o_position_controller
% % [Kb_psi_o,gg_psi_o] = balreal(K_psi_o);gg_psi_o
% % K_psi_o = modred(Kb_psi_o,[3],'MatchDC');%
% % disp('Reduced Order Controller Kb_psi_o')
% % zpk(K_psi_o)

%% Design Analysis for psi_o_position_controller
AA = f_Maps_PKW(P_psi_o, K_psi_o_rot);
AA.W1 = W1_psi_o;
AA.W2 = W2_psi_o;
AA.W3 = W3_psi_o;
%%%
f_Plot_Sigma_Resp(AA, wvec, 'b', '-')
damp(pole(AA.To)) %% closed loop poles
%%%
figure(100)
step(AA.Try, 'b',linspace(0, 3, 1001)) %% time response
    %%linspace(0, 1, 1001)
```

```
grid on; hold on
title('Try for psi_o_position_controller',...
    'Interpreter','none','FontSize',13,'FontName','Times New Roman')
%%%
figure(101)
step(AA.Tru, 'b', linspace(0, 3, 1001)) %%control response
grid on; hold on
title('Tru for psi_o_position_controller',...
    'Interpreter','none','FontSize',13,'FontName','Times New Roman')
%%%
figure(200)
rlocus(AA.Lo)

%% UPDATE SIMULINK BLOCK
load_system('PositionController');

%%%% Set controller paramaters
%%
%%%%Position Controller paramater
set_param('PositionController/Outer Azimuth Position Controller/K_psi_o_rot', 'Numerator', mat2str(num),...
                              'Denominator', mat2str(den));


disp('SBD UPDATED (PositionController.slx K_psi_o_rot value is updated)')
```

psi-i-position-controller.m (SISO)

```
clc
clearvars
close all

equilibrium_point

bode_plot_opts = bodeoptions;
```

```
bode_plot_opts.FreqUnits = 'rad/s';
bode_plot_opts.Title.FontSize = 14;
bode_plot_opts.XLabel.FontSize = 14;
bode_plot_opts.YLabel.FontSize = 14;
bode_plot_opts.TickLabel.FontSize = 14;
bode_plot_opts.Grid = 'on';


wvec = logspace(-3, 4, 1001);

%% Outer Azimuth Axis Position Controller Design (psi_i_position_controller)
%% 1) psi_i_position_controller (1*1 SISO System)
%%%%% The position controllers were designed with H_infinity controller methodology

disp('Plant from ta to psi_i = P_psi_i')
P_psi_i = zpk(H(4,4))

%%

n_y_psi_i = size(P_psi_i,1);       % Number of Outputs for Plant ta to psi_i
n_u_psi_i = size(P_psi_i,2);       % Number of Inputs for Plant ta to psi_i
n_s_psi_i = size(P_psi_i,'order'); % Number of States for Plant ta to psi_i


%% Weighting Functions for psi_i_position controller
%% W1  (sensitivity)
Ms_psi_i = 10;     %% 'Ms' helps adjust overshoot in sensitivity graph.
wb_psi_i = 2*pi*1.2;        %% 'wb' helps adjust bandwith range.
Eps_psi_i = 0.001;          %% Eps is a minimum value in sensitivity function.
```

```
k_psi_i = 1;                %% 'k' provides steeper transition .
W1_psi_i = tf([1/(Ms_psi_i)^(1/k_psi_i) wb_psi_i], [1 wb_psi_i*(Eps_psi_i)^(1/k_psi_i)])^k_psi_i; %%general form.

%% W2  (control sensitivity)
Eps_psi_i = 0.01;
wbu_psi_i = 1e4;
Mu_psi_i = 1e-4;
k_psi_i=1;
% W2_psi_i = tf([1 wbu_psi_i/(Mu_psi_i^(1/k_psi_i))],[ Eps_psi_i^(1/k_psi_i) wbu_psi_i])^k_psi_i   %% general form.
% W2_psi_i = tf([1 wbu_psi_i/Mu_psi_i], [Eps_psi_i wbu_psi_i]);
W2_psi_i = tf(Mu_psi_i, 1)  %% any fixed function. % W2_psi_i = tf([0 Mu_psi_i], [0 1])
%W2_psi_i = tf(1/Mu_psi_i, 1);%% inverse Mu_psi_i


%% W3  (complemantary sensitivity)
% My_psi_i = 10^(20/20) ;
% wbc_psi_i= 2*pi*50;
% Eps_psi_i = 0.01;
% W3_psi_i = tf([1 wbc_psi_i/My_psi_i], [Eps_psi_i wbc_psi_i]);
W3_psi_i=[];

%%
aug = false;
blt = true;

%% Augment with Integrators at the Input for psi_i_position_controller

if aug
```

```
    Paug_psi_i = f_Augment_at_Input(P_psi_i);
else
    Paug_psi_i = ss(P_psi_i);
end

%% Bilinear Transformation for psi_i_position_controller

if blt
    p2_psi_i = -1e8; p1_psi_i = -1;
    Pt_psi_i=bilin(Paug_psi_i, 1,'Sft_jw',[p2_psi_i
       p1_psi_i]);
else
    Pt_psi_i=Paug_psi_i;
end

%% Augmented Plant for psi_i_position_controller
G_psi_i = augw(Pt_psi_i,W1_psi_i,W2_psi_i,W3_psi_i); %%
   augmented plant

%% Hinf Controller Design Methodology for
   psi_i_position_controller
design_opts = hinfsynOptions;
design_opts.Method='RIC';%'LMI';%'MAXE';
design_opts.Display='on';
[Kt_psi_i,CL,GAM,INFO] = hinfsyn(G_psi_i,n_y_psi_i,
   n_u_psi_i,design_opts);

%% Inverse Bilinear Transformation for
   psi_i_position_controller
if blt
    K_psi_i=bilin(Kt_psi_i,-1,'Sft_jw',[p2_psi_i p1_psi_i
       ]);
else
    K_psi_i = Kt_psi_i;
end
n_k_psi_i = size(K_psi_i,'order'); % Number of States

```

```
%% Augment with Integrators for psi_i_position_controller
if aug
    K_psi_i = f_Augment_at_Output(K_psi_i);
end
disp('Outer Azimuth Position Controller = K_psi_i')
zpk(K_psi_i)

%% Controller Design (rule of thumb) for
   psi_i_position_controller
figure(1)
bode(K_psi_i, 'r',bode_plot_opts)
hold on

[zz, pp, kk] = zpkdata(K_psi_i,'v')

K_psi_i_rot=zpk(zz,[pp([2 3]);0 ],kk);

zpk(K_psi_i_rot)
clearvars zz pp kk

disp('Rule of Thumb Outer Azimuth Position Controller =
   K_psi_i_rot')
bode (K_psi_i_rot,'b',bode_plot_opts)
set(findall(gcf, 'Type', 'line'), 'LineWidth', 2)
set(gcf, 'Position', [100 100 800 600])

%K_psi_i_rot=K_psi_i
[num,den] = tfdata(K_psi_i_rot, 'v');

% str = ['test_pdf.pdf']
% set(gcf,'PaperPosition', [0 0 800 600])
% set(gcf,'PaperPositionMode','Auto',...
%          'PaperUnits','centimeters',...
%          'PaperSize',[10 7.5])
% print(gcf,str,'-dpdf','-r600', '-loose', '-fillpage')
% disp('DONE')
```

```
%% Model Reduction for psi_i_position_controller
% [Kb_psi_i,gg_psi_i] = balreal(K_psi_i);gg_psi_i
% K_psi_i = modred(Kb_psi_i,[],'MatchDC');%
% disp('Reduced Order Controller Kb_psi_i')
% zpk(K_psi_i)

%% Design Analysis for psi_i_position_controller
aa = f_Maps_PKW(P_psi_i, K_psi_i_rot);
aa.W1 = W1_psi_i;
aa.W2 = W2_psi_i;
aa.W3 = W3_psi_i;
%%%
f_Plot_Sigma_Resp(aa, wvec, 'b', '-')
damp(pole(aa.To)) %% closed loop poles
%%%
figure(100)
step(aa.Try, 'b', linspace(0, 1, 1001)) %% time response linspace(0, 1, 1001)
grid on; hold on
title('Try for psi_i_position_controller',...
    'Interpreter','none','FontSize',13,'FontName','Times New Roman')
%%%
figure(101)
step(aa.Tru, 'b', linspace(0, 0.1, 1001)) %%control response
grid on; hold on
title('Tru for psi_i_position_controller',...
    'Interpreter','none','FontSize',13,'FontName','Times New Roman')
%%%
figure(200)
rlocus(aa.Lo)

%%  UPDATE SIMULINK BLOCK
load_system('PositionController');

```

```
%%%% Set controller paramaters
%%
%%%%Position Controller paramater
set_param('PositionController/Inner Azimuth Position
   Controller/K_psi_i_rot', 'Numerator', mat2str(num),...
                                  'Denominator', mat2str(den));


disp('SBD UPDATED (PositionController.slx K_psi_i_rot
   value is updated)')
```

theta-o-position-controller.m (SISO)

```
clc
clearvars
close all

equilibrium_point


bode_plot_opts = bodeoptions;
bode_plot_opts.FreqUnits = 'rad/s';
bode_plot_opts.Title.FontSize = 14;
bode_plot_opts.XLabel.FontSize = 14;
bode_plot_opts.YLabel.FontSize = 14;
bode_plot_opts.TickLabel.FontSize = 14;
bode_plot_opts.Grid = 'on';


wvec = logspace(-3, 4, 1001);

%% 2) theta_o_position_controller (1*1 SISO System)
%%% From t_E to theta_o  (Position Controller Design)


disp('Plants from t_E to theta_o = P_theta_o')%%%% 1*1
   SISO Plant
P_theta_o = zpk(H(2,2))

```

```
return
%%

n_y_theta_o = size(P_theta_o,1);        % Number of Outputs for plant t_E to theta_o
n_u_theta_o = size(P_theta_o,2);        % Number of Inputs for plant t_E to theta_o
n_s_theta_o = size(P_theta_o,'order'); % Number of States for plant t_E to theta_o


%% Weighting Functions for theta_o position controller
%% W1  (sensitivity)
%%%Parameters
Ms_theta_o = 10;
wb_theta_o = 2*pi*0.5;
Eps_theta_o = 0.001;
k_theta_o = 1;
W1_theta_o = tf([1/(Ms_theta_o)^(1/k_theta_o) wb_theta_o], [1 wb_theta_o*(Eps_theta_o)^(1/k_theta_o)])^k_theta_o; %%general form.


%zpk(W1_theta_o)

%% W2  (control sensitivity) for theta_o position controller
%%%Parameters
Eps_theta_o = 250;
wbu_theta_o = 1000;
Mu_theta_o = 1e-2;
k_theta_o=1;

W2_theta_o = tf(Mu_theta_o, 1);    %% any fixed function.
%%%W2_theta_o = tf(1/Mu_theta_o, 1); %%inverse W2_theta_o
zpk(W2_theta_o)

```

```
%% W3  (complemantary sensitivity) for theta_o position controller
% My_theta_o = 10^(20/20) ;
% wbc_theta_o= 2*pi*50;
% Eps_theta_o = 0.01;
% W3_theta_o = tf([1 wbc_theta_o/My_theta_o], [Eps_theta_o wbc_theta_o]);
W3_theta_o=[];

%%
aug = false;
blt = true;

%% Augment with Integrators at the Input for theta_o position controller
if aug
    Paug_theta_o = f_Augment_at_Input(P_theta_o);
else
    Paug_theta_o =ss(P_theta_o);
end

%% Bilinear Transformation for theta_o position controller
if blt
    p2_theta_o = -1e8; p1_theta_o =-0.01; %-0.2  -0.55 -0.09
    Pt_theta_o=bilin(Paug_theta_o, 1,'Sft_jw',[p2_theta_o p1_theta_o]);
else
    Pt_theta_o=Paug_theta_o;
end

%% Augmented Plant for theta_o position controller
G_theta_o = augw(Paug_theta_o,W1_theta_o,W2_theta_o,W3_theta_o); %%augmented plant

```

```matlab
%% Hinf Design for theta_o position controller
design_opts = hinfsynOptions;
design_opts.Method='RIC';%'LMI';%'MAXE';
design_opts.Display='on';
[Kt_theta_o,CL,GAM,INFO] = hinfsyn(G_theta_o,n_y_theta_o,
    n_u_theta_o,design_opts);

%% Inverse Bilinear Transformation for theta_o position
    controller
if blt
    K_theta_o=bilin(Kt_theta_o,-1,'Sft_jw',[p2_theta_o
        p1_theta_o]);
else
    K_theta_o = Kt_theta_o;
end
n_k = size(K_theta_o,'order'); % Number of States


%% Augment with Integrators at the Output for theta_o
    position controller
if aug
    K_theta_o= f_Augment_at_Output(K_theta_o);
end
disp('Outer_Inner Elevation Position Controller =
    K_theta_o')
zpk(K_theta_o)


%% Controller Design (rule of thumb) for
    theta_o_position_controller
figure(1)
bode(K_theta_o, 'r',bode_plot_opts)
hold on

[zz, pp, kk] = zpkdata(K_theta_o,'v')

K_theta_o_rot=zpk(zz,[pp([1 2 4]);0],kk);
```

```
zpk(K_theta_o_rot)
clearvars zz pp kk

disp('Rule of Thumb Outer Elevation Position Controller = K_theta_o_rot')
bode (K_theta_o_rot,'b',bode_plot_opts)
set(findall(gcf, 'Type', 'line'), 'LineWidth', 2)
set(gcf, 'Position', [100 100 800 600])

%K_theta_o_rot=K_theta_o
[num, den] = tfdata(K_theta_o_rot, 'v');

%% Model Reduction for theta_o position controller
% % [Kb_theta_o,gg_theta_o] = balreal(K_theta_o); gg_theta_o
% % K_theta_o_rot = modred(Kb_theta_o,[4],'MatchDC');
% % disp('Reduced Order Controller Kb_theta_o')

%% Design Analysis
EE = f_Maps_PKW(P_theta_o, K_theta_o_rot);
EE.W1 = W1_theta_o;
EE.W2 = W2_theta_o;
EE.W3 = W3_theta_o;
%%%
f_Plot_Sigma_Resp(EE, wvec, 'b', '-')
damp(pole(EE.To)) %% closed loop poles
%%%
figure(100)
step(EE.Try, 'b', linspace(0, 1, 1001)) %% time response
grid on; hold on
title('Try for theta_o_position_controller',...
'Interpreter','none','FontSize',13,'FontName','Times New Roman')
%%%
figure(101)
step(EE.Tru, 'b', linspace(0, 1, 1001)) %%control
```

```
    response
grid on; hold on
title('Tru for theta_o_position_controller',...
'Interpreter','none','FontSize',13,'FontName','Times New
    Roman')

%% UPDATE SIMULINK BLOCK
load_system('PositionController');

%%%% Set controller paramaters
%%
%%%%Position Controller paramater
set_param('PositionController/Outer Elevation Position
    Controller/K_theta_o_rot', 'Numerator', mat2str(num),
    ...
                         'Denominator', mat2str(den));



disp('SBD UPDATED (PositionController.slx K_theta_o_rot
    value is updated)')
```

theta-i-position-controller.m (SISO)

```
clc
clearvars
close all

equilibrium_point


bode_plot_opts = bodeoptions;
bode_plot_opts.FreqUnits = 'rad/s';
bode_plot_opts.Title.FontSize = 14;
bode_plot_opts.XLabel.FontSize = 14;
bode_plot_opts.YLabel.FontSize = 14;
bode_plot_opts.TickLabel.FontSize = 14;
bode_plot_opts.Grid = 'on';

```

```

wvec = logspace(-3, 4, 1001);

%% 3) theta_i_position_controller (1*1 SISO System)
%%% From t_e to theta_i  (Position Controller Design)

disp('Plants from t_e to theta_i = P_theta_i')%%%% 1*1 SISO Plant
P_theta_i = zpk(H(3,3))
return
%%

n_y_theta_i = size(P_theta_i,1);        % Number of Outputs for plant t_e to theta_i
n_u_theta_i = size(P_theta_i,2);        % Number of Inputs for plant t_e to theta_i
n_s_theta_i = size(P_theta_i,'order'); % Number of States for plant t_e to theta_i


%% Weighting Functions for theta_i position controller
%% W1  (sensitivity)
%%%Parameters
Ms_theta_i = 10;
wb_theta_i = 2*pi*0.7;
Eps_theta_i = 0.001;
k_theta_i = 1;
W1_theta_i = tf([1/(Ms_theta_i)^(1/k_theta_i) wb_theta_i ], [1 wb_theta_i*(Eps_theta_i)^(1/k_theta_i)])^k_theta_i; %%general form.


%zpk(W1_theta_i)

%% W2  (control sensitivity) for theta_i position controller
%%%Parameters
```

```
Eps_theta_i = 0.01;
wbu_theta_i = 1000;
Mu_theta_i = 1e-6;
k_theta_i=1;

W2_theta_i = tf(Mu_theta_i , 1);    %% any fixed function.
% % W2_theta_i = tf(1/Mu_theta_i , 1); %% inverse
   W2_theta_i
%zpk(W2_theta_i)


%% W3  (complemantary sensitivity) for theta_i position
   controller
% My_theta_i = 10^(20/20) ;
% wbc_theta_i= 2*pi*50;
% Eps_theta_i = 0.01;
% W3_theta_i = tf([1 wbc_theta_i/My_theta_i], [
   Eps_theta_i wbc_theta_i]);
W3_theta_i=[];

%%
aug = false;
blt = true;

%% Augment with Integrators at the Input for theta_i
   position controller
if aug
    Paug_theta_i = f_Augment_at_Input(P_theta_i);
else
    Paug_theta_i = ss(P_theta_i);
end

%% Bilinear Transformation for theta_i position
   controller
if blt
    p2_theta_i = -1e8; p1_theta_i = -2;
    Pt_theta_i=bilin(Paug_theta_i , 1,'Sft_jw',[p2_theta_i
```

```
        p1_theta_i]);
else
    Pt_theta_i=Paug_theta_i;
end

%% Augmented Plant for theta_i position controller
G_theta_i = augw(Paug_theta_i,W1_theta_i,W2_theta_i,
   W3_theta_i); %%augmented plant

%% Hinf Design for theta_i position controller
design_opts = hinfsynOptions;
design_opts.Method='RIC';%'LMI';%'MAXE';
design_opts.Display='on';
[Kt_theta_i,CL,GAM,INFO] = hinfsyn(G_theta_i,n_y_theta_i,
   n_u_theta_i,design_opts);

%% Inverse Bilinear Transformation for theta_i position
   controller
if blt
    K_theta_i=bilin(Kt_theta_i,-1,'Sft_jw',[p2_theta_i
       p1_theta_i]);
else
    K_theta_i = Kt_theta_i;
end
n_k = size(K_theta_i,'order'); % Number of States


%% Augment with Integrators at the Output for theta_i
   position controller
if aug
    K_theta_i= f_Augment_at_Output(K_theta_i);
end
disp('Inner Elevation Position Controller = K_theta_i')
zpk(K_theta_i)


%% Controller Design (rule of thumb) for
```

```
    theta_i_position_controller
figure(1)
bode(K_theta_i, 'r',bode_plot_opts)
hold on


[zz, pp, kk] = zpkdata(K_theta_i,'v')

K_theta_i_rot=zpk(zz,[pp([1 2 3]);0],kk);

zpk(K_theta_i_rot)
clearvars zz pp kk


disp('Rule of Thumb Outer Elevation Position Controller = K_theta_i_rot')
bode (K_theta_i_rot,'b',bode_plot_opts)
set(findall(gcf, 'Type', 'line'), 'LineWidth', 2)
set(gcf, 'Position', [100 100 800 600])

%K_theta_i_rot=K_theta_i
[num, den] = tfdata(K_theta_i_rot, 'v');


% %% Model Reduction for theta_i position controller
% [Kb_theta_i,gg_theta_i] = balreal(K_theta_i);gg_theta_i
% K_theta_i = modred(Kb_theta_i,[],'MatchDC');
% disp('Reduced Order Controller Kb_theta_i')
% zpk(K_theta_i)

%% Design Analysis
ee = f_Maps_PKW(P_theta_i, K_theta_i_rot);
ee.W1 = W1_theta_i;
ee.W2 = W2_theta_i;
ee.W3 = W3_theta_i;
%%%
f_Plot_Sigma_Resp(ee, wvec, 'b', '-')
```

```
damp(pole(ee.To)) %% closed loop poles
%%%
figure(100)
step(ee.Try, 'b') %% time response
grid on; hold on
title('Try for theta_i_position_controller',...
'Interpreter','none','FontSize',13,'FontName','Times New
    Roman')
%%%
figure(101)
step(ee.Tru, 'b') %%control response
grid on; hold on
title('Tru for theta_i_position_controller',...
'Interpreter','none','FontSize',13,'FontName','Times New
    Roman')

%%  UPDATE SIMULINK BLOCK
load_system('PositionController');

%%%% Set controller paramaters
%%
%%%%Position Controller paramater
set_param('PositionController/Inner Elevation Position
    Controller/K_theta_i_rot', 'Numerator', mat2str(num),
    ...
                                'Denominator', mat2str(den));



disp('SBD UPDATED (PositionController.slx K_theta_i_rot
    value is updated)')
```

theta-o-theta-i-position-controller.m (MIMO)

```
clc
clearvars
close all

equilibrium_point
```

```
bode_plot_opts = bodeoptions;
bode_plot_opts.FreqUnits = 'rad/s';
bode_plot_opts.Title.FontSize = 14;
bode_plot_opts.XLabel.FontSize = 14;
bode_plot_opts.YLabel.FontSize = 14;
bode_plot_opts.TickLabel.FontSize = 14;
bode_plot_opts.Grid = 'on';


wvec = logspace(-3, 4, 1001);


%% 2) theta_o_theta_i_position_controller (2*2 MIMO System)
%%% From t_E and t_e to theta_o and theta_i (Position Controller Design)

disp('Plants from t_E and t_e to theta_o and theta_i = P_theta_o_theta_i')%%%% 2*2 MIMO Plant
P_theta_o_theta_i = zpk(H(2:3,2:3))


%%

n_y_theta_o_theta_i = size(P_theta_o_theta_i,1);        % Number of Outputs for plant t_E and t_e to theta_o and theta_i
n_u_theta_o_theta_i = size(P_theta_o_theta_i,2);        % Number of Inputs  for plant t_E and t_e to theta_o and theta_i
n_s_theta_o_theta_i = size(P_theta_o_theta_i,'order'); % Number of States  for plant t_E and t_e to theta_o and theta_i
```

```
%% Weighting Functions for theta_o_theta_i position controller
%% W1  (sensitivity)
%%%Parameters
Eps_theta_o_theta_i = 0.001%0.00001;
Ms1_theta_o_theta_i = 1e1; wb1_theta_o_theta_i = 2*pi*0.1;
Ms2_theta_o_theta_i = 1e1; wb2_theta_o_theta_i = 2*pi*0.5;
q = 1; p =1;
%%%%Weighting function 1
W1_theta_o_theta_i = [tf([1/(Ms1_theta_o_theta_i^(1/q)) wb1_theta_o_theta_i], [1 wb1_theta_o_theta_i*(Eps_theta_o_theta_i^(1/q))])^q 0;
      0 tf([1/(Ms2_theta_o_theta_i^(1/p)) wb2_theta_o_theta_i], [1 wb2_theta_o_theta_i*(Eps_theta_o_theta_i^(1/p))])^p];

%zpk(W1_theta_o_theta_i)

%% W2  (control sensitivity) for theta_o_theta_i position controller
%%%Parameters
wbu1_theta_o_theta_i = 2*pi*100; Mu1_theta_o_theta_i =1e-3;
wbu2_theta_o_theta_i = 2*pi*100; Mu2_theta_o_theta_i =1e-6;
%%%%Weighting function 2
W2_theta_o_theta_i = [tf([1 wbu1_theta_o_theta_i/Mu1_theta_o_theta_i], [Eps_theta_o_theta_i wbu1_theta_o_theta_i]) 0;
      0 tf([1 wbu2_theta_o_theta_i/Mu2_theta_o_theta_i], [Eps_theta_o_theta_i wbu2_theta_o_theta_i])];
%zpk(W2_theta_o_theta_i)

% % W2_theta_o_theta_i = [tf(1/Mu1_theta_o_theta_i, 1) 0; 0 tf(1/Mu2_theta_o_theta_i, 1)]; %%inverse   %% any
```

```
fixed function.
W2_theta_o_theta_i = [tf(Mu1_theta_o_theta_i , 1) 0; 0 tf(
    Mu2_theta_o_theta_i , 1)];
%% W3  (complemantary sensitivity) for theta_o_theta_i
    position controller
%%%Parameters
 My1_theta_o_theta_i = 10^(20/20); wbc1_theta_o_theta_i=
    2*pi*5;
 My2_theta_o_theta_i = 10^(20/20); wbc2_theta_o_theta_i=
    2*pi*75;
 v = 1; w = 1;
%%%%Weighting function 3
W3_theta_o_theta_i = [tf([1 wbc1_theta_o_theta_i/(
    My1_theta_o_theta_i^(1/v))], [(Eps_theta_o_theta_i^(1/
    v)) wbc1_theta_o_theta_i])^v 0;
    0 tf([1 wbc2_theta_o_theta_i/(My2_theta_o_theta_i^(1/
        w))], [(Eps_theta_o_theta_i^(1/w))
        wbc2_theta_o_theta_i])^w];
W3_theta_o_theta_i=[];
%zpk(W3_theta_o_theta_i)

%%
aug = false;
blt = true;

%% Augment with Integrators at the Input for
    theta_o_theta_i position controller
if aug
    Paug_theta_o_theta_i = f_Augment_at_Input(
        P_theta_o_theta_i);
else
    Paug_theta_o_theta_i = ss(P_theta_o_theta_i);
end

%% Bilinear Transformation for theta_o_theta_i position
    controller
if blt
```

```
    p2_theta_o_theta_i = -1e8; p1_theta_o_theta_i = -0.8;
    Pt_theta_o_theta_i=bilin(Paug_theta_o_theta_i, 1,'Sft_jw',[p2_theta_o_theta_i p1_theta_o_theta_i]);
else
    Pt_theta_o_theta_i=Paug_theta_o_theta_i;
end

%% Augmented Plant for theta_o_theta_i position controller
G_theta_o_theta_i = augw(Paug_theta_o_theta_i,W1_theta_o_theta_i,W2_theta_o_theta_i,W3_theta_o_theta_i); %%augmented plant

%% Hinf Design for theta_o_theta_i position controller
design_opts = hinfsynOptions;
design_opts.Method='RIC';%'LMI';%'MAXE';
design_opts.Display='on';
[Kt_theta_o_theta_i,CL,GAM,INFO] = hinfsyn(G_theta_o_theta_i,n_y_theta_o_theta_i,n_u_theta_o_theta_i,design_opts);

%% Inverse Bilinear Transformation for theta_o_theta_i position controller
if blt
    K_theta_o_theta_i=bilin(Kt_theta_o_theta_i,-1,'Sft_jw',[p2_theta_o_theta_i p1_theta_o_theta_i]);
else
    K_theta_o_theta_i = Kt_theta_o_theta_i;
end
n_k = size(K_theta_o_theta_i,'order'); % Number of States


%% Augment with Integrators at the Output for theta_o_theta_i position controller
if aug
    K_theta_o_theta_i= f_Augment_at_Output(K_theta_o_theta_i);
```

```
end
disp('Outer_Inner Elevation Position Controller = K_theta_o_theta_i')
zpk(K_theta_o_theta_i)

%% Model Reduction for theta_o_theta_i position controller
[Kb_theta_o_theta_i,gg_theta_o_theta_i] = balreal(K_theta_o_theta_i);gg_theta_o_theta_i
K_theta_o_theta_i = modred(Kb_theta_o_theta_i,[],'MatchDC');
disp('Reduced Order Controller Kb_theta_o_theta_i')
zpk(K_theta_o_theta_i)



%% Design Analysis
EE = f_Maps_PKW(P_theta_o_theta_i, K_theta_o_theta_i);
EE.W1 = W1_theta_o_theta_i;
EE.W2 = W2_theta_o_theta_i;
EE.W3 = W3_theta_o_theta_i;
%%%
f_Plot_Sigma_Resp(EE, wvec, 'b', '-')
damp(pole(EE.To)) %% closed loop poles
%%%
figure(100)
step(EE.Try, 'b') %% time response
grid on; hold on
title('Try for theta_o_theta_i_position_controller',...
'Interpreter','none','FontSize',13,'FontName','Times New Roman')
%%%
figure(101)
step(EE.Tru, 'b') %%control response
grid on; hold on
title('Tru for theta_o_theta_i_position_controller',...
'Interpreter','none','FontSize',13,'FontName','Times New
```

```
    Roman')




%%  UPDATE SIMULINK BLOCK
load_system('PositionController');

%%%% Set controller paramaters
%%
%%%%Position Controller paramater
% % set_param('PositionController/Outer_Inner Elevation
    Position Controller/K_theta_o_theta_i','A',...
% %      'K_theta_o_theta_i.A','B','K_theta_o_theta_i.B','
    C','K_theta_o_theta_i.C','D','K_theta_o_theta_i.D');

set_param('PositionController/Outer_Inner Elevation
    Position Controller/K_theta_o_theta_i',...
     'A',mat2str(K_theta_o_theta_i.A),...
     'B',mat2str(K_theta_o_theta_i.B),...
     'C',mat2str(K_theta_o_theta_i.C),...
     'D',mat2str(K_theta_o_theta_i.D));

disp('SBD UPDATED (PositionController.slx
    K_theta_o_theta_i value is updated)')
```

wz-outer-rate-controller.m

```
clc
clearvars
close all
equilibrium_point

bode_plot_opts = bodeoptions;
bode_plot_opts.FreqUnits = 'rad/s';
bode_plot_opts.Title.FontSize = 14;
bode_plot_opts.XLabel.FontSize = 14;
bode_plot_opts.YLabel.FontSize = 14;
bode_plot_opts.TickLabel.FontSize = 14;
```

```
bode_plot_opts.Grid = 'on';


wvec = logspace(-3, 4, 1001);


%%
wc = 2*pi*0.5;
F1 = tf(wc,[1 wc]);  %%%low pass filter
[num1,den1] = tfdata(F1,'v');


%% 1) gyro_z_axis_rate_controller (1*1 SISO System)

%%% From t_A to w_z (Rate Controller Design)

disp('Plants from t_A to w_z= P_w_z')%%%% 1*1 SISO Plant
P_w_z = zpk(H(5,1))


%%
n_y_w_z = size(P_w_z,1);        %Number of Outputs for plant from t_A to w_z
n_u_w_z = size(P_w_z,2);        %Number of Inputs for plant from  t_A to w_z
n_s_w_z = size(P_w_z,'order'); %Number of States for plant from  t_A to w_z



%% Weighting Functions for w_z controller
%% W1  (sensitivity)

Ms_w_z =10;       %% 'Ms' helps adjust overshoot in sensitivity graph.
wb_w_z = 2*pi*0.5;        %% 'wb' helps adjust bandwith range.
```

```
Eps_w_z = 0.001;          %% Eps is a minimum value in
    sensitivity function.
k_w_z =1;                 %% 'k' provides steeper transition
    .
%W1_w_z = tf([1/(Ms_w_z ^(1/k_w_z)) wb_w_z], [1 wb_w_z*(
    Eps_w_z ^(1/k_w_z))])^k_w_z;%%general form.(1*2)

W1_w_z = tf([1/Ms_w_z wb_w_z], [1 wb_w_z*Eps_w_z])

%% W2  (control sensitivity)
% Eps_w_z =0.001;   Eps1_w_z = 0.001;
% wbu_w_z = 2*pi*100;    wbu1_w_z = 2*pi*100;
% k_w_z=1;               k1_w_z=1;

%  Mu_w_z = 1e7;  Mu1_w_z = 10^(0.00001/20);
Mu1_w_z = 1e-10;  Mu2_w_z =1e-2;
% W2_w_z = tf([1 wbu_w_z/(Mu_w_z^(1/k_w_z))],[Eps_w_z^(1/
    k_w_z) wbu_w_z])^k_w_z   %% general form.
% W2_w_z = tf([1 wbu_w_z/Mu_w_z], [Eps_w_z wbu_w_z]);
%W2_w_z = tf(1/Mu_w_z, 1);            %% any fixed
    function.
% W2_w_z = [tf([1 wbu_w_z/(Mu1_w_z^(1/k_w_z))],[Eps_w_z
    ^(1/k_w_z) wbu_w_z])^k_w_z   0;
%   0      tf([1 wbu1_w_z/(Mu2_w_z^(1/k1_w_z))],[Eps1_w_z
    ^(1/k1_w_z) wbu1_w_z])^k1_w_z]; %% general form.

% W2_w_z= [tf(1/Mu1_w_z, 1)  0;
%            0    tf(1/Mu2_w_z, 1)];  %% any fixed
    function(2*2)


W2_w_z = tf(Mu1_w_z, 1);


%% W3  (complemantary sensitivity)
My_w_z = 10^(0.01/20) ;
wbc_w_z= 2*pi*5;
```

```
Eps_w_z = 0.0001;
v=1;

% W3_w_z = tf([1 wbc_w_z/My_w_z], [Eps_w_z wbc_w_z]);
W3_w_z = tf([1 wbc_w_z/(My_w_z^(1/v))], [(Eps_w_z^(1/v))
    wbc_w_z])^v;
W3_w_z=[];

%%
aug =true;
blt = true;


%% Augment with Integrators at the Input for w_z
    controller(outer controller)

if aug
    Paug_w_z = f_Augment_at_Input(P_w_z);
else
    Paug_w_z =ss(P_w_z);
end


%% Bilinear Transformation for w_z controller (outer
    controller)

if blt
    p2_w_z = -1e8; p1_w_z = -1;
    Pt_w_z=bilin(Paug_w_z, 1,'Sft_jw',[p2_w_z p1_w_z]);
else
    Pt_w_z=Paug_w_z;
end

%% Augmented Plant for w_z controller
G_w_z = augw(Pt_w_z,W1_w_z,W2_w_z,W3_w_z); %%augmented
    plant

```

```
%% Hinf Controller Design Methodology for w_z controller
design_opts = hinfsynOptions;
design_opts.Method='RIC';%'LMI';%'MAXE';
design_opts.Display='on';
[Kt_w_z,CL,GAM,INFO] = hinfsyn(G_w_z,n_y_w_z,n_u_w_z,
   design_opts);

%% Inverse Bilinear Transformation for w_z controller
if blt
    K_w_z=bilin(Kt_w_z,-1,'Sft_jw',[p2_w_z p1_w_z]);
else
    K_w_z = Kt_w_z;
end
n_k_w_z = size(K_w_z,'order'); % Number of States

%% Augment with Integrators for w_z controller
if aug
    K_w_z = f_Augment_at_Output(K_w_z);
end
disp('Outer Azimuth Position Controller = K_w_z')
zpk(K_w_z)


%% Controller Design (rule of thumb) for w_z controller
% figure(1)
% bode(K_w_z, 'r', bode_plot_opts)
% hold on

[zz, pp, kk] = zpkdata(K_w_z,'v')

% K_w_z_rot=zpk(zz,[pp([1 3]); 0],kk);%choose zz, pp, kk
%  K_w_z_rot=zpk(zz,[pp([2 4 5]);0],kk);%choose zz, pp,
   kk

% zpk(K_w_z_rot)
clearvars zz pp kk

```

```
% disp('Rule of Thumb Outer Azimuth Rate Controller =
    K_w_z_rot')
% bode (K_w_z_rot,'b',bode_plot_opts)
% set(findall(gcf, 'Type', 'line'), 'LineWidth', 2)
% set(gcf, 'Position', [100 100 800 600])

K_w_z_rot=K_w_z;
[num den] = tfdata(K_w_z_rot, 'v');

% str = ['test_pdf.pdf']
% set(gcf,'PaperPosition', [0 0 800 600])
% set(gcf,'PaperPositionMode','Auto',...
%          'PaperUnits','centimeters',...
%          'PaperSize',[10 7.5])
% print(gcf,str,'-dpdf','-r600', '-loose', '-fillpage')
% disp('DONE')


%% Model Reduction for w_z controller
% % [Kb_w_z,gg_w_z] = balreal(K_w_z_rot);gg_w_z
% % K_w_z = modred(Kb_w_z,[],'MatchDC');%
% % disp('Reduced Order Controller Kb_w_z')
% % zpk(K_w_z)


%% Design Analysis for w_z controller
HH = f_Maps_PKW(P_w_z, K_w_z_rot);
HH.W1 = W1_w_z;
HH.W2 = W2_w_z;
HH.W3 = W3_w_z;
%%%
f_Plot_Sigma_Resp(HH, wvec, 'b', '-')
damp(pole(HH.To)) %% closed loop poles
%%%
figure(100)
step(HH.Try, 'b', linspace(0, 5, 1001)) %% time response
grid on; hold on
```

```
title('Try for psi_o_position_controller',...
    'Interpreter','none','FontSize',13,'FontName','Times New Roman')
%%%
figure(101)
step(HH.Tru, 'b', linspace(0, 5, 1001)) %%control response
grid on; hold on
title('Tru for psi_o_position_controller',...
    'Interpreter','none','FontSize',13,'FontName','Times New Roman')
%%%
figure(200)
rlocus(HH.Lo)



%%  UPDATE SIMULINK BLOCK
load_system('Ratecontroller');

%%%% Set controller paramaters
%%
%%%%%%% Rate Controller paramater


set_param('Ratecontroller/wz/K_d', 'Numerator', mat2str(num),...
                           'Denominator', mat2str(den));
%% High pass and low pass filter parameter
set_param('Ratecontroller/wz/LPF', 'Numerator', mat2str(num1),...
                           'Denominator', mat2str(den1));

set_param('Ratecontroller/wz/lpf', 'Numerator', mat2str(num1),...
                           'Denominator', mat2str(den1));

```

```
disp('SBD UPDATED (Ratecontroller.slx K_w_z value is
   updated)')
```

wz-inner-rate-controller.m

```
clc
clearvars
close all
equilibrium_point

bode_plot_opts = bodeoptions;
bode_plot_opts.FreqUnits = 'rad/s';
bode_plot_opts.Title.FontSize = 14;
bode_plot_opts.XLabel.FontSize = 14;
bode_plot_opts.YLabel.FontSize = 14;
bode_plot_opts.TickLabel.FontSize = 14;
bode_plot_opts.Grid = 'on';


wvec = logspace(-3, 4, 1001);


%% Cut-off frequency for high pass filter
wc = 2*pi*0.5;
F2 = tf([1 0],[1 wc]);  %%% high pass filter
[num2,den2] = tfdata(F2,'v'); %%% for set_param

%% 1) gyro_z_axis_rate_controller (1*1 SISO System)
%%% From t_a to w_z (Rate Controller Design)


disp('Plants from t_A to w_z= P_w_z')%%%% 1*1 SISO Plant
P_w_z = zpk(H(5,4))

%%
n_y_w_z = size(P_w_z,1);        %Number of Outputs for
   plant from t_a to w_z
n_u_w_z = size(P_w_z,2);        %Number of Inputs for
   plant from  t_a to w_z
```

```
n_s_w_z = size(P_w_z,'order'); %Number of States for plant from  t_a to w_z


%% Weighting Functions for w_z controller
%% W1  (sensitivity)

Ms_w_z =10;       %% 'Ms' helps adjust overshoot in sensitivity graph.
wb_w_z = 2*pi*100;        %% 'wb' helps adjust bandwith range.
Eps_w_z = 0.001;          %% Eps is a minimum value in sensitivity function.
k_w_z =1;                %% 'k' provides steeper transition.
%W1_w_z = tf([1/(Ms_w_z ^(1/k_w_z)) wb_w_z], [1 wb_w_z*(Eps_w_z ^(1/k_w_z))])^k_w_z;%%general form.(1*2)

W1_w_z = tf([1/Ms_w_z wb_w_z], [1 wb_w_z*Eps_w_z])

%% W2  (control sensitivity)
% Eps_w_z =0.001;   Eps1_w_z = 0.001;
% wbu_w_z = 2*pi*100;    wbu1_w_z = 2*pi*100;
% k_w_z=1;              k1_w_z=1;

%  Mu_w_z = 1e7;  Mu1_w_z = 10^(0.00001/20);
Mu1_w_z = 1e-6;  Mu2_w_z =1e-2;
% W2_w_z = tf([1 wbu_w_z/(Mu_w_z^(1/k_w_z))],[Eps_w_z^(1/k_w_z) wbu_w_z])^k_w_z   %% general form.
% W2_w_z = tf([1 wbu_w_z/Mu_w_z], [Eps_w_z wbu_w_z]);
%W2_w_z = tf(1/Mu_w_z, 1);              %% any fixed function.
% W2_w_z = [tf([1 wbu_w_z/(Mu1_w_z^(1/k_w_z))],[Eps_w_z^(1/k_w_z) wbu_w_z])^k_w_z   0;
%   0      tf([1 wbu1_w_z/(Mu2_w_z^(1/k1_w_z))],[Eps1_w_z^(1/k1_w_z) wbu1_w_z])^k1_w_z]; %% general form.

```

```
% W2_w_z= [tf(1/Mu1_w_z, 1)  0;
%              0     tf(1/Mu2_w_z, 1)];  %% any fixed
    function(2*2)

 W2_w_z = tf(Mu1_w_z, 1);
% % W2_w_z = tf(1/Mu1_w_z, 1);


%% W3  (complemantary sensitivity)
My_w_z = 10^(0.01/20) ;
wbc_w_z= 2*pi*5;
Eps_w_z = 0.0001;
v=1;

% W3_w_z = tf([1 wbc_w_z/My_w_z], [Eps_w_z wbc_w_z]);
W3_w_z = tf([1 wbc_w_z/(My_w_z^(1/v))], [(Eps_w_z^(1/v))
    wbc_w_z])^v;
W3_w_z=[];

%%
aug = true;
blt = true;


%% Augment with Integrators at the Input for w_z
    controller(inner controller)

if aug
    Paug_w_z = f_Augment_at_Input(P_w_z);
else
    Paug_w_z =ss(P_w_z);
end


%% Bilinear Transformation for w_z controller (inner
    controller)

```

```
if blt
    p2_w_z = -1e8; p1_w_z = -1;
    Pt_w_z=bilin(Paug_w_z, 1,'Sft_jw',[p2_w_z p1_w_z]);
else
    Pt_w_z=Paug_w_z;
end

%% Augmented Plant for w_z controller
G_w_z = augw(Pt_w_z,W1_w_z,W2_w_z,W3_w_z); %%augmented plant

%% Hinf Controller Design Methodology for w_z controller
design_opts = hinfsynOptions;
design_opts.Method='RIC';%'LMI';%'MAXE';
design_opts.Display='on';
[Kt_w_z,CL,GAM,INFO] = hinfsyn(G_w_z,n_y_w_z,n_u_w_z,design_opts);

%% Inverse Bilinear Transformation for w_z controller
if blt
    K_w_z=bilin(Kt_w_z,-1,'Sft_jw',[p2_w_z p1_w_z]);
else
    K_w_z = Kt_w_z;
end
n_k_w_z = size(K_w_z,'order'); % Number of States

%% Augment with Integrators for w_z controller
if aug
    K_w_z = f_Augment_at_Output(K_w_z);
end
disp('Outer Azimuth Position Controller = K_w_z')
zpk(K_w_z)


%% Controller Design (rule of thumb) for w_z controller
% figure(1)
% bode(K_w_z, 'r', bode_plot_opts)
```

```matlab
% hold on

[zz, pp, kk] = zpkdata(K_w_z,'v')

% K_w_z_rot=zpk(zz,[pp([1 3]); 0],kk);%choose zz, pp, kk
% K_w_z_rot=zpk(zz,[pp([2]);0],kk);%choose zz, pp, kk

% zpk(K_w_z_rot)
% clearvars zz pp kk
%
% disp('Rule of Thumb Outer Azimuth Rate Controller =
    K_w_z_rot')
% bode (K_w_z_rot,'b',bode_plot_opts)
% set(findall(gcf, 'Type', 'line'), 'LineWidth', 2)
% set(gcf, 'Position', [100 100 800 600])

K_w_z_rot=K_w_z;
[num den] = tfdata(K_w_z_rot, 'v'); %%%% for  set_param

% str = ['test_pdf.pdf']
% set(gcf,'PaperPosition', [0 0 800 600])
% set(gcf,'PaperPositionMode','Auto',...
%          'PaperUnits','centimeters',...
%          'PaperSize',[10 7.5])
% print(gcf,str,'-dpdf','-r600', '-loose', '-fillpage')
% disp('DONE')


%% Model Reduction for w_z controller
% % [Kb_w_z,gg_w_z] = balreal(K_w_z);gg_w_z
% % K_w_z = modred(Kb_w_z,[3],'MatchDC');%
% % disp('Reduced Order Controller Kb_w_z')
% % zpk(K_w_z)


%% Design Analysis for w_z controller
UU = f_Maps_PKW(P_w_z, K_w_z_rot);
```

```
UU.W1 = W1_w_z;
UU.W2 = W2_w_z;
UU.W3 = W3_w_z;
%%%
f_Plot_Sigma_Resp(UU, wvec, 'b', '-')
damp(pole(UU.To)) %% closed loop poles
%%%
figure(100)
step(UU.Try, 'b', linspace(0, 1, 1001)) %% time response
grid on; hold on
title('Try for psi_o_position_controller',...
    'Interpreter','none','FontSize',13,'FontName','Times
       New Roman')
%%%
figure(101)
step(UU.Tru, 'b', linspace(0, 1, 1001)) %%control
   response
grid on; hold on
title('Tru for psi_o_position_controller',...
    'Interpreter','none','FontSize',13,'FontName','Times
       New Roman')
%%%
figure(200)
rlocus(UU.Lo)



%%  UPDATE SIMULINK BLOCK
load_system('Ratecontroller');

%%%% Set controller paramaters
%%
%%%%%%% Rate Controller paramater


set_param('Ratecontroller/wz/K_i', 'Numerator', mat2str(
   num),...
```

```
                            'Denominator', mat2str(den));
%% High pass and low pass filter parameter

set_param('Ratecontroller/wz/HPF', 'Numerator', mat2str(
    num2),...
                            'Denominator', mat2str(den2));

set_param('Ratecontroller/wz/hpf', 'Numerator', mat2str(
    num2),...
                            'Denominator', mat2str(den2));
disp('SBD UPDATED (Ratecontroller.slx K_w_z value is
    updated)')
```

wy-inner-rate-controller.m

```
clc
clearvars
close all
equilibrium_point

bode_plot_opts = bodeoptions;
bode_plot_opts.FreqUnits = 'rad/s';
bode_plot_opts.Title.FontSize = 14;
bode_plot_opts.XLabel.FontSize = 14;
bode_plot_opts.YLabel.FontSize = 14;
bode_plot_opts.TickLabel.FontSize = 14;
bode_plot_opts.Grid = 'on';


wvec = logspace(-3, 4, 1001);


%% Cut-off frequency for high pass filter
wc = 2*pi*0.5;
F2 = tf([1 0],[1 wc]);  %%% high pass filter
[num2,den2] = tfdata(F2,'v'); %%% for set_param

%% 1) gyro_y_axis_rate_controller (1*1 SISO System)
%%% From t_e to w_y (Rate Controller Design)
```

```
disp('Plants from t_e to w_y= P_w_y')%%%% 1*1 SISO Plant
P_w_y = zpk(H(6,3))

%%
n_y_w_y = size(P_w_y,1);        %Number of Outputs for plant from t_e to w_y
n_u_w_y = size(P_w_y,2);        %Number of Inputs for plant from  t_e to w_y
n_s_w_y = size(P_w_y,'order'); %Number of States for plant from  t_e to w_y


%% Weighting Functions for w_y controller
%% W1  (sensitivity)

Ms_w_y =5;      %% 'Ms' helps adjust overshoot in sensitivity graph.
wb_w_y = 2*pi*80;        %% 'wb' helps adjust bandwith range.
Eps_w_y = 0.001;          %% Eps is a minimum value in sensitivity function.
k_w_y =1;                 %% 'k' provides steeper transition.
%W1_w_y = tf([1/(Ms_w_y ^(1/k_w_y)) wb_w_y], [1 wb_w_y*(Eps_w_y ^(1/k_w_y))])^k_w_y;%%general form.(1*2)

W1_w_y = tf([1/Ms_w_y wb_w_y], [1 wb_w_y*Eps_w_y])

%% W2  (control sensitivity)
% Eps_w_y =0.001;   Eps1_w_y = 0.001;
% wbu_w_y = 2*pi*100;    wbu1_w_y = 2*pi*100;
% k_w_y=1;                k1_w_y=1;

%  Mu_w_y = 1e7;  Mu1_w_y = 10^(0.00001/20);
Mu1_w_y = 1e7;  Mu2_w_y =1e2;
```

```
% W2_w_y = tf([1 wbu_w_y/(Mu_w_y^(1/k_w_y))],[Eps_w_y^(1/
    k_w_y) wbu_w_y])^k_w_y   %% general form.
% W2_w_y = tf([1 wbu_w_y/Mu_w_y], [Eps_w_y wbu_w_y]);
%W2_w_y = tf(1/Mu_w_y, 1);            %% any fixed
    function.
% W2_w_y = [tf([1 wbu_w_y/(Mu1_w_y^(1/k_w_y))],[Eps_w_y
    ^(1/k_w_y) wbu_w_y])^k_w_y   0;
%   0      tf([1 wbu1_w_y/(Mu2_w_y^(1/k1_w_y))],[Eps1_w_y
    ^(1/k1_w_y) wbu1_w_y])^k1_w_y]; %% general form.

% W2_w_y= [tf(1/Mu1_w_y, 1)  0;
%             0    tf(1/Mu2_w_y, 1)];  %% any fixed
    function(2*2)


W2_w_y = tf(1/Mu1_w_y, 1);


%% W3  (complemantary sensitivity)
My_w_y = 10^(0.01/20) ;
wbc_w_y= 2*pi*5;
Eps_w_y = 0.0001;
v=1;

% W3_w_y = tf([1 wbc_w_y/My_w_y], [Eps_w_y wbc_w_y]);
W3_w_y = tf([1 wbc_w_y/(My_w_y^(1/v))], [(Eps_w_y^(1/v))
    wbc_w_y])^v;
W3_w_y=[];

%%
aug = true;
blt = true;


%% Augment with Integrators at the Input for w_y
    controller(inner controller)

```

```
if aug
    Paug_w_y = f_Augment_at_Input(P_w_y);
else
    Paug_w_y =ss(P_w_y);
end


%% Bilinear Transformation for w_y controller (inner
   controller)

if blt
    p2_w_y = -1e20; p1_w_y = -0.08;
    Pt_w_y=bilin(Paug_w_y, 1,'Sft_jw',[p2_w_y p1_w_y]);
else
    Pt_w_y=Paug_w_y;
end

%% Augmented Plant for w_y controller
G_w_y = augw(Pt_w_y,W1_w_y,W2_w_y,W3_w_y); %%augmented
   plant

%% Hinf Controller Design Methodology for w_y controller
design_opts = hinfsynOptions;
design_opts.Method='RIC';%'LMI';%'MAXE';
design_opts.Display='on';
[Kt_w_y,CL,GAM,INFO] = hinfsyn(G_w_y,n_y_w_y,n_u_w_y,
   design_opts);

%% Inverse Bilinear Transformation for w_y controller
if blt
    K_w_y=bilin(Kt_w_y,-1,'Sft_jw',[p2_w_y p1_w_y]);
else
    K_w_y = Kt_w_y;
end
n_k_w_y = size(K_w_y,'order'); % Number of States

%% Augment with Integrators for w_y controller
```

```
if aug
    K_w_y = f_Augment_at_Output(K_w_y);
end
disp('Inner Elevation Position Controller = K_w_y')
zpk(K_w_y)

%% Controller Design (rule of thumb) for w_y controller
% figure(1)
% bode(K_w_y, 'r', bode_plot_opts)
% hold on

[zz, pp, kk] = zpkdata(K_w_y,'v')

% K_w_y_rot=zpk(zz,[pp([1 3]); 0],kk);%choose zz, pp, kk
% K_w_y_rot=zpk(zz,[pp([2]);0],kk);%choose zz, pp, kk

% zpk(K_w_y_rot)
% clearvars zz pp kk
%
% disp('Rule of Thumb Outer Azimuth Rate Controller = K_w_y_rot')
% bode (K_w_y_rot,'b',bode_plot_opts)
% set(findall(gcf, 'Type', 'line'), 'LineWidth', 2)
% set(gcf, 'Position', [100 100 800 600])

K_w_y_rot=K_w_y;
[num den] = tfdata(K_w_y_rot, 'v'); %%%% for  set_param

% str = ['test_pdf.pdf']
% set(gcf,'PaperPosition', [0 0 800 600])
% set(gcf,'PaperPositionMode','Auto',...
%          'PaperUnits','centimeters',...
%          'PaperSize',[10 7.5])
% print(gcf,str,'-dpdf','-r600', '-loose', '-fillpage')
% disp('DONE')
```

```
%% Model Reduction for w_y controller
% % [Kb_w_y,gg_w_y] = balreal(K_w_y);gg_w_y
% % K_w_z = modred(Kb_w_y,[3],'MatchDC');%
% % disp('Reduced Order Controller Kb_w_y')
% % zpk(K_w_y)


%% Design Analysis for w_y controller
UU = f_Maps_PKW(P_w_y, K_w_y_rot);
UU.W1 = W1_w_y;
UU.W2 = W2_w_y;
UU.W3 = W3_w_y;
%%%
f_Plot_Sigma_Resp(UU, wvec, 'b', '-')
damp(pole(UU.To)) %% closed loop poles
%%%
figure(100)
step(UU.Try, 'b', linspace(0, 1, 1001)) %% time response
grid on; hold on
title('Try for psi_o_position_controller',...
    'Interpreter','none','FontSize',13,'FontName','Times New Roman')
%%%
figure(101)
step(UU.Tru, 'b', linspace(0, 1, 1001)) %%control response
grid on; hold on
title('Tru for psi_o_position_controller',...
    'Interpreter','none','FontSize',13,'FontName','Times New Roman')
%%%
figure(200)
rlocus(UU.Lo)



%%  UPDATE SIMULINK BLOCK
```

```
load_system('Ratecontroller');

%%%% Set controller paramaters
%%
%%%%%%% Rate Controller paramater


set_param('Ratecontroller/wy/K_i', 'Numerator', mat2str(
    num),...
                            'Denominator', mat2str(den));
%% High pass and low pass filter parameter

set_param('Ratecontroller/wy/HPF', 'Numerator', mat2str(
    num2),...
                            'Denominator', mat2str(den2));

set_param('Ratecontroller/wy/hpf', 'Numerator', mat2str(
    num2),...
                            'Denominator', mat2str(den2));
disp('SBD UPDATED (Ratecontroller.slx K_w_y value is
    updated)')
```

==

APPENDIX B

SIMULINK BLOCKS

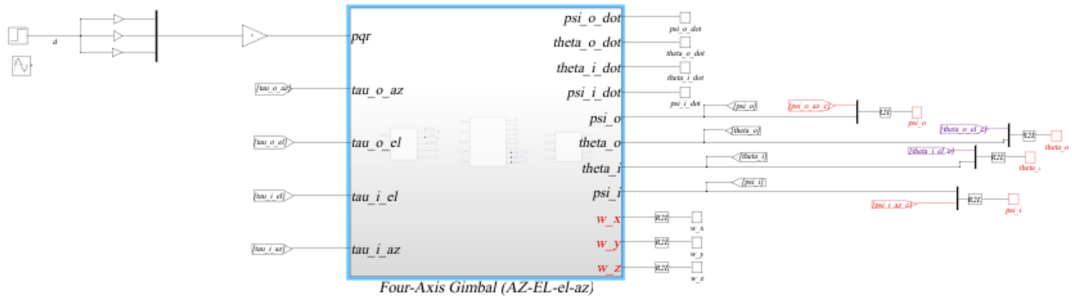

Figure B.1: Four Axis Gimbal(AZ-EL-el-az).

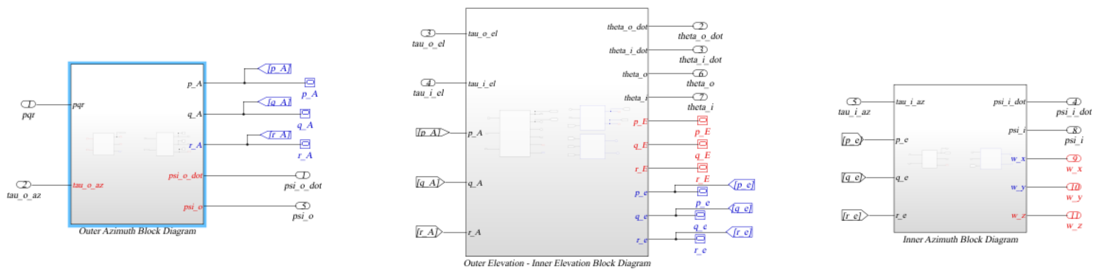

Figure B.2: Four Axis Gimbal Block Inside.

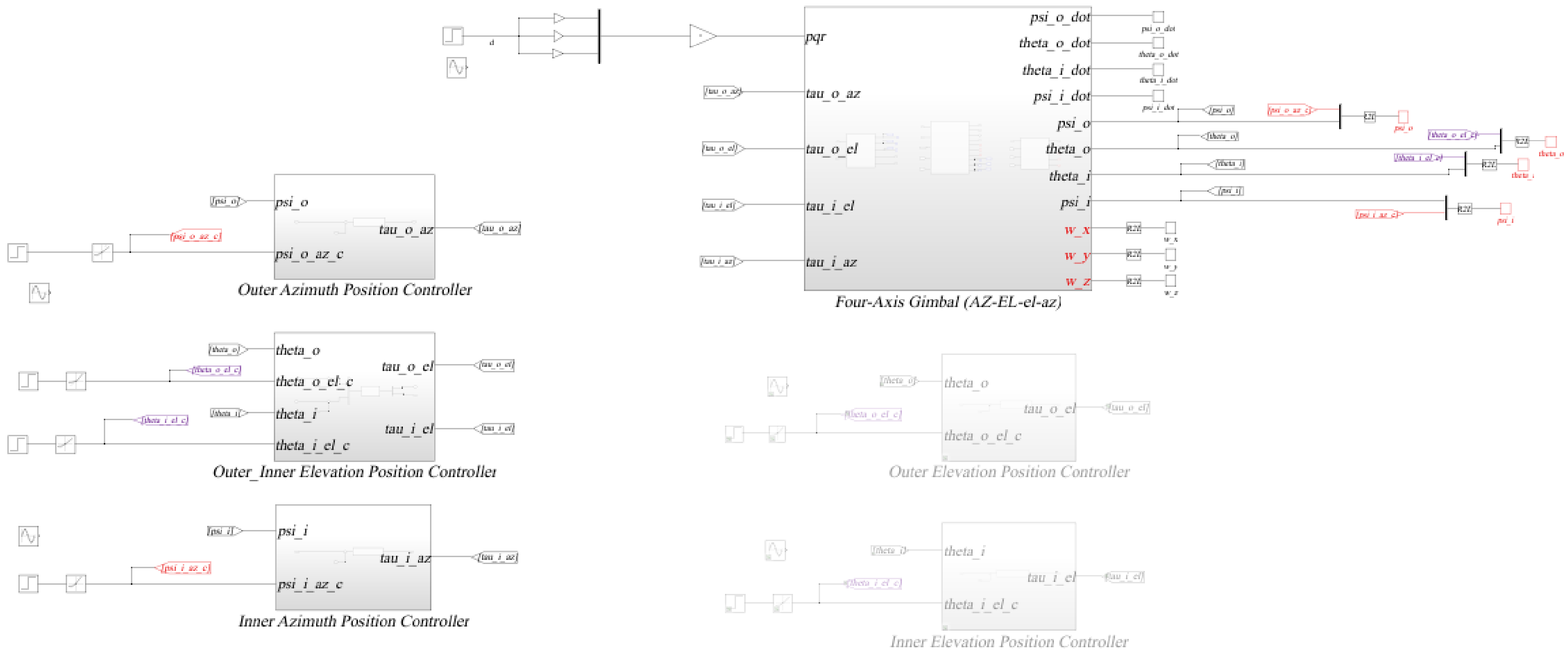

Figure B.3: Position Controller Design.

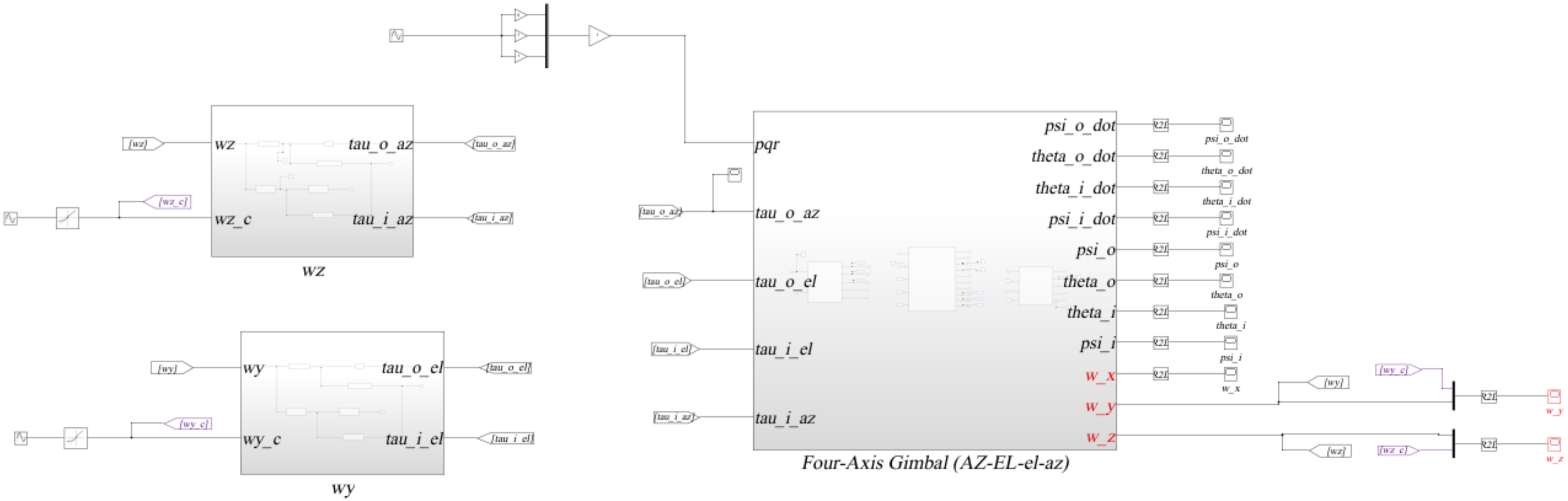

Figure B.4: Rate Controller Design.